UNIVERSITEIT VAN PRETORIA
UNIVERSITY OF PRETORIA
YUNIBESITHI YA PRETORIA

STUDY OF FLOW AND HEAT TRANSFER FEATURES OF NANOFLUIDS USING MULTIPHASE MODELS: EULERIAN MULTIPHASE AND DISCRETE LAGRANGIAN APPROACHES

by

MOSTAFA MAHDAVI

Submitted in partial fulfilment of the requirements for the degree

Philosophiae Doctor (Mechanical Engineering)

in the

Department of Mechanical and Aeronautical Engineering

Faculty of Engineering, Built Environment and Information Technology
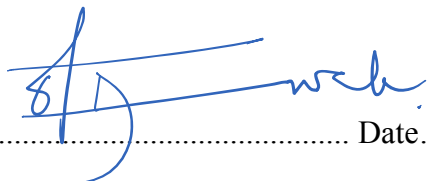
University of Pretoria

Pretoria

2016

DECLARATION

I, Mostafa Mahdavi, hereby declare that the matter embodied in this thesis, *Study of flow and heat transfer features of nanofluids by CFD models: Eulerian multiphase and discrete Lagrangian approaches*, is the result of investigations carried out under the supervision of Dr M Sharifpur and Prof JP Meyer in the Department of Mechanical and Aeronautical Engineering, University of Pretoria, South Africa, towards the awarding of the degree *Philosophiae Doctor*. I also declare that this thesis has not been submitted elsewhere for any degree or diploma. In keeping with the general practice in reporting scientific observations, due acknowledgment was made whenever the work described was based on the findings of other researchers.

Signature... Date…………………………………………

ACKNOWLEDGEMENTS

I would like to express my gratitude to my supervisor, Prof. Mohsen Sharifpur, for his guidance throughout this study, for creating a good supervisor-student relationship and for creating time for all my challenges.

My thanks and appreciation also go to my co-supervisor and Head of the Department of Mechanical and Aeronautical Engineering at the University of Pretoria, Prof. Josua P Meyer, for his technical and financial support, which allowed me to successfully complete this study.

I would also like to thank Ms Tersia Evans (Departmental Postgraduate Administrator). She provided a warm friendly atmosphere in the department, which was important in the completion of my PhD degree.

ABSTRACT

Title: Study of flow and heat transfer features of nanofluids by CFD models: Eulerian multiphase and discrete Lagrangian approaches

Author: Mostafa Mahdavi

Supervisors: Prof. Mohsen Sharifpur and Prof. Josua P Meyer

Department: Mechanical and Aeronautical Engineering

University: University of Pretoria

Degree: *Philosophiae Doctor* (Mechanical Engineering)

Choosing correct boundary conditions, flow field characteristics and employing right thermal fluid properties can affect the simulation of convection heat transfer using nanofluids. Nanofluids have shown higher heat transfer performance in comparison with conventional heat transfer fluids. The suspension of the nanoparticles in nanofluids creates a larger interaction surface to the volume ratio. Therefore, they can be distributed uniformly to bring about the most effective enhancement of heat transfer without causing a considerable pressure drop. These advantages introduce nanofluids as a desirable heat transfer fluid in the cooling and heating industries. The thermal effects of nanofluids in both forced and free convection flows have interested researchers to a great extent in the last decade.

Investigating the interaction mechanisms happening between nanoparticles and base fluid is the main goal of the study. These mechanisms can be explained via different approaches through some theoretical and numerical methods. Two common approaches regarding particle-fluid interactions are Eulerian-Eulerian and Eulerian-Lagrangian. The dominant conceptions in each of them are slip velocity and interaction forces respectively. The mixture multiphase model as part of the Eulerian-Eulerian approach deals with slip mechanisms and somehow mass diffusion from the nanoparticle phase to the fluid phase. The slip velocity can be induced by a pressure gradient, buoyancy, virtual mass, attraction and repulsion between particles. Some of the diffusion processes can be caused by the gradient of temperature and concentration.

The discrete phase model (DPM) is a part of the Eulerian-Lagrangian approach. The interactions between solid and liquid phase were presented as forces such as drag, pressure gradient force, virtual mass force, gravity, electrostatic forces, thermophoretic and Brownian forces. The energy transfer from particle to continuous phase can be introduced through both convective and conduction terms on the surface of the particles.

A study of both approaches was conducted in the case of laminar and turbulent forced convections as well as cavity flow natural convection. The cases included horizontal and vertical pipes and a rectangular cavity. An experimental study was conducted for cavity flow to be compared with the simulation results. The results of the forced convections were evaluated with data from literature. Alumina and zinc oxide nanoparticles with different sizes were used in cavity experiments and the same for simulations. All the equations, slip mechanisms and forces were implemented in ANSYS-Fluent through some user-defined functions.

The comparison showed good agreement between experiments and numerical results. Nusselt number and pressure drops were the heat transfer and flow features of nanofluid and were found in the ranges of the accuracy of experimental measurements. The findings of the two approaches were somehow different, especially regarding the concentration distribution. The mixture model provided more uniform distribution in the domain than the DPM. Due to the Lagrangian frame of the DPM, the simulation time of this model was much longer. The method proposed in this research could also be a useful tool for other areas of particulate systems.

Keywords: *Nanofluid, Eulerian-Eulerian, Eulerian-Lagrangian, mixture model, discrete phase model, slip velocity, interaction forces, ANSYS-Fluent, user-defined functions*

LIST OF FIGURES

LIST OF TABLES

NOMENCLATURE

A	Hamaker constant (J)
A_p	particle surface area (m^2)
C_c	Cunningham slip correction factor (-)
C_D	drag coefficient (-)
c_i	concentration (mol/L)
C_L	lift coefficient (-)
C_{ML}	rotational lift coefficient (-)
C_p	specific heat (J/kg.K)
C_ω	rotational drag coefficient (-)
D, d	diameter (m)
d_c	molecule diameter (m)
D_B	diffusion coefficient (-)
D_T	thermophoresis coefficient (-)
E	energy source term (W/m^3)
$\mathbf{f}$	force per mass vector (N/kg)
F	Faraday constant (C/mol)
$\mathbf{F}$	force vector (N)
$\tilde{F}$	non-dimensional force ratio (-)
f_d	drag function (-)
$\boldsymbol{g}$	gravity vector (m/s^2)
G_w	Gaussian weight function (-)
h	enthalpy (J/kg), with subscripts
h	heat transfer coefficient ($W/m^2.K$)
I_0	ionic strength (mol/L)
I_p	moment of inertia ($kg.m^2$)
$\mathbf{J}$	mass flux diffusion ($kg/m^2.s$)
k	thermal conductivity ($W/m.^oK$)
K_B	Boltzmann constant ($m^2.kg/^oK.s^2$)

Kn	Knudsen number (-)
L	length (m)
m	mass (kg)
$\mathbf{M}$	momentum source term vector ($kg/m^2.s^2$)
$\dot{m}$	mass flow rate (kg/s)
Nu	Nusselt number (-)
$N_{particle}$	number of particles in a parcel (-)
p	pressure (N/m^2)
Pr	Prandtl number (-)
$\mathbf{q}''$	heat flux vector (W/m^2)
q''	heat flux (W/m^2)
Q_s	heat transfer (W)
r	radial direction (m)
R	gas universal constant (J/mol.K)
Ra	Rayleigh number (-)
Re	Reynolds number (-)
Re_w	vorticity Reynolds number (-)
T	temperature (K)
T_{ref}	freezing temperature (K)
T^*	non-dimensional temperature
u	velocity magnitude (m/s)
$\mathbf{V}$	velocity vector (m/s)
V	volume (m^3)
$\mathbf{V}_{km}$, $\mathbf{V}_{cm}$, $\mathbf{v}_{pm}$	drift velocity vector (m/s)
V_R	potential energy (J)
$\mathbf{v}_{slip}$	slip velocity vector (m/s)
$\langle \mathbf{x.x} \rangle$	mean square displacement (m)
X, Y, Z	coordinate directions (m)
z_i	charge (-)

Greek symbols

α	volume fraction (-)
β	thermal expansion coefficient (K^{-1})
δ	particle-to-particle distance (m)
Δt	particle time step (s)
ε_0	vacuum permittivity (C/V.m)
ε_r	relative permittivity (-)
Γ	mass source term (kg/m^3.s)
$\dot{\gamma}$	shear rate (1/s)
κ	Debye-Huckel parameter (1/m)
λ	mean free path of the liquid phase (m)
μ	viscosity (Pa.s)
ν	kinematic viscosity (m^2/s)
ω_p	particle angular velocity vector (rad/s)
$\mathbf{\Omega}$	relative angular velocity of the fluid and particle (rad/s)
ρ	density (kg/m^3)
ψ	surface potential (V)
$\mathbf{\tau}$	shear stress vector (Pa)
τ	particle relaxation time (s)
θ	shape factor (-)
$\bar{\theta}_{parcel}$	particle variables
ζ_i	Gaussian white noise function (-)

Subscripts

b	bulk
B	Brownian
c	continuous phase
$c\text{-}ave$	average on the cold wall
$drag$	drag force

EDL	electric double layer
fr	freezing
h-ave	average on the hot wall
in	inlet to a cell
k	a phase of mixture
lift	lift force
m	mixture
nf	nanofluid
out	outlet of a cell
p	particle
pressure	pressure gradient force
virtual-mass	virtual mass force
VDW	Van der Waals
w	wall

PUBLICATIONS IN JOURNALS AND CONFERENCE PROCEEDINGS

The following articles and conference papers were published while this study was in progress. It provided independent peer reviews, and very valuable feedback from reviewers was implemented.

Published articles in international journals

1. **M. Mahdavi**, M. Sharifpur and J.P. Meyer, CFD modelling of heat transfer and pressure drops for nanofluids through vertical tubes in laminar flow by DPM and mixture model, International Journal of Heat and Mass Transfer, vol. 88, 803-813, 2015.

2. **M. Mahdavi**, M. Sharifpur, H. Ghodsinezhad and J.P. Meyer, Experimental and numerical study on thermal and hydro-dynamic characteristics of laminar natural convective flow inside a rectangular cavity with water, EG-water and air, Experimental Thermal and Fluid Science, vol. 78, 50-64, 2016.

3. **M. Mahdavi**, M. Sharifpur and J.P. Meyer, Simulation study of convective and hydrodynamic turbulent nanofluids by turbulence models, International Journal of Thermal Sciences, vol. 110, 36-51, 2016.

4. **Mostafa Mahdavi**, M. Sharifpur and J.P. Meyer, Implementation of diffusion and electrostatic forces to produce a new slip velocity in multiphase approach of nanofluids, Powder Technology, Vol. 307, 1 February 2017, pp. 153-162.

5. **Mostafa Mahdavi**, M. Sharifpur and J.P. Meyer, A new combination of nanoparticles mass diffusion flux and slip mechanism approaches with electrostatic forces in a natural convective cavity flow, International Journal of Heat and Mass Transfer, Vol. 106, March 2017, pp. 980–988.

Manuscripts accepted

6. **M. Mahdavi**, M. Sharifpur, H. Ghodsinezhad and J.P. Meyer, Experimental and numerical investigation on a water-filled cavity natural convection to find proper

thermal boundary conditions for simulation, Journal of Heat Transfer Engineering. Accepted, 2016.

Manuscripts submitted

7. **Mostafa Mahdavi**, M. Sharifpur and J.P. Meyer, Aggregation study of Brownian nanoparticles in convective phenomena, submitted to International Journal Heat and Mass Transfer, manuscript number: HMT_2017_438.

Published refereed conference papers

8. **M. Mahdavi**, M. Sharifpur and J.P. Meyer, Comparative study on simulation of convective Al_2O_3-water nanofluid by using ANSYS-Fluent, The 15th International Heat Transfer Conference (IHTC-15), August 10-15, 2014, Kyoto, Japan.

9. **M. Mahdavi**, H. Ghodsinezhad, M. Sharifpur and J.P. Meyer, Boundary condition investigation for cavity flow natural convection, 11th International Conference on Heat Transfer, Fluid Mechanics and Thermodynamics (HEFAT 2015), July 20-23, 2015, Kruger National Park, South Africa.

10. **M. Mahdavi**, M. Sharifpur and J.P. Meyer, Natural convection study of Brownian nano-size particles inside a water-filled cavity by Lagrangian-Eulerian tracking approach, 12th International Conference on Heat Transfer, Fluid Mechanics and Thermodynamics (HEFAT 2016), July 10-14, 2016, Malaga, Spain.

11. **Mostafa Mahdavi**, M. Sharifpur and J.P. Meyer, Development of a novel method for slip velocity of fluid structure interactions by employing effects of electrostatic attraction on the surface of nano-scale particles, The Sixth International Conference on Structural Engineering, Mechanics and Computation (SEMC 2016), September 5-7, 2016, Cape Town, South Africa.

CHAPTER 1: INTRODUCTION

BACKGROUND

Enhancement of heat transfer and improvement of performance are some of the most important issues in industrial equipment. Some of the applications can be found in heat exchangers, solar collectors, boilers, etc.

Due to the low thermal conductivity of the liquid phase compared with that of metallic solids, heat transfer improvement via mixing nanoparticles with liquid has caught much attention in recent years. This mixture is commonly called nanofluid. The order of magnitude of particle sizes can be 10^2 nm. High uniformity of distribution of nanoparticles inside the liquid can provide a new fluid with higher conductivity, density and viscosity. In spite of the increase in thermal conductivity, the negative side of the rise in viscosity cannot be ignored.

There are two main approaches to model particulate systems. In the multiphase mixture model, both solid and liquid phases are assumed continuum and the relative velocity between two phases is small. Nonetheless, it might have a considerable impact on the particle phase's final distribution. The conventional slip velocity in ANSYS-Fluent is the acceleration due to gravitational and centrifugal forces. The essential part of the mixture model is the thermophysical properties of the nanofluid mixture. There are a large number of empirical and theoretical correlations for nanofluid mixture properties in literature. The reliability of those correlations for a wide range of nanofluids is still in doubt. In addition, the phenomena of aggregation and sedimentation can be considered the unknown and unexplained parts in the mixture model due to nature of this model to the solid-liquid mixture.

In the Lagrangian discrete phase model, only the liquid phase is the continuum and all the nanoparticles are tracked separately. The effect of the particles on each other is expressed in terms of the interaction forces. The exchange of momentum and energy between solid and liquid is established through the source terms. The important forces on the

nanoparticles can be different depending on the particle size. Other phenomena such as collision, clustering and sedimentation are still not fully explained for this size of particles. One of the main advantages of this approach is to provide a more realistic distribution of nanoparticles inside the liquid phase.

AIM OF THE RESEARCH

The aim of this research is to fully investigate the affecting parameters in governing equations for both the mixture and DPM approaches when the heat transfer fluid is a nanofluid. Due to the incomplete built-in models in CFD software packages, further development will be implemented through user-defined functions using ANSYS-Fluent.

RESEARCH OBJECTIVES

The specific objectives of this research are as follows:

1. The flow in horizontal and vertical pipes is modelled by ANSYS-Fluent. Because this research has been going on for three years as a PhD work, three versions of ANSYS-Fluent, namely 15.0, 16.0 and 17.0 are used. Forced convection flow is investigated with the presence of nanoparticles. The results are compared with experimental data from literature. The experimental work is particularly borrowed from previous studies. The capabilities and weaknesses of both the mixture model and DPM are also evaluated.

2. A two- and a three-dimensional analysis of natural convective flow in a water-filled cavity are presented and compared with experimental measurements to find the actual boundary conditions.

3. New mathematical approaches are implemented into the ANSYS-Fluent through some UDFs for both the mixture model and DPM.

4. The results of new approaches are compared with the measurements of nanofluid-filled cavity taken in this research. The capabilities of these are explained compared with the conventional methods.

SCOPE OF THE STUDY

In this research, the application of both Eulerian and Lagrangian approaches for nanofluids modelling are studied. The interactions between solid and liquid phases are explained and the available parameters and correlations are implemented into the models. The simulations cover laminar and turbulent forced convections as well as natural convection in cavities. The findings of forced convections are compared with experimental measurements from literature. Some experiments are conducted for the case of cavity flow natural convection with nanofluids.

.

ORGANISATION OF THE THESIS

A brief study of other researches is presented in Chapter 2. The literature review mainly covers the experimental and theoretical investigations of nanofluid flows. Both the mixture model and discrete phase modelling are extensively explained and the new modifications in both are proposed in Chapter 3. The results of some simulations conducted in terms of these proposed approaches are discussed in Chapter 4. The final conclusions and some recommendations for future work are provided in Chapter 5.

CHAPTER 2:   LITERATURE REVIEW

INTRODUCTION

Nanotechnology can be involved in many sections of technology and industry, for instance, energy management, medicine, information technology, environmental science, thermal storage and food safety. Nanofluids have shown higher heat transfer performance in comparison with conventional heat transfer fluids, therefore, they have captured the interest of many researchers in recent years. Nanoparticles are suspended in conventional heat transfer fluids (base fluids) to produce stable nanofluids. On the other hand, the advantage of nanoparticles compared with microparticles is a higher surface area per volume, which clearly enhances heat transfer rate. In addition, the random movement of ultrafine particles can be another reason for the heat transfer enhancement. Experimental findings explain that the heat transfer improvement by nanofluids can vary from a small percentage [1] to a few times higher than the case for pure base fluid (without particles) [2]. All the studies can be categorised into three sections, namely experimental, numerical and theoretical studies. In each section, different types of flows are briefly explained.

EXPERIMENTAL STUDIES OF NANOFLUID

Both force and natural convection have been experimentally investigated in the literature. A large number of these are associated with pipe flow, either laminar or turbulence. Also, there are some reports about the increase of heat performance in heat exchangers.

2.1.1   Nanofluid laminar forced convective flow

Experimental studies of nanofluid laminar flow in pipes (both of horizontal and vertical cases) have been conducted by different researchers [3–15]. Wen and Ding [3] studied the enhancement of heat transfer for alumina nanofluid in a horizontal pipe with Reynolds number up to 1950. The nanoparticle concentration was kept below 2% vol., but the enhancement was measured up to 50% in some tests. This is contrary to Rea et al. [7], who showed that the conventional correlations failed to correctly predict heat transfer

coefficient. The main reasons were pointed out, namely the particle migration, disturbed hydrodynamic and thermal boundary layers.

Yang et al. [4] used two different base fluids from water, mixed with graphite nanoparticles with an aspect ratio of 0.02. The nanofluid mixture was reported stable and no settling was observed. Because the result of heat transfer for the nanofluid was different from the one calculated based on static thermophysical properties for single-phase flow, the homogeneous behaviour of the nanofluid mixture was questioned. They suggested that new correlations were essential for nanofluid heat transfer features.

He et al. [5] investigated the hydrodynamic and heat transfer characteristics of TiO_2 nanofluid in a vertical pipe under both laminar and turbulent conditions. The volume fraction was less than 1.2% vol. They observed a slight effect of particle size on heat transfer coefficient. Even though the enhancement of heat transfer was reported up to 40%, the impacts on pressure drops were found almost negligible compared with pure water. The traditional correlations for heat transfer in pipe flows underpredicted the results.

Kim et al. [6] investigated alumina and carbonic nanofluid in a laminar and turbulent horizontal pipe flow with constant heat flux. The volume fraction for both was chosen about 3% vol. The increase in heat transfer coefficient was found higher in the case of alumina nanofluid. The particle migration was stated as the main cause of enhancement in heat transfer at the entrance.

Anoop et al. [8] proposed a new correlation for the local Nusselt number for alumina nanofluid up to 8 wt% in terms of particle size and volume fraction. The measurements were conducted in the developing region of a laminar pipe flow with constant heat flux and were found to be higher than those for the fully developed part of the pipe. They also reported the enhancement in local heat transfer coefficient to be more than 30% compared with pure water.

Improvement of heat transfer and increased nanofluid thermal conductivity in a horizontal pipe were measured by Kolade et al. [9]. The Reynolds number was up to 1600 for

5

alumina nanoparticles in DI water up to 2% vol. and carbon nanotubes in silicone oil up to 0.2% vol. It was shown that the dynamic nanofluid thermal conductivity in the pipe can somehow differ from the static measurements. Also, the structure of carbon nanotube was the contributing factor to higher enhancement compared with alumina nanofluid.

Zhang [11] and Rea et al. [7] conducted experimental studies of silica, alumina and zirconia nanofluid in two vertical pipes in the laminar regime. One of the pipes was used to measure pressure loss and the other one for heat transfer coefficient. The highest value of performance was reported for alumina 6% vol. with 27% in heat transfer coefficient compared with pure water. On the other hand, the increase in heat transfer was measured 3% for zirconia at 1.32% vol. Rea et al. [7] state that the traditional correlations for the calculating of pressure loss and heat transfer coefficient in pipes are valid for nanofluid by using the thermophysical properties of the mixture. Zhang [11] observed only a small increase in heat transfer performance for silica nanofluid up to 5% vol. In most of the cases, the increase was reported at the order of the uncertainty of the experiment, i.e. 10%.

Liu and Yu [16] conducted some experiments for alumina nanofluid up to 5% vol. in a horizontal minichannel tube with Reynolds number from 600 to 4500. They explain that the enhancement of heat transfer with nanofluid can only happen either in laminar or fully developed turbulent flow. The reason for this is the size distribution of the particles especially in the turbulent section. The interactions between nanoparticles and base fluid are presented as the main cause of changes in fluid flow features. They state that the turbulence intensity and instability reduce under the effect of particle-fluid interactions. They also state that the presence of the particle distribution gradient is unavoidable, being maximum at the centre line of the tube and decreasing towards the wall. Consequently, the velocity profile will be affected by this non-homogeneity.

The friction factor of alumina nanofluid at 6% vol. in a laminar pipe flow was experimentally measured by Tang et al. [14]. The study of shear rate proved the Newtonian behaviour of the mixture for a wide range of temperatures. The measured friction factor was found close to the calculations from conventional correlations for

6

single phase in pipe flows. Nonetheless, the transition Reynolds number was observed to be 1500, which was different from single-phase liquids, previously mentioned as being 2300.

Utomo et al. [15] studied the impacts of the presence of alumina, titania and carbon nanotube in a horizontal pipe. The results of the local Nusselt number, heat transfer coefficient and pressure drops were found in the range of 10% error of traditional correlations for straight pipes. The SEM images showed the presence of diameter distribution from 120 nm to 200 nm in average in the case of alumina nanoparticles, which was different from the nanoparticle size reported by the manufacturer. They state that the nanofluid mixture is highly homogeneous and the influences of Brownian diffusion, thermophoresis, viscosity gradient and non-uniform shear rate can be negligible in heat transfer.

In summary, literature review in this section shows that there is no full agreement on the impacts of nanoparticles on heat transfer and pressure losses in laminar flow and further theoretical exploration is necessary.

2.1.2   Nanofluid turbulent forced convective flow

Due to the presence of a higher order of velocity in turbulent flow, it is expected that the nanoparticles mainly follow the streamlines. But the reciprocal interactions between particles and turbulent eddies during the lifetime of the eddies can be important. There are also a large number of experimental studies for nanofluid in turbulent flows and commonly in pipes [17-32].

One of the earliest experimental reports comes from the study by Pak and Cho [17]. Two nanoparticles were employed in the tests, alumina with 13 nm and titania with 27 nm in size. The mixture viscosity of alumina nanofluid was found much higher than that of titania nanofluid. Viscosity of the nanofluid is the most significant parameter in flow pressure drops; 30% pressure drops was reported for 3% volume fraction. A new correlation for the Nusselt number was proposed in terms of the Reynolds and Prandtl numbers based on mixture properties. It was found that the heat transfer showed a

7

decrease in nanofluid compared with pure water under similar inlet average velocity. This was attributed to the decrease of the Reynolds number in nanofluid.

Xuan and Li [18] proposed a correlation for Cu-water nanofluid Nusselt number in terms of the Reynolds, Prandtl and Peclet numbers and volume fraction up to 2% vol. The results of friction factor showed almost no impact by the presence of nanoparticles compared with pure water, while the heat transfer was highly influenced by changes in the nanoparticle volume fraction.

Williams et al. [19] reported that the conventional correlations for pressure drops and heat transfer features for turbulent pipe flow were sufficiently enough to predict the nanofluid behaviour in a horizontal pipe with constant heat flux. In other words, the appropriate correlations for nanofluid mixture properties had to be measured in each case. Alumina and zirconia nanofluid were used in the tests up to 3.6% vol. and 0.9% vol. respectively.

Yu et al. [20] studied the heat transfer and pressure loss of silicon cardide-water nanofluid in a horizontal pipe for Reynolds number from 3 300 to 13 000. They explained that the traditional correlations for heat transfer coefficient in turbulent flows provided 14% to 32% underprediction compared with the measurements. The pumping power of SiC-water was also compared with that of alumina nanofluid and it was found less for SiC-water. Under constant average inlet velocity, the nanofluid heat transfer coefficient was found less than for pure water.

Duangthongsuk and Wongwises [21] investigated the effect of the presence of titania nanofluid in a double-tube counterflow heat exchanger with turbulent flow. The growth in heat transfer coefficient was only observed for volume fraction up to 1% vol. The heat transfer coefficient improvement was 26% compared with that of pure water at 1% vol., while heat transfer was found to be 14% smaller than for pure water for 2% vol. The correlation of Nusselt number suggested by Pak and Cho [17] was only proper for volume fraction less than 0.2%. New correlations were proposed for Nusselt number and pressure drops in terms of Reynolds and Prandtl numbers and volume fraction.

The flow characteristics of alumina nanofluid inside a horizontal tube with twisted tape insert were studied by Sundar and Sharma [22] under turbulent flow Reynolds number between 10 000 and 22 000. The positive effect of nanofluid on heat transfer was observed higher than the negative effect on pressure loss. The presence of nanoparticles on heat transfer was found to be effective in all the ranges of volume fraction. The conventional correlations underestimated the Nusselt number for turbulent pipe single-phase flow. Two correlations were proposed for Nusselt number and friction coefficient in terms of Reynolds and Prandtl numbers, volume fraction and twist ratio. Some other experimental studies of nanofluid are described in Table 2-1.

Table 2-1 Summary of some experimental studies of turbulent nanofluid flow

Authors	Geometry	Nanoparticles	Remarks
Torii et al. [23]	Horizontal pipe flow with constant heat flux	Diamond, Al_2O_3, CuO, base fluid is water	Deterioration of heat transfer due to nanoparticle aggregation, slight increase in pressure loss, the aggregated size of the particles is much higher than the one reported by manufacturer.
Ferrouillat et al. [24]	Counterflow shell-and-tube heat exchanger, fixed temperature on the wall of the tube	SiO_2-water	Particle stability problem at high temperature, only the measured thermal conductivity and viscosity are introduced as the main criteria of the benefits of nanoparticles. Accordingly, a dimensionless number based on heat transfer and pressure drops is defined.
Sajadi and Kazemi [25]	Horizontal tube with wall temperature condition	TiO_2-water	Even small amount of nanoparticles enhanced heat transfer, the increase in volume fraction makes not many changes in heat transfer, previous correlations fail to predict Nusselt number properly, a new correlation is proposed.

Asirvatham et al. [26]	Counter-current flow with tube-in-tube	Silver-water	Considerable increase of heat transfer enhancement, a correlation is proposed for Nusselt number based on mixture properties and in terms of Reynolds number, Prandtl number and volume fraction.
Suresh et al. [27]	Plain and helically dimpled tube, with constant heat flux	CuO-water	Enhancement of heat transfer is much higher than pressure loss for volume fraction less than 0.3%. The mixture transport properties are explained as the main reasons of the abnormal behaviour of nanofluid.
Sundar et al. [28]	Horizontal copper tube subject to constant heat flux	Magnetite Fe_3O_4-water	The conventional correlation for Nusselt number for single-phase pipe flow underestimates the results. The positive effects of heat transfer improvement are higher than negative effects.
Azmi et al. [29]	Horizontal pipe flow under heat flux condition	SiO_2-water	There is a volume fraction at which the maximum heat transfer coefficient happens, and then it decreases. The friction factor goes up and down with growth in nanoparticle concentration and Reynolds number respectively.
Sahin et al. [30]	Horizontal tube under constant heat flux	Al_2O_3-water	Oscillation is observed in the trend of increase or decrease in heat transfer. The optimum value for volume fraction with the highest heat transfer is 0.5%. Volume fraction higher than 1% is not recommended for the purposes of heat transfer.

Wusiman et al. [31]	Horizontal tube under heat flux condition, from laminar to turbulent regime	Cu-water and Al_2O_3-water	The enhancement of heat transfer was found higher in laminar regime than others. The trend also decreases in transition flow. The heat transfer coefficient even gets worse with increase in nanoparticle concentration in transition flow. The trend is more gentle in turbulent flow but less affected by increase in concentration.
Sundar et al. [32]	Horizontal tube under heat flux condition	magnetic Ni in distilled water	The improvement in Nusselt number is much higher than negative effects on friction factor. The previous correlations in a single-phase pipe flow fail to properly predict Nusselt number. Ni-water nanofluid is introduced as the best in terms of thermal performance. Correlations are proposed for Nusselt number and friction factor as a function of Reynolds and Prandtl numbers and concentration.

It is concluded that the presence of nanoparticles has fewer effects on main flow in turbulent regime comparing to the previous section in laminar one. Although, the enhancement is still observable and needs to be discussed in modelling.

2.1.3   Nanofluid natural convective flow

Due to complexities and difficulties, and also the probability of sedimentation, the number of experimental studies in natural convection with the presence of nanoparticles is limited [33-46]. Buoyancy is the driving force in natural convection and it is induced in the continuous phase. Putra et al. [33] investigated the heat transfer characteristics of Al_2O_3-water and CuO-water nanofluid in a horizontal cylinder, heated and cooled down from both ends. The fluid was found highly homogeneous with no instability in the flow. The slip mechanism between particles and fluid and sedimentation played an important

role. Deterioration in heat transfer was observed in all the cases, depending on the density, concentration and aspect ratio of the cylinder.

Nanofluid natural convective flow between two circular disks was experimentally studied by Wen and Ding [34]. Titanium dioxide nanoparticles with the nominal size of 34 nm were mixed with water. After providing the nanofluid at a given concentration and size measurement, the average size was observed to be 170 nm, which was much higher than the nominal size. To stabilise the nanoparticles inside the liquid, the pH was set around 3 with zeta potential from 25 to 50 mV. The negative impacts of nanoparticles on heat transfer were seen in any concentration compared with those for pure water. Also, the Nusselt number dropped with an increase in concentration, even as small as 0.19% vol.

Nnanna [35] conducted an experimental study in a vertically heated cavity with isothermal walls and alumina nanofluid up to 8% vol. in the laminar regime. The enhancement of the Nusselt number was reported for volume fraction up to 2%, and then it decreased. The trend for the Nusselt number indicated that it highly depended on volume fraction, even at small changes of concentration. A correlation for the Nusselt number was proposed in terms of Rayleigh number and volume fraction.

Alumina nanofluid with 250 nm in size was used in two cavities with an aspect ratio of 10.9 and 50.7 under the laminar regime at different inclination angles by Chang et al. [36]. In a vertical situation, no dependency on nanoparticle concentration was observed by the Nusselt and Rayleigh numbers, while the Nusselt number decreased with changes in inclination angle and increase in particle concentration compared with the conditions for pure water. The abnormal behaviour of heat transfer in the cavity was due to the size of the nanoparticles and the possibility of sedimentation at higher volume fraction. Thermophoresis was also mentioned as being important only for particle size less than 100 nm.

Li and Peterson [37] explained some of the main phenomena causing deterioration in heat transfer in the natural convective regime. They used alumina nanofluid up to 6% vol. in a rectangular enclosure. On the other hand, the visualisation of the flow and thermal patterns was conducted by polystyrene-water with 850 nm in size. Some of the reasons

12

mentioned for the deterioration of heat transfer are as follows: the rise in mixture viscosity, stirring and mixing effects of the Brownian motions, the impacts of smoothed gradient temperature, non-uniformity of particle distribution, aggregation in nanoparticles, sedimentation and other interactions between nanoparticles. Table 2-2 provides some other experimental studies of nanofluid in natural convection.

Table 2-2 Summary of some experimental studies of natural convective nanofluid flow

Authors	Geometry	Nanoparticles	Remarks
Ho et al. [38]	Three different rectangular cavities with two-dimensional behaviour	Al_2O_3-water, from 0.1% to 4% vol.	Increase in heat transfer coefficient is only observed for volume fraction less than 0.1%. It is stated that this enhancement cannot be explained by changes in the thermophysical properties of nanofluid. Other phenomena involved in particle migration might be important.
Ni et al. [39]	Cavity with isothermal condition at the top and heat flux at the bottom	Al_2O_3-water under turbulent and somehow transition flow	The transition occurs at critical Rayleigh number $Ra=2.5\times10^9$. Nu is almost the same for both pure water and nanofluid for Ra less than critical value. For higher, Nu decreases. Mass diffusion of nanoparticles is mentioned as the reason. Velocity is not affected by the presence of nanoparticles.
Mahrood et al. [40]	Vertical cylinder, heated from the bottom and cooled down from the top	Al_2O_3 and TiO_2 nanoparticles mixed with solution of carboxymethyl cellulose and distilled water. The mixture is non-Newtonian nanofluids	Enhancement in heat transfer was observed in low concentration. Heat transfer coefficient of nanofluid is less than pure water for volume fraction above 1%. An optimum concentration is found for both nanofluids corresponding to maximum heat transfer. The effect of the enclosure aspect ratio cannot be ignored.

13

Hu et al. [41]	Vertically heated walls of a cavity, heated by silicone gel heater on one side and cooled down by circulating water on other side	TiO_2-water	The deterioration of heat transfer is seen in nanofluid compared with water. Viscosity is the key parameter more important than thermal conductivity in natural convection in laminar regime.
Rao and Srivastava [42]	Vertically heated flat plate in nanofluid medium	Al_2O_3-water at very small concentration, only up to 0.02% vol.	The transient changes in thermal boundary layer are visualised by laser interferometry method. Therefore, two-dimensional temperature profiles are recorded. Interestingly, the enhancement of heat transfer reaches up to 21% at this tiny concentration. The images show that the presence of nanoparticle clearly influences the thermal boundary layer.
Ho et al. [43]	Rectangular cavity heated from the top and cooled down from the bottom	Al_2O_3-water up to 4% vol.	The experiments are employed to validate the numerical methods and investigate the effects of thermophoresis and Brownian movements of the nanoparticles. It is claimed that sedimentation plays an important role in natural convection. Adding nanoparticles to the base fluid enhances the heat transfer in all the cases in laminar regime.
Li et al. [44]	Square cavity with vertically heated walls	ZnO nanoparticles in the mixture of ethylene glycol and deionised water	The deterioration of heat transfer in nanofluid is reported for all the cases compared with base fluid. The critical value for Rayleigh number is mentioned as 7.4×10^7. There is a slight change in Nu trend in terms of Ra when

14

			it is below or above critical value.
Moradi et al. [45]	Vertical cylindrical enclosure heated from the bottom and cooled down from the top	Al_2O_3 and TiO_2 nanopartilces in water	The effects of nanoparticles in water on heat transfer are small or deteriorated. The enhancement may only be seen in low Ra. The impacts of changes in inclination angle are noticeable.
Rao and Srivastava [46]	Vertically heated wall cavity, hot and cold walls at the bottom and top respectively.	Al_2O_3-water up to 0.04% vol.	The presence of nanoparticles has considerable positive effects on heat transfer. Nanoparticles clearly change thermal field of the fluid. Roll-like structures appear or break into smaller structures with changes in concentration. This eventually enhances the heat transfer.

In conclusion, even though the negative impacts of nanoparticles in base fluid was observed in some experiments, it is worthwhile to make an attempt to find the areas that enhancement can be achieved regarding to particles type and size. Theoretical modelling can be recommended in this matter.

THEORETICAL STUDIES OF NANOFLUID

A large part of the theoretical analysis of nanofluid is associated with numerical simulations. Other theoretical works are concerned with the modelling of transport properties of nanofluid to be employed for numerical purposes. Therefore, two main approaches should be studied. First, both nanoparticles and base fluid are assumed continuous phase and the conventional Navier-Stokes is valid for both of them. The only interaction between them is the slip mechanism. This approach is the most common numerical approach in terms of numerical simulations of nanofluid. Second, the base fluid is considered the only continuous phase and nanoparticle is assumed to be a discrete phase. The second approach is still undeveloped and needs many phenomena involved. Hence, only a few studies are available and more are definitely needed.

15

One of the most applicable models based on the first approach mentioned above is the mixture model from multiphase models. This model will be extensively explained in the next chapter. Also, some reports are available which consider only the single-phase equations with nanofluid mixture properties. Many researchers have used the mixture and single phase models to simulate nanofluid in different flow regimes [47-61].

Xuan and Roetzel [47] explain that many phenomena are involved in particle-fluid interactions such as gravity, friction force between the fluid and solid particles, Brownian force and Brownian diffusion, sedimentation, aggregation, collision, clustering and dispersion. They used single-phase equations in their model, considering nanofluid mixture properties from some previous analytical models. They introduced a new parameter in energy equation as the total thermal dispersion coefficient. It included both effects of thermal diffusivity of the flow or conduction and thermal dispersion or diffusion of the nanoparticles in both laminar and turbulent flow. They stated that their proposed approach was not complete and further development was needed in the special case of ultrafine particles.

Maiga et al. [48] considered nanofluid as a highly homogeneous single-phase fluid in a laminar pipe flow and only used mixture thermophysical properties from previous classical correlations in their equations. Alumina nanofluid was mixed in two different base fluids, water and ethylene glycol. They assumed that there was no concentration gradient in the nanofluid and that nanoparticles were uniformly distributed. This assumption is, however, contrary to some experimental observations and theoretical analyses [42, 46, 47].

Buongiorno [49] used scale analysis to show that the slip velocity between nanoparticle and fluid was negligible and only the mass diffusion of the particles was important in thermal transport. He states that, firstly, the nanoparticles can be treated as continuum because of the small Knudsen number. Secondly, the slip mechanisms due to the inertia of the nanoparticles, diffusiophoresis, Magnus effect, wall lubrication and gravity can be neglected. Only diffusion due to thermophoresis and Brownian was mentioned scalable in nanofluid. Therefore, the momentum equation was written similar to the single-phase

flow and the energy equation contained the effects of the particle thermal diffusion into the base fluid. Also, the mass equation for the nanofluid was solved similar to the continuty for the fluid considering the influences of the diffusion terms. Buongiorno [49] shows that the turbulent diffusivity is stronger than Brownian concentration diffusion in turbulent flow and should be considered in equations. Some other theoretical and numerical analyses of nanofluid are explained in Table 2-3.

Table 2-3 Summary of some theoretical studies of nanofluid flows

Authors	Geometry and model	Nanoparticles	Remarks
Akbarinia and Laur [50]	A circular curved tube with laminar regime. The default mixture model in ANSYS-Fluent was employed. The slip velocity was the default function, only considering the effects of gravity and centrifugal force.	Alumina nanofluid up to 1% vol.	The impact of nanoparticle diameter was investigated, from 10 nm to 30 μm. Nanoparticle distribution was reported uniform at small diameter, while it was non-uniform at higher size and concentrated to the outer bend of the tube. They concluded that nanofluid was completely homogeneous.
Bianco et al. [51]	Turbulent flow in a tube with constant heat flux. Both single- and mixture phase models were used. The mixture model was the default from ANSYS-Fluent and no contribution to the model. The thermophysical properties were borrowed from literature.	Alumina nanofluid	The numerical simulation was validated by the previous studies of heat transfer in a pipe flow without particles. The concentration distribution was observed close to the wall.
Moghari et al. [52]	Laminar conjugate convective flow in an annulus. The default mixture model from ANSYS-Fluent was employed. More complicated nanofluid properties from literature were used. No contribution to the model.	Alumina nanofluid	Heat transfer enhancement was observed with increase in concentration and not much negative effects on pressure loss.

17

Haddad et al. [53]	A cavity with heated and cooled walls at the bottom and top respectively. Concentration and thermophoretic diffusion terms were implemented in energy and mass equations. No-slip velocity was considered in momentum equation. The validation was done by comparing with other numerical studies of nanofluid.	Alumina nanofluid	The effects of nanoparticle concentration and temperature gradients on simulation results of heat transfer were found surprisingly noticeable.
Pakravan and Yaghoubi [54]	Laminar cavity flow. Mixture model was used considering the concentration and thermophoretic diffusion terms as slip mechanisms. High resolution in grid generation was necessary.	Alumina nanofluid	Distribution of nanoparticles in the cavity was observed. The drops in Nusselt number due to increase in volume fraction were considerable. Thermophoretic coefficient was the key parameter in simulations.
Di Schio et al. [55]	Laminar channel flow. Concentration and thermophoretic diffusion terms were implemented in energy and mass equations. No-slip mechanisms in equations.	Alumina nanofluid	There was a noticeable distribution of nanoparticle concentration. The thermophoresis and the Brownian diffusion were found important terms in simulations of nanofluid.
Shariat et al. [56]	Laminar mixed convection in an elliptic duct. The default mixture model from ANSYS-Fluent was employed. The simulation results were validated by previous studies for duct flow without particles. No contribution to the model.	Alumina nanofluid	Brownian motions were considered through thermal conductivity of the nanofluid. A weak concentration gradient was seen in the duct cross-sections. The effect of particle size was studied.
Goodarzi et al. [57]	A cavity with heated and cooled walls at the bottom and top respectively. The default mixture model from ANSYS-	Cu-water nanofluid	Validated by previous studies without nanoparticles. Different turbulent models were investigated.

18

	Fluent was employed. No contribution to the model.		
Hejazian et al. [58]	Turbulent mixed convection tube flow. Both Euler and mixture models from multi-phase approach were employed. The default models from ANSYS-Fluent were used. No contribution to the models.	Alumina nanofluid	Not much difference was found between the prediction of both models. Mixture model was recommended for the case of nanofluid simulations.
Abbassi et al. [59]	Vertical annulus with cosine heat flux at inner-tube wall. The default mixture model from ANSYS-Fluent was employed. No contribution to the models.	Alumina nanofluid	Increase in concentration led to increase in heat transfer coefficient and decrease in Nusselt number.
Garoosi et al. [60]	Mixed convection of nanofluids in a square cavity with internal and external heating. The default mixture model from ANSYS-Fluent was employed. No contribution to the models.	Cu- and TiO_2-water nanofluid	It was found that in each case, a volume fraction corresponded to the maximum amount of Nusselt number. The drag and gravity forces can be important in some cases.
Kakaç and Pramuanjaroe-nkij [61]	Single-phase and two-phase models. Review paper.		The most recent review of nanofluid simulations.

Due to many solid-liquid interactions involved in nanofluid medium, there are a few studies of discrete phase model in literature, explained in Table 2-4.

Table 2-4 Summary of theoretical studies of discrete phase modelling of nanofluid flows

Authors	Geometry and model	Particles	Remarks
He et al. [62]	Laminar tube flow. The Lagrangian method was used considering the nanofluid	TiO_2-water nanofluid	Heat transfer coefficient was more affected by thermal conductivity than viscosity.

19

	mixture properties in continuous phase equations. The default interaction forces in ANSYS-Fluent were employed. No particle-particle interaction.		The effects of Brownian force, the lift force and the thermophoretic force were almost negligible.
Bianco et al. [63]	Laminar pipe flow. The default Lagrangian method in ANSYS-Fluent and single-phase model were used. No particle-particle interaction.	Alumina nanofluid	The results of heat transfer can be clearly different considering the temperature-dependent properties. The final findings of both models were found similar.
Jin [64]	Laminar and turbulent pipe flow and two-dimensional. No particle-particle interaction. The default interaction forces in ANSYS-Fluent were employed. Random walk model was used as stochastic tracking method.	Carbon nanoparticles with 500 nm size in water	Nanoparticles were un-uniformly distributed in a cross-section, concentrated between the centre line and wall. The turbulence intensity increased.
Laín and Sommerfeld [65]	Turbulent pipe and channel flow. Both two-way coupling (particle-fluid interaction) and four-way coupling (particle-particle interaction) were used with very small time step, considering the particle-wall collision as well.	Spherical glass beads with a diameter of 130 μm	The results were validated by properly extracted previous experimental data. Particle concentration distribution was graphically explained. Wall roughness influenced the particle concentration area in a cross-section.
Tahir and Mital [66]	Laminar pipe flow. No particle-particle interaction. The default interaction forces in ANSYS-Fluent were employed.	Alumina nanofluid	Reynolds number and particle concentration were presented as the most and least important parameters in increase of heat transfer coefficient. A noticeable change was observed in results by changing particle diameter from 50 nm to 100 nm.

20

Bahremand et al. [67]	Turbulent flow in a helical coiled tube. CFX-Solver was used for simulation with adding a subroutine using FORTRAN to add Brownian motion.	Water-silver nanofluid	It was found that the single-phase approach underestimated the heat transfer results compared with the experiments, while the results of discrete phase model were almost accurate. The impacts of nanoparticle migration on flow velocity and kinetic energy were small.

In conclusion, literature review in this section shows that there are many other phenomena involved in nanoparticles interactions and theoretical studies are still in developing parts. Thus, further investigations are essentially needed concerning to solid-liquid interactions in nanoscale.

CONCLUSION

An extensive review of nanofluid flow in literature was presented in this section. Broad ranges of experimental studies on various geometries with different nanoparticles were explained. Most of the works in forced convection reported enhancement in heat transfer, while both enhancement and deterioration in heat transfer were observed in natural convection.

The literature showed that most studies used the multiphase approach and the mixture model. The available mixture model properly works for liquid-liquid or liquid-gas flows with high connectivity at the interface. But it seems that due to many phenomena involved in nanoscale between particles and fluid, it is essential to consider other aspects of this field. Some examples of these aspects are diffusion due to concentration and gradient of temperature or slip mechanisms caused by some forces. However, the role of other forces such as attractive Van der Waals and repulsive electrostatic double-layer forces and also the substitution of these in mixture equations should be investigated.

Discrete phase modelling or DPM can be the other appropriate approach for nanofluid simulations. This model was developed for particles in sizes larger than nanoscale. Hence

21

many of the interactions involved in micro-sizes might be negligible in nano-sizes and other phenomena should be implemented. It was shown that only a few studies were conducted for nanofluid using this model and not much manipulation of the model in CFD software. Clustering and sedimentation must also be present in CFD code.

From an experimental aspect, only a few exact measurements of nanofluids are available in the literature of experimental works showing the precise amount of heat transfer and hydrodynamic feature enhancement. No studies providing the concentration distribution during convective heat transfer have been found. Also, the experimental study borrowed from literature was carefully chosen to cover at least both heat transfer and hydrodynamic features of the flow with high accuracy. Further experimental studies are recommended.

3

CHAPTER 3:   METHODOLOGY

INTRODUCTION

The extensive details of the mixture model and discrete phase modelling are explained in this chapter. As a first step, the governing equations for the multiphase mixture model are expressed in proper forms. Then, the proposed modifications in the model are added to the equations. The discrete phase model is subsequently presented considering the interactions between the particles and liquid.

MULTIPHASE MIXTURE MODEL

3.1.1   Two-phase model equations

This model is also a part of the Eulerian-Eulerian approach of two-phase flow modelling. In single-phase simulations of nanofluid, the conventional Navier-Stokes equations are solved numerically considering the mixture properties. Therefore, the nanofluid is assumed completely homogeneous and consequently, no concentration distribution is explained. The Eulerian-Eulerian approach in multiphase flows is based on the assumption that each phase in the domain can be treated as a continuum. Therefore, the equations of continuity, momentum and energy are written for each phase separately. It is important to ensure that nanoparticle flow in a liquid can be treated as a continuum. The criterion is the Knudsen number defined as the mean free path to a length scale:

$$Kn = \frac{\lambda}{d_p}$$

(3.1)

Buongiorno [49] states that the length scale should be the particle diameter. Considering the mean free path of water 0.3 nm and particle size of 100 nm, the Knudsen number will be much less than 0.1. It means the medium of nanoparticles phase can be assumed continuum. Therefore, the Eulerian-Eulerian multiphase approach can be a valid method for simulation purposes. In terms of this approach, the governing equations are expressed

23

for each phase separately and only some source terms and interactions are present in the equation.

Mass equation for each phase:

$$\frac{\partial(\alpha_k \rho_k)}{\partial t} + \nabla \cdot (\alpha_k \rho_k \mathbf{v}_k) = \Gamma_k \qquad (3.2)$$

Because no mass transfer occurs between nanoparticles and fluid (neither produced nor destroyed), Γ_k is zero.

Momentum equation for each phase:

$$\frac{\partial}{\partial t}(\alpha_k \rho_k \mathbf{v}_k) + \nabla \cdot (\alpha_k \rho_k \mathbf{v}_k \mathbf{v}_k) = -\nabla(\alpha_k p_k) + \nabla \cdot (\alpha_k \boldsymbol{\tau}_k) + \alpha_k \rho_k \mathbf{g} + \mathbf{M_k} \qquad (3.3)$$

Energy equation:

$$\frac{\partial}{\partial t}\left(\alpha_k \rho_k h_k\right) + \nabla \cdot \left(\alpha_k \rho_k \mathbf{v}_k h_k\right) = -\nabla \cdot \left(\alpha_k \mathbf{q}_k''\right) + \frac{D_k}{Dt}(\alpha_k p_k) + \alpha_k \boldsymbol{\tau}_k : \nabla \mathbf{v}_k + E_k \qquad (3.4)$$

As can be seen, $\mathbf{M_k}$ and E_k are the source terms due to interactions between the two phases. The details of the derivation of the mentioned equations can be found in a book by Ishii and Hibiki [68].

3.1.2 Mixture model governing equations

The mixture model is a part of the two-phase model approach in multiphase flows. Strong coupling between two phases is assumed in this model, which can be the case in nanofluid flows. It was shown in the previous chapter that most of the studies in nanofluids were concerned with the mixture model, even though not many developments have been presented in the model in recent years. Therefore, some ideas and methods are developed into this model in this research.

The governing equations for each phase are combined with others and new sets of equations are defined based on mixture variables and properties. The strong coupling can

24

be presented through slip or drift velocity. The mixture model is properly presented as follows:

Mixture variables and properties definition:

Mixture velocity:

$$\mathbf{v}_m = \frac{\sum_{k=1}^{2} \alpha_k \rho_k \mathbf{v}_k}{\rho_m} \tag{3.5}$$

Mixture pressure:

$$p_m = \sum_{k=1}^{2} \alpha_k p_k \tag{3.6}$$

Mixture enthalpy:

$$h_m = \frac{\sum_{k=1}^{2} \alpha_k \rho_k h_k}{\rho_m} \tag{3.7}$$

Mixture stress tensor:

$$\sum_{k=1}^{2} \alpha_k \boldsymbol{\tau}_k = \boldsymbol{\tau}_m \tag{3.8}$$

$$\boldsymbol{\tau}_m = \mu_m \left[\left(\nabla \mathbf{v}_m \right) + \left(\nabla \mathbf{v}_m \right)^T \right] \tag{3.9}$$

Mixture other terms:

$$\sum_{k=1}^{2} \alpha_k \rho_k \mathbf{g} = \mathbf{g} \sum_{k=1}^{2} \alpha_k \rho_k = \rho_m \mathbf{g} \tag{3.10}$$

$$\sum_{k=1}^{2} \mathbf{M_k} \equiv \mathbf{M}_m \tag{3.11}$$

Mixture continuity equation:

$$\sum_{k=1}^{2} \frac{\partial(\alpha_k \rho_k)}{\partial t} + \sum_{k=1}^{2} \nabla \cdot (\alpha_k \rho_k \mathbf{v}_k) = 0 \tag{3.12}$$

$$\frac{\partial \rho_m}{\partial t} + \nabla \cdot (\rho_m \mathbf{v}_m) = 0 \tag{3.13}$$

The drift and slip velocity are defined as the relative velocity between one phase to the mixture and two phases respectively:

$$\mathbf{V}_{km} = \mathbf{v}_k - \mathbf{v}_m \tag{3.14}$$

$$\mathbf{v}_{slip} = \mathbf{v}_p - \mathbf{v}_c \tag{3.15}$$

Momentum equation of the mixture:

$$\frac{\partial}{\partial t} \sum_{k=1}^{2} (\alpha_k \rho_k \mathbf{v}_k) + \nabla \cdot \sum_{k=1}^{2} (\alpha_k \rho_k \mathbf{v}_k \mathbf{v}_k) = -\nabla \sum_{k=1}^{2} (\alpha_k p_k)$$
$$+ \nabla \cdot \sum_{k=1}^{2} (\alpha_k \boldsymbol{\tau}_k) + \sum_{k=1}^{2} \alpha_k \rho_k \mathbf{g} + \sum_{k=1}^{2} \mathbf{M_k} \tag{3.16}$$

With manipulation of the terms, the equation should be rearranged based on mixture variables and properties:

26

$$\sum_{k=1}^{2} \alpha_k \rho_k \mathbf{v}_k \mathbf{v}_k = \sum_{k=1}^{2} \alpha_k \rho_k \mathbf{v}_k (\mathbf{v}_m + \mathbf{V}_{km})$$

$$= \sum_{k=1}^{2} \alpha_k \rho_k \mathbf{v}_k \mathbf{v}_m + \sum_{k=1}^{2} \alpha_k \rho_k \mathbf{v}_k \mathbf{V}_{km}$$

$$= \rho_m \mathbf{v}_m \mathbf{v}_m + \mathbf{v}_m \sum_{k=1}^{2} \alpha_k \rho_k (\mathbf{v}_k - \mathbf{v}_m) + \sum_{k=1}^{2} \alpha_k \rho_k \mathbf{V}_{km} \mathbf{V}_{km} \qquad (3.17)$$

$$= \rho_m \mathbf{v}_m \mathbf{v}_m + \mathbf{v}_m \sum_{k=1}^{2} \alpha_k \rho_k \mathbf{v}_k - \mathbf{v}_m \sum_{k=1}^{2} \alpha_k \rho_k \mathbf{v}_m + \sum_{k=1}^{2} \alpha_k \rho_k \mathbf{V}_{km} \mathbf{V}_{km}$$

$$\sum_{k=1}^{2} \alpha_k \rho_k \mathbf{v}_k \mathbf{v}_k = \rho_m \mathbf{v}_m \mathbf{v}_m + \sum_{k=1}^{2} \alpha_k \rho_k \mathbf{V}_{km} \mathbf{V}_{km} \qquad (3.18)$$

Hence a form of the mixture momentum equation is:

$$\frac{\partial (\rho_m \mathbf{v}_m)}{\partial t} + \nabla \cdot (\rho_m \mathbf{v}_m \mathbf{v}_m) = -\nabla p_m + \nabla \cdot \boldsymbol{\tau}_m + \rho_m \mathbf{g} + \mathbf{M}_m - \nabla \cdot \sum_{k=1}^{2} \alpha_k \rho_k \mathbf{V}_{km} \mathbf{V}_{km} \qquad (3.19)$$

A similar way of derivation was also presented by Ishii and Hibiki [68] and Manninen et al. [69]. There is only one difference between this version of momentum equation and the one presented in the ANSYS-Fluent 17.0 Theory guide. The sign of the drift flux on the right-hand side is positive in the ANSYS-Fluent 17.0 Theory guide (the reason is unknown to the author). The same problem was found in previous versions and also 16.0 and 17.0, recently released. It was reported to the company anyway.

Because only mixture variables and properties along with the special form of slip velocity should be present in the momentum equation, further manipulation is needed to replace the drift flux term.

Relation between two drift velocities:

$$\mathbf{V}_{cm} = -\frac{\alpha_p \rho_p}{\alpha_c \rho_c} \mathbf{V}_{pm} \qquad (3.20)$$

27

The subscripts *p* and *c* represent particle and continuous phase with the definition of drift mass flux for nanoparticles:

$$\mathbf{J}_p = \alpha_p \rho_p \mathbf{V}_{pm} \tag{3.21}$$

Thus:

$$
\begin{aligned}
\sum \alpha_k \rho_k \mathbf{V}_{km} \mathbf{V}_{km} &= \alpha_c \rho_c \mathbf{V}_{cm} \mathbf{V}_{cm} + \alpha_p \rho_p \mathbf{V}_{pm} \mathbf{V}_{pm} \\
&= \alpha_c \rho_c \left(\frac{\alpha_p \rho_p}{\alpha_c \rho_c} \right)^2 \mathbf{V}_{pm} \mathbf{V}_{pm} + \alpha_p \rho_p \mathbf{V}_{pm} \mathbf{V}_{pm} \\
&= \mathbf{J}_p \mathbf{J}_p \frac{\rho_m}{(1-\alpha_p)\alpha_p \rho_c \rho_p}
\end{aligned}
\tag{3.22}
$$

The final form of the momentum equation reaches to:

$$
\begin{aligned}
\frac{\partial(\rho_m \mathbf{v}_m)}{\partial t} + \nabla \cdot (\rho_m \mathbf{v}_m \mathbf{v}_m) &= -\nabla p_m + \nabla \cdot \boldsymbol{\tau}_m + \rho_m \mathbf{g} + \mathbf{M}_m \\
&\quad - \nabla \cdot \left(\mathbf{J}_p \mathbf{J}_p \frac{\rho_m}{(1-\alpha_p)\alpha_p \rho_c \rho_p} \right)
\end{aligned}
\tag{3.23}
$$

The drift flux can be rewritten in terms of slip velocity as:

$$\mathbf{V}_{pm} = \frac{\alpha_c \rho_c}{\rho_m} \mathbf{v}_{slip} \tag{3.24}$$

The energy equation of the mixture obtains from the combination of the energy equation for each phase:

$$
\begin{aligned}
\sum_{k=1}^{2} \frac{\partial}{\partial t}(\alpha_k \rho_k h_k) + \sum_{k=1}^{2} \nabla \cdot (\alpha_k \rho_k \mathbf{v}_k h_k) &= -\sum_{k=1}^{2} \nabla \cdot (\alpha_k \mathbf{q}_k'') + \sum_{k=1}^{2} \frac{D_k}{Dt}(\alpha_k p_k) \\
&\quad + \sum_{k=1}^{2} \alpha_k \boldsymbol{\tau}_k : \nabla \mathbf{v}_k + \sum_{k=1}^{2} E_k
\end{aligned}
\tag{3.25}
$$

28

The second and third terms on the right-hand side are the net mechanical works and the fourth term is the net energy transfer between two phases.

The mixture variables are:

$$\sum_{k=1}^{2} \left(\alpha_k \rho_k h_k \right) = \rho_m h_m \tag{3.26}$$

$$\sum_{k=1}^{2} \left(\alpha_k \mathbf{q}_k'' \right) = \mathbf{q}_m'' \tag{3.27}$$

$$\sum_{k=1}^{2} E_k = E_m \tag{3.28}$$

Then, based on drift flux model:

$$\begin{aligned}
\sum_{k=1}^{2} \alpha_k \rho_k \mathbf{v}_k h_k &= \sum_{k=1}^{2} \alpha_k \rho_k (\mathbf{v}_m + \mathbf{V}_{km}) h_k \\
&= \rho_m \mathbf{v}_m h_m + \sum_{k=1}^{2} \alpha_k \rho_k \mathbf{V}_{km} h_k
\end{aligned} \tag{3.29}$$

$$\begin{aligned}
\sum \alpha_k \rho_k \mathbf{V}_{km} h_k &= \alpha_c \rho_c \mathbf{V}_{cm} h_c + \alpha_p \rho_p \mathbf{V}_{pm} h_p \\
&= -\alpha_c \rho_c \frac{\alpha_p \rho_p}{\alpha_c \rho_c} \mathbf{V}_{pm} h_c + \alpha_p \rho_p \mathbf{V}_{pm} h_p \\
&= \mathbf{J}_p \left(h_p - h_c \right)
\end{aligned} \tag{3.30}$$

The general form reaches to:

$$\begin{aligned}
\frac{\partial}{\partial t} \left(\rho_m h_m \right) + \nabla \cdot \left(\rho_m \mathbf{v}_m h_m \right) &= -\nabla \cdot \mathbf{q}_m + \sum_{k=1}^{2} \frac{D_k}{Dt} (\alpha_k p_k) \\
&\quad + \sum_{k=1}^{2} \alpha_k \boldsymbol{\tau}_k : \nabla \mathbf{v}_k + E_m - \mathbf{J}_p \left(h_p - h_c \right)
\end{aligned} \tag{3.31}$$

29

Some simplification can be mentioned here: due to the ranges of velocity and shear stresses, the mechanical works can be ignored; the net heat transfer between nanoparticles and fluid can be zero; the thermodynamic equilibrium can be applied, i.e. $h = C_p T$ and $T_p = T_c = T_m$ [69].

3.1.3 Constitutive equations of mixture

Due to newly defined variables in mixture equations, some closure relations are needed to reach the adequate number of equations.

Equation of volume fraction:

$$\sum_{k=1}^{2} \alpha_k = \alpha_p + \alpha_c = 1 \tag{3.32}$$

Mass balance for nanoparticles with constant density:

$$\frac{\partial \alpha_p}{\partial t} + \nabla \cdot (\alpha_p \mathbf{v}_p) = 0 \tag{3.33}$$

$$\frac{\partial \alpha_p}{\partial t} + \nabla \cdot (\alpha_p \mathbf{v}_m) = -\nabla \cdot (\alpha_p \mathbf{V}_{pm})$$
$$= -\frac{1}{\rho_p} \nabla \cdot \mathbf{J}_p \tag{3.34}$$

The other forms of this equation can be found in [69]. The key parameter in the mixture model is slip velocity, which is explained in the following section.

3.1.4 Slip mechanisms in the mixture model

Slip velocity is the relative velocity between the nanoparticles and the fluid in which they are immersed. Typically, the slip velocity should include all the slip mechanisms involved in the phase interface. The algebraic form of the slip velocity used in ANSYS-Fluent only covers gravitational and centrifugal effects. Therefore, other phenomena in nanoscale ranges should be implemented. The slip velocity used in ANSYS-Fluent:

$$\mathbf{v}_{slip} = \frac{\rho_p d_p^2}{18 \mu_c f_d} \frac{(\rho_p - \rho_m)}{\rho_p} \left[\mathbf{g} - (\mathbf{v}_m . \nabla) \mathbf{v}_m - \frac{\partial \mathbf{v}_m}{\partial t} \right] \tag{3.35}$$

The terms in the bracket are acceleration. The drag function, f_d, is defined as:

$$f_d = \begin{cases} 1 + 0.15 Re_p^{0.687} & Re_p \leq 1000 \\ 0.0183 Re_p & Re_p > 1000 \end{cases} \tag{3.36}$$

Particle Reynolds number:

$$Re_p = \frac{d_p \rho_c |\mathbf{v}_{slip}|}{\mu_c} \tag{3.37}$$

This slip velocity may be adequate in micro-size particle flows, but further development is definitely needed in nanoscale. Therefore, a new slip velocity based on other interaction forces is developed in this study. A scale analysis will reveal the importance of each phenomenon.

3.1.5 Development of a modified slip velocity: slip velocity approach

Because each force involved in the interaction between the nanoparticles and fluid is responsible for producing a small amount of drag force, the equivalent slip velocity can easily be obtained. It consists of buoyancy, centrifugal effect, virtual mass, pressure gradient, diffusion due to Brownian and thermophoresis, lift, attractive Van der Waals and repulsive electric double layer.

Virtual mass and pressure gradient per mass of particle [69]:

$$\mathbf{f}_{Virtual-mass} = 0.5 \frac{\rho_c}{\rho_p} \left(\mathbf{v}_p \nabla \mathbf{v}_c - \frac{d\mathbf{v}_p}{dt} \right) \tag{3.38}$$

31

$$\mathbf{f}_{\text{Pr}essure} = \frac{\rho_c}{\rho_p} \mathbf{v}_p \nabla \mathbf{v}_c \qquad (3.39)$$

Drag force per mass of particle:

$$\mathbf{f}_{drag} = \frac{f_d}{\tau} \mathbf{v}_{slip} \qquad (3.40)$$

$$\tau = \frac{\rho_p d_p^2}{18 \mu_c} \qquad (3.41)$$

Particle relaxation time, τ, is the time it takes for a particle to reach 63% of the fluid velocity.

Diffusion due to Brownian and thermophoresis [1, 49]:

$$\mathbf{J}_p = -\frac{\rho_p K_B T}{3 \pi \mu_c d_p} \nabla \alpha_p - S_T \alpha_p \frac{\rho_p}{\rho_c} \frac{\mu_c}{T} \nabla T \qquad (3.42)$$

$$S_T = 0.26 \frac{k_c}{k_p + 2k_c} \qquad (3.43)$$

The slip velocity due to diffusion is calculated through the relation between drift flux, drift velocity and slip velocity.

Lift force per mass of the particle [70]:

$$\mathbf{f}_{lift} = C_L \frac{\rho_c}{\rho_p} \alpha_p \left(\mathbf{v}_p - \mathbf{v}_c \right) \times \left(\nabla \times \mathbf{v}_c \right) \qquad (3.44)$$

$$C_L = 6.46 \frac{3}{2 \pi \sqrt{Re_\omega}} \qquad (3.45)$$

$$Re_\omega = \frac{\rho_c \left| \nabla \times \mathbf{v}_c \right| d_p^2}{\mu_c} \tag{3.46}$$

Attractive Van der Waals force [71]:

$$\left| \mathbf{f} \right|_{VDW} = \frac{6}{\pi \rho_p d_p^3} \frac{A}{6 d_p} \frac{1}{x^2 (x+1)^3 (x+2)^2} \tag{3.47}$$

$$x = \frac{\delta}{d_p} \tag{3.48}$$

where A and δ are Hamaker constant and surface-to-surface distance of two approaching particles. The amount of Hamaker constant is available for some common solid liquid mixtures [71, 72], shown in Table 3-1 for some materials, for instance, 4.44×10^{-20} J in the case of alumina nanofluid.

Table 3-1 Hamaker constant for some particles in different media [71, 72]

Materials	$A/10^{-20}$ J	
	Vacuum	Water
Polystyrene	7.9	1.3
Gold	40	30
Silver	50	40
Al_2O_3	30	4.44
Copper	40	30
Water	4.0	
Pentane	3.8	0.34
Decane	4.8	0.46
Hexadecane	5.2	0.54
Quartz (fused)	6.5	0.83
Quartz (crystalline)	8.8	1.70
Fused Silica	6.6	0.85
Calcite	10.1	2.23
Calcium fluoride	7.2	1.04
Sapphire	15.6	5.32

33

Poly (methyl methacrylate)	7.1	1.05
Poly (vinyl chloride)	7.8	1.30
Polyisoprene	6.0	0.74
Poly (tetrafluoroethylene)	3.8	0.33

Electrical double-layer repulsion force:

$$V_R = \pi d_p \varepsilon_0 \varepsilon_r \psi^2 \exp(-\kappa\delta) \qquad \kappa d_p < 10 \tag{3.49}$$

$$V_R = \pi d_p \varepsilon_0 \varepsilon_r \psi^2 Ln\left[1 - exp(-\kappa\delta)\right] \quad \kappa d_p > 10 \tag{3.50}$$

$$\left|\mathbf{f}\right|_{EDL} = -\frac{6}{\pi\rho_p d_p^3}\frac{dV_R}{d\delta} \tag{3.51}$$

where V_R is the repulsion energy on the surface of a particle. The amount of vacuum and relative permittivity of the medium is $\varepsilon_0 = 8.854 \times 10^{12} CV^{-1}m^{-1}$ and $\varepsilon_r = 80$ for water respectively. ψ is the potential on the surface of the electrical double layer over charged surface group, which can be approximated by zeta potential on the surface of the diffuse layer. Because the small zeta potential means fewer repulsion barriers and consequently produces stronger agglomeration inside the nanofluid, the approaching potential to zero is avoided in all the simulations. κ is Debye-Huckel parameter and defined as:

$$\kappa = \sqrt{\frac{2000F^2 I_0}{\varepsilon_0 \varepsilon_r RT}} \tag{3.52}$$

$F = 96485 \ Cmol^{-1}, \ R = 8.31 \ Jmol^{-1}K^{-1}$

where F and R are Faraday and gas universal constants. The ionic strength is simply calculated by knowing the concentration (c_i) and the charge (z_i) of the species. With the assumption of the presence of only two ions (H^+ and OH^-) in the mixture, it gives:

$$I_0 = \frac{1}{2}\sum_i c_i z_i = \frac{1}{2}\begin{cases} 10^{-(14-PH)} & PH > 7 \\ 10^{-PH} & PH \leq 7 \end{cases} \tag{3.53}$$

It is noted that the inverse amount of Debye-Huckel parameter can be scaled as Debye length or the thickness of the electrical double layer $L_D = \kappa^{-1}\, m$. This length can be used as a cut-off distance to avoid overlapping of diffuse layer of nanoparticles. It means that the attractive and repulsive electrostatic forces are only active in the program until the surface-to-surface distance of the particles is higher than $2L_D$.

Finally, the drag force is equal to the other forces. This provides the final form of the slip velocity as follows:

$$\begin{aligned} \mathbf{v}_{slip} &= \mathbf{v}_{Brownian} + \mathbf{v}_{Thermophoresis} + \mathbf{v}_{Virtual-mass} + \mathbf{v}_{Pressure} \\ &\quad + \mathbf{v}_{lift} + \mathbf{v}_{Buoyancy-centrifugal} + \mathbf{v}_{VDW} + \mathbf{v}_{EDL} \end{aligned} \tag{3.54}$$

Each term on the right-hand side is the slip velocity associated with the force.

3.1.6 Development of a modified slip velocity: diffusion approach

This approach is more or less similar to the above-mentioned one. The idea behind the diffusion approach is the possibility of stronger diffusion terms in some nanofluid cases, particularly natural convective flow. The only difference between this approach and the previous one is that thermophoretic and Brownian motion are expressed as diffusion terms in mass, momentum and energy equations. The other slip phenomena remain the same. Therefore, the governing equations are modified as follows:

Mixture continuity:

$$\frac{\partial \rho_m}{\partial t} + \nabla \cdot (\rho_m \mathbf{v}_m) = 0 \tag{3.55}$$

Mass equation for nanoparticles:

35

$$\frac{\partial \alpha_p}{\partial t} + \nabla.(\alpha_p \rho_p \mathbf{v}_m) = -\nabla.(\alpha_p \rho_p \mathbf{V}_{pm}) + \rho_p D_B \nabla^2 \alpha + \rho_p D_T \frac{\nabla^2 T}{T} \tag{3.56}$$

$$D_T = 0.26 \frac{k_c}{k_p + 2k_c} \alpha_p \frac{\mu_c}{\rho_c} \tag{3.57}$$

$$D_B = \frac{K_B T}{3\pi \mu_c d_p} \tag{3.58}$$

Momentum equation of the mixture:

$$\frac{\partial (\rho_m \mathbf{v}_m)}{\partial t} + \nabla.(\rho_m \mathbf{v}_m \mathbf{v}_m) = -\nabla P_m + \nabla.\tau_m + \rho_m g - \nabla.\frac{\alpha_p}{(1-\alpha_p)} \frac{\rho_p \rho_m}{\rho_c} \mathbf{V}_{pm} \mathbf{V}_{pm} \tag{3.59}$$

Energy equation of the mixture:

$$\nabla.(\rho_m C_{p_m} \mathbf{v}_m T_m) = -\nabla.\mathbf{q}''_m - \nabla.\left[\alpha_p \rho_p \mathbf{V}_{pm} T_m (C_{p_p} - C_{p_c}) \right]$$
$$+\rho_p C_{p_p} \left[D_B \nabla \alpha.\nabla T + D_T \frac{\nabla T.\nabla T}{T} \right] \tag{3.60}$$

The source terms in all the equations are implemented through some UDFs in ANSYS-Fluent.

3.1.7 Mixture thermophysical properties

Due to buoyancy effects of the base fluid in natural convection, a high accurate density correlation by curve fitting from Kröger [73] for water was employed in all the equations:

$$\rho_c = 0.0000152322 T^3 - 0.0183891979 T^2 + 6.6564073561 T$$
$$+ 243.4039040229 \tag{3.61}$$

The linear combination of density for nanoparticles and base fluid is the most common and highly valid assumption in the mixture properties.

$$\rho_m = \sum_{k=1}^{2} \alpha_k \rho_k \tag{3.62}$$

$$C_{P_m} = \frac{\sum_{k=1}^{2} \alpha_k \rho_k C_{P_k}}{\rho_m} \tag{3.63}$$

Michaelides [74] shows that the thermal expansion coefficient of the nanofluid mixture must be calculated in the same way as the density. Considering the element changes of temperature and volume under constant pressure leads to:

$$\beta = \frac{1}{V}\left(\frac{\partial V}{\partial T}\right)_P \tag{3.64}$$

$$\delta V_p = \beta_p V \alpha_p \delta T \qquad and \qquad \delta V_c = \beta_c V (1 - \alpha_p)\delta T \tag{3.65}$$

and a linear summation of the element volume:

$$\delta V = \left[\beta_p \alpha_p + \beta_c(1 - \alpha_p)\right]V \delta T \tag{3.66}$$

$$\beta_m = \frac{1}{V}\left(\frac{\partial V}{\partial T}\right)_P = \beta_p \alpha_p + \beta_c(1 - \alpha_p) \tag{3.67}$$

The transport properties of the nanofluid viscosity and thermal conductivity are borrowed from reference [75]:

$$\frac{k_m}{k_c} = 1 + 4.4 Re^{0.4} Pr^{0.66} \left(\frac{T}{T_{fr}}\right)^{10} \left(\frac{k_p}{k_c}\right) \alpha_p^{0.66} \tag{3.68}$$

$$Re_B = \frac{\rho_c u_B d_p}{\mu_c} \tag{3.69}$$

37

$$u_B = \frac{2K_B T}{\pi \mu_c d_p^2} \tag{3.70}$$

$$\frac{\mu_m}{\mu_c} = \frac{1}{1 - 34.87 \left(d_p / d_c \right)^{-0.3} \alpha_p^{1.03}} \tag{3.71}$$

where T_{fr} and d_c are water freezing temperature and molecule diameter as 0.3nm. These correlations were presented to be valid for different types of nanoparticles, such as alumina, copper, TiO2, SiO2, etc. Also, the size can go up to more than 200 nm and volume fraction up to 7% vol.

ANSYS-Fluent is employed to simulate the nanofluid. All the above-mentioned slip mechanisms are implemented as a new slip velocity equation into the mixture model through the user-defined function (UDF). The UDF is divided into three sections: adjust function to define gradient of concentration, slip velocity function and mixture thermophysical properties. The mixture model UDF is presented in Appendix A.

DISCRETE PHASE MODELLING (DPM)

The basic difference between this model and the mixture model is that DPM assumes there is only base fluid as the continuous phase and the nanoparticles are non-continuous suspended in the fluid. In DPM, nanoparticles are tracked as a large number of particles and all the energy or force interactions are introduced as momentum or energy source terms in the governing equations. The rest of the Navier-Stokes equations are treated as usual for the base fluid. A differential form of force balance equation is applied to a particle suspended in the flow to calculate the trajectory of the particle. Here, the focus is only on the interaction forces and particle equation because the flow equations are similar to those of the single-phase model.

The forces on a particle in a fluid can be categorised into three sections: the forces between particles such as electrostatic forces, the interaction forces between nanoparticles and fluid such as drag, the interaction forces between nanoparticles and walls.

38

Due to the small size, it can be expected that the nanoparticles mostly follow the base flow regime and two situations can be presumed for the particles at the vicinity of the walls. They can either stick on or fully rebound from the walls. The sticking situation can happen when clustering occurs in the main flow, otherwise the rebound situation would apply.

There are many interactions between fluid and nanoparticles. All the forces along with particle-particle forces are solved in Newton's equation of the motion for a single particle and the results are extended to the rest of the particles. The possible affecting forces are explained here. Newton's equation of force balance in Lagrangian frame for nanoparticles is written as:

$$m_p \frac{d\mathbf{v}_p}{dt_p} = \mathbf{F}_{drag} + m_p \frac{\vec{g}(\rho_p - \rho_{nf})}{\rho_p} + \mathbf{F}_{lift} + \mathbf{F}_{virtual} + \mathbf{F}_{Magnus}$$
$$+ \mathbf{F}_{thermo} + \mathbf{F}_B + \mathbf{F}_{VDW} + \mathbf{F}_{EDL} \qquad (3.72)$$

t_p is the travelling time of a nanoparticle from the point of injection until it reaches its final fate in the domain (sticking on a wall or leaving the domain).

3.1.8 Forces between particles

The main attraction forces between particles can be divided into a short range due to chemical reactions and a long range by Van der Waals forces. The long range forces are only present for particle-particle distance much more than 1 °A. This force is caused by the fluctuating of negative electrons around a positive nucleus in an atom, which induces constant changing dipole moments and electric fields. Eventually, the interactions between magnetic fields will lead to the Van der Waals attraction forces. The impact distances of Van der Waals force can be much higher than the London and Lifshitz theory of distances, from 1 nm to 100 nm [76]. Three types of Van der Waals forces are found in literature [76]: Keesom-orientation force from interactions of randomly orienting dipole-dipole, Debeye-induction force between dipoles and induced dipoles, London-dispersion force from fluctuating dipole-induced dipole. Among all, the first two are the result of molecules with permanent dipole movements. Because the last force is bigger than the

others, it will be taken into account in simulations. The Van der Waals force can be expressed in terms of Lifshitz Van der Waals constant. This constant is linearly connected to the Hamaker constant, which will be used in this study. The attraction force is similar to equation (3.47) for two-sphere particles. At the limit as the particles approach each other, it can be rewritten as:

$$\left.\mathbf{F}\right|_{VDW} = \frac{A}{24d_p x^2} \tag{3.73}$$

and for a particle approaching a flat wall:

$$\left.\mathbf{F}\right|_{VDW} = \frac{A}{12d_p x^2} \tag{3.74}$$

The other particle-to-particle force is the repulsive electrical double-layer force, as presented in equations (3.49) (3.50) and (3.51).

The combination of the mentioned forces is a part of DLVO theory as explained by [77]. Because one of the forces is attractive and the other one is repulsive, the net of them will be applied.

3.1.9 Forces induced by the presence of fluid

Drag force:

The correlation of drag force should be the same everywhere in the domain because of the small size of the nanoparticles.

$$\mathbf{F}_{drag} = \frac{m_p}{\tau} \frac{C_D Re_p}{24 C_c} \left(\mathbf{v}_c - \mathbf{v}_p \right) \tag{3.75}$$

$$Re_p = \frac{\rho_c d_p \left| \mathbf{v}_c - \mathbf{v}_p \right|}{\mu_c} \tag{3.76}$$

Drag coefficient for a smooth spherical particle is introduced as:

$$C_D = a_1 + \frac{a_2}{Re_p} + \frac{a_3}{Re_p^2} \tag{3.77}$$

The constant values a_i are available for a wide range of Reynolds numbers [78]. Because the nanoparticles are ultrafine, $Re_p<<1$ and $a_1=a_3=0$ and $a_2=24$ give $C_D = \frac{24}{Re_p}$. The Cunningham slip correction factor, C_c, is used when the no-slip boundary condition for a continuum cannot be preserved over a particle or solid wall. Since the Knudsen number in this study is much less than 0.1 and highly continuum, it gives $C_c=1$:

$$C_c = 1 + Kn\left[2.514 + 0.8e^{-0.55/Kn} \right] \tag{3.78}$$

For non-spherical particles with the sphericity, θ, smaller than unity, the following expression is used by Haider and Levenspiel [79]:

$$C_D = \frac{24}{Re_p}(1 + b_1 Re_p^{b_2}) + \frac{b_3 Re_p}{b_4 + Re_p} \tag{3.79}$$

$$\theta = \frac{a}{A} \tag{3.80}$$

$$b_1 = \exp(2.3288 - 6.4581\,\theta + 2.4486\,\theta^2) \tag{3.81}$$

$$b_2 = 0.0964 + 0.5565\,\theta \tag{3.82}$$

$$b_3 = \exp(4.905 - 13.8944\theta + 18.4222\theta^2 - 10.2599\theta^3) \tag{3.83}$$

$$b_4 = \exp(1.4681 + 12.258\theta - 20.7322\theta^2 + 15.8855\theta^3) \tag{3.84}$$

where a and A_p are the surface of a spherical particle with the same volume as the actual particle and surface area of the particle respectively. Basically, the drag force at the vicinity of a wall would be different from the core region of the fluid, but due to

41

nanoscale size, this can be neglected and only sticking on and rebounding from the wall would be the case.

Because the centrifugal force (force due to rotating of a particle on a circle) is mainly caused by the presence of other forces in the flow field, it can be safely ignored in calculations. On the other hand, the lift induced by the rotation of the particle around its axis in uniform flow or Magnus force can also be negligible in terms of the nanosize of the particles. However, it can be important if the flow is highly rotational and the inertia of the particles is noticeable.

Magnus force. Similar to the force balance equation, the particle angular velocity, $\boldsymbol{\omega}_p$, can be obtained from particle conservation of angular momentum equation as follows [80]:

$$I_p \frac{d\boldsymbol{\omega}_p}{dt} = \frac{\rho_c}{2}\left(\frac{d_p}{2}\right)^5 C_\omega \boldsymbol{\Omega} \tag{3.85}$$

As can be seen, similar to Newton's law of motion, the acceleration of the particle torque (left-hand side of equation (3.71)) is damped by the rotational drag coefficient, C_ω, and relative angular velocity of the fluid and particle, $\boldsymbol{\Omega}$:

$$\boldsymbol{\Omega} = \frac{1}{2}\nabla \times \mathbf{v}_c - \boldsymbol{\omega}_p \tag{3.86}$$

The moment of inertia for a spherical particle is expressed as:

$$I_p = \frac{\pi}{60}\rho_p d_p^5 \tag{3.87}$$

The rotational drag coefficient [81]:

$$C_\omega = \frac{6.45}{\sqrt{Re_{\omega_p}}} + \frac{32.1}{Re_{\omega_p}} \tag{3.88}$$

$$Re_{\omega_p} = \frac{\rho_c |\mathbf{\Omega}| d_p^2}{4\mu_c} \qquad (3.89)$$

Therefore, the rotational flow condition is important for the presence of Magnus force in the solution ($Re_{\omega_p} \neq 0$). The general form of Magnus lift force can be written as:

$$\mathbf{F}_{Magnus} = \frac{1}{2} A_p C_{ML} \rho_c \frac{|\mathbf{v}_c - \mathbf{v}_p|}{|\mathbf{\Omega}|} \left[(\mathbf{v}_c - \mathbf{v}_p) \times \mathbf{\Omega} \right] \qquad (3.90)$$

where A_p and C_{ML} are projected particle surface area and rotational lift coefficient respectively. This coefficient is calculated from the following correlation [80]:

$$C_{ML} = 0.45 + \left(\frac{Re_{\omega_p}}{Re_p} - 0.45 \right) exp\left(-0.05684 Re_{\omega_p}^{0.4} Re_p^{0.3}\right) \quad , 10 < Re_p < 140 \qquad (3.91)$$

$$Re_p = \frac{\rho_c d_p |\mathbf{v}_c - \mathbf{v}_p|}{\mu_c} \qquad (3.92)$$

Another correlation for Magnus force is presented by Varaksin et al. [82]:

$$\mathbf{F}_{Magnus} = k_M \rho_c \left(\frac{d_p}{2} \right)^3 \left[(\mathbf{v}_c - \mathbf{v}_p) \times \mathbf{\omega}_p \right] \quad , Re_{\omega_p} = \frac{\rho_c |\mathbf{\omega}| d_p^2}{\mu_c} << 1 \qquad (3.93)$$

For the lower limit of Reynolds numbers, it gives $k_M = \pi$. The other general form of the coefficient:

$$k_M = 0.534 Re_{\omega_p}^{-0.64} Re_p^{0.715} \qquad (3.94)$$

Saffman lift force. Due to induced pressure difference on both sides of a particle in a shear flow, a force known as the Saffman lift force acts on the particle. Because strong shear stress is mainly found close to walls, the lift force will be perpendicular to the walls, presented as [70, 83]:

43

$$\mathbf{F}_{lift} = 20.3\mu_c d_p^2 (\mathbf{v}_c - \mathbf{v}_p)\sqrt{\frac{\dot{\gamma}\rho_c}{\mu_c}}\,\text{sgn}(\dot{\gamma}) \tag{3.95}$$

where $\dot{\gamma}$ is the shear rate mainly important at the vicinity of the walls.

Pressure gradient force. It comes from any static pressure gradient field in the flow on a particle [84]:

$$\mathbf{F}_{pressure} = m_p \left(\frac{\rho_{nf}}{\rho_p}\right)\mathbf{v}_p \nabla \mathbf{v}_c \tag{3.96}$$

Virtual mass force. Changes in the velocity of a mass of the fluid due to acceleration of particle movement will lead to virtual mass force. This force is available only when the interactions between particle and fluid are present [84]:

$$\mathbf{F}_{virtual} = 0.5 m_p \left(\frac{\rho_{nf}}{\rho_p}\right)\frac{d}{dt}(\mathbf{v}_c - \mathbf{v}_p) \tag{3.97}$$

Thermophoretic force. It is caused by higher kinetic energy of a particle with higher temperature. It produces stronger movement in one region and finally, the gradient of temperature will be the driving diffusion force for particles with higher temperature. The following equation can be the thermophoresis force for particles with lower thermal conductivity [85]:

$$\mathbf{F}_{thermo} = -D_T \frac{\nabla T}{T} \tag{3.98}$$

$$D_T = 0.78 \frac{\pi \mu_c^2 d_p}{\rho_c}\frac{k_c}{2k_c + k_p} \tag{3.99}$$

There is no conclusive agreement on the thermophoretic coefficient in literature, especially for nanofluids. This coefficient can depend on base fluid, nanoparticles, thermal conductivity of the particles and temperature. The factor in equation (3.86) was found to be 0.017 for water-based nanofluid by Ahmed and Eslamian [86], rather than

44

0.78. Michaelides [87] proposes a new form of thermophoresis force based on molecular dynamic simulation:

$$\mathbf{F}_{thermo} = 3\pi\mu_c d_p \mathbf{v}_{thermo} = 3\pi\mu_c d_p \left[-C_1 \left(\frac{d_p}{d_0} \right)^{-C_2} \frac{\mu_c}{\rho_c} \frac{\nabla T}{T} \right] \tag{3.100}$$

The C_i constants vary depending on the type of nanofluid.

Brownian motion or diffusion force? It is the random motion of particles suspended in a fluid. It may result in collision among other particles or molecules. Brownian movement is induced by the kinetic energy or temperature of the particles. There are two approaches in the literature for this force: Brownian diffusion force [49] and Brownian random force in the base fluid [88]. The diffusion force approach is expressed as:

$$\mathbf{F}_{Brownian} = 3\pi\mu_c d_p \mathbf{v}_{diffusion} \tag{3.101}$$

$$\mathbf{v}_{diffusion} = \frac{J_p}{\rho_p \alpha_p} = -D_B \frac{\nabla \alpha_p}{\alpha_p} \tag{3.102}$$

where D is particle mass diffusivity or diffusion coefficient:

$$D_B = \frac{K_B T}{3\pi\mu_c d_p} \tag{3.103}$$

The other time-averaged Brownian velocity for nanofluids with no effects of random movement can be written as:

Koo and Kleinstreuer [89]:

$$\left| \overline{\mathbf{v}}_B \right| = \sqrt{\frac{18 K_B T}{\pi \rho_p d_p^3}} \tag{3.104}$$

Patel et al. [90]:

$$\left|\overline{\mathbf{v}}_B\right| = \frac{2K_BT}{\pi\mu_c d_p^2}$$

(3.105)

One possibility of modelling the Brownian force can be adding unit-variance Gaussian random numbers to the Brownian velocity mentioned above.

The other approach to the Brownian force is to consider any motions by a small time step regarding the acting of the force in arbitrary directions. It is presented as:

$$\mathbf{F}_B = \zeta_i\sqrt{\frac{6\pi d_p\mu_c K_BT}{\Delta t_p}}$$

(3.106)

where ζ_i is the unit-variance random number produced by a Gaussian white noise process. Michaelides [74] obtained a new form of random motion force by solving the Langevin equation as follows:

$$\mathbf{F}_B = \frac{1}{6}d_p^3\rho_p\zeta_i\sqrt{\frac{2K_BT}{3\pi d_p\mu_c\Delta t_p^3}}$$

(3.107)

and mean square displacement of the particle:

$$\left\langle \mathbf{x}.\mathbf{x}\right\rangle = \frac{2K_BT}{3\pi d_p\mu_c}t_p$$

(3.108)

3.1.10 Energy equation of the nanoparticles

The basic form of the heat transfer equation for a particle in a flow can easily be referred to as the balance of changes in temperature in the travelling path, known as transient or Lagrangian frame, and convection on the particles:

$$m_pC_{p_p}\frac{dT_p}{dt} = hA_p(T_c - T_p)$$

(3.109)

46

Because radiation heat transfer was not investigated in this research, the associated term was ignored from the equation. This ordinary differential equation can easily be solved to reach final form of temperature in each time step. Then, it gives:

$$T_p^{t+\Delta t} = T_c + \left[T_p^t - T_c \right] e^{-\frac{A_p h}{m_p C_{p_p}} \Delta t} \tag{3.110}$$

The important parameter is heat transfer coefficient for flow over a spherical particle [91]:

$$Nu = \frac{h d_p}{k_c} = 2.0 + 0.6 Re_p^{0.5} Pr^{1/3} \tag{3.111}$$

$$Pr = \frac{C_{p_c} \mu_c}{k_c} \tag{3.112}$$

The other less mentioned form of particle heat transfer equation is proposed by Michaelides and Feng [92]:

$$m_p C_{p_p} \frac{d T_p}{d t} = m_c C_{p_c} \frac{D T_c}{D t} - 2 \pi d_p k_c (T_p - T_c) \tag{3.113}$$

where $m_c = \frac{1}{6} \pi \rho_c d_p^3$ mc is the mass of the fluid occupying the particle place. The first term on the right-hand side (material derivative) is the heat transferred by the fluid being in place of the particle. This term is similar to the virtual mass term in force balance equation of the particles. The second term is obviously due to heat conduction from the surface of the nanoparticle. The significance of this term can mainly be seen in the case of nanosize with small particle Reynolds number and density ratio close to unity. The solution of this ODE will lead to:

$$T_p^{t+\Delta t} = c_3 + \left[T_p^t - c_3 \right] e^{-c_4 \Delta t} \tag{3.114}$$

$$c_3 = \frac{m_c C_{p_c}}{2 \pi d_p k_c} \frac{D T_c}{D t} + T_c \tag{3.115}$$

47

$$c_4 = \frac{m_c C_{p_c}}{2\pi d_p k_c}$$

(3.116)

3.1.11 Coupling between continuous phase and discrete nanoparticles

It is important to consider the impacts of nanoparticles on the base fluid. In the case of ignoring this coupling, the nanoparticles will be tracked under the effects of the mentioned forces during the given time in the domain. Otherwise, the effects of nanoparticle momentum and energy should be seen in fluid equations as some source terms. The exchanges of momentum and energy are:

$$\mathbf{F}_s = \sum \left(\frac{18\mu_c}{\rho_p d_p^2} \frac{C_D Re_p}{24} (\mathbf{v}_p - \mathbf{v}_c) + \mathbf{F}_{other} \right) \dot{m}_p \Delta t$$

(3.117)

$$Q_s = \dot{m}_p c_{p_p} (T_{p_{in-cell}} - T_{p_{out-cell}})$$

(3.118)

These source terms are presented on the right-hand side of fluid momentum and energy equations. Because there is no mass exchange, particle flow rate $\dot{m}_p$ in each cell will be conserved. $T_{p_{in}}$ and $T_{p_{out}}$ are particle temperature at the inlet and outlet of a cell respectively. They are calculated according to the time of tracking of the nanoparticles.

3.1.12 Numerical considerations of discrete phase modelling

Both 2D and 3D models were employed in this study for the cases and the results showed that it was important to use a 3D model in nanofluid flow in some geometries, especially with the presence of gravity in the Lagrangian approach. It could be argued that 2D axisymmetric could only capture radial migration of nanoparticles inside the fluid, while the difference between a 3D model and 2D axisymmetric simulation results proved that nanoparticles migrated from the wall both radially and tangentially. Also, the simulations showed that gravity could not be neglected when DPM was used and the absence of gravity force underestimated pressure drops in, for example, vertical tubes. The CFD software employed in this research to solve the governing equations was Fluent 15.0,

48

using the control volume approach. Because new versions of the CFD software are released every year, the newest version was also used in simulations, ANSYS-Fluent 17.0. The SIMPLE method was employed to couple pressure and velocity in equations, the QUICK scheme for volume fraction and the second-order upwind for interpolating other parameters. In the case of natural convection, it was found that the coupled solver provided the best convergence for simulations. Both the pressure interpolation schemes, i.e. standard and linear, showed the same results for pressure drops in DPM. It is noted that the PRESTO! interpolation scheme is not recommended for pressure discretisation in DPM. Because pressure values are needed on the faces of each control volume to discretise in momentum equation, standard and linear schemes evaluate pressure on the face based on the cell values at neighbourhoods, with the assumption of zero pressure gradient at the wall. The PRESTO! scheme estimates pressure on the face via continuity balance based on staggered control volume with non-zero pressure gradient on the wall [93]. Using the PRESTO! scheme provides unreal pressure distribution results in the case of the tube entrance with DPM. It may come from the solution method of DPM, especially with a high number of particles in each computational cell (order of 10^{10}). Also, nanoparticles are injected into the flow at the entrance uniformly, while a boundary layer starts forming in base flow and produces slip velocity between base flow and nanoparticles at the vicinity of the wall. The number of particles in each computational cell is in the order of 10^{10} and more. It can probably produce a considerable amount of source terms in momentum equation and pressure drops predicted by the PRESTO! scheme, because of the solution method of this scheme at the vicinity of the wall. There is a notable difference between particle and flow velocities at the entrance, because of the undeveloped particle and flow boundary layer. In spite of the standard or linear interpolation schemes, the PRESTO! scheme interpolates pressure at the face centre of a cell (it can be called face pressure instead of cell pressure) where particles are interred in the cell. The large difference between particle and flow velocities at the entrance produces a large body force at the face of a cell (staggered grid), which makes an unreal large amount of pressure interpolated by the PRESTO! scheme. The only way to overcome this problem seems to provide very small time steps. A particle Lagrangian time step depends on the size of the cell that a parcel passes, the smaller the size, the

49

shorter the time step. Simulation showed some improvement with very fine mesh at the entrance with the PRESTO! scheme, but the geometry required grids with the same size as DNS to overcome this issue completely, which was not the main goal of this study.

One of the most important rules of the Lagrangian tracking method is that a particle never skips a computational cell. Hence each computational cell is divided into a number of sub-cells, known as parcels, based on time steps and the number of steps that a particle should pass in each cell. A nanoparticle in each parcel is representative of the entire nanoparticles on that parcel and heat transfer and motion equations are solved only for this nanoparticle and extended to others. Therefore, the distribution effects of these nanoparticles on parcels in the neighbourhood are not usually applied to the equations, which can be called a point-particle approach. For this aim, the node-based averaging method is employed to consider those influences from the Lagrangian frame onto the Eulerian field. The Gaussian distribution function is used to interpolate the neighbouring parcel's impact on the centroid parcel, as the following [94]:

$$\overline{\theta}_{parcel} = \sum N_{particle} G_w \theta_{particle} \tag{3.119}$$

$$G_w = \left(\frac{a}{\pi}\right)^{3/2} \exp\left(-a \frac{\left|x_{parcel} - x_{particle}\right|^2}{\Delta x^2}\right) \tag{3.120}$$

where $\overline{\theta}_{parcel}$, $N_{particle}$, G_w, $\theta_{particle}$, Δx, x_{parcel} and $x_{particle}$ are particle variables affected by nodes in the neighbourhood (which are 26 cells for the structured quad mesh in three-dimensional structure meshes), number of particles in the parcel, Gaussian weight function, particle variable in the node, characteristic length of the cell, parcel location in the neighbourhood and particle location respectively. *a* is a constant which changes the width of Gaussian function. The number of particles in each parcel can be calculated as:

$$N_{particle} = \dot{m}_p \frac{\Delta t}{m_p} \tag{3.121}$$

Particle variables $\theta_{particl}$ are achieved from DPM equations and then the new number of variables $\bar{\theta}_{parcel}$ affected by neighbouring cells will be calculated. This new value is incorporated into the source terms of the base fluid equations. The simulations showed that the results by DPM with node-based averaging were in better agreement with experiments and the residuals indicated improved convergence than without the node-based averaging method. Some researcher believes that the existence of interpolation operators such as Gaussian kernel function can improve and accelerate the numerical solution [94, 95], especially in the case of a dense number of nanoparticles in each computational cell. Moreover, the grid study proves that a structured mesh with higher uniformity can provide more precise results by DPM than other meshes. However, a higher number of cells is needed in modelling nanofluid by DPM compared with other single-phase flows in the same geometry.

CONCLUSION

Two common approaches regarding the simulation of nanofluids were extensively explained in this chapter. In conclusion, there are some advantages and disadvantages of using each of the methods. In the mixture model, the thermophysical properties of the nanofluid play the key role in the accuracy of the final results. In DPM, on the other hand, there is no need for empirical thermophysical properties, while reaching the appropriate heat transfer features cannot be easy. Therefore, the capabilities of both approaches were investigated with some modification presented in this chapter and experimental data were borrowed from literature for further validation.

4

CHAPTER 4:   SIMULATION RESULTS AND DISCUSSION

INTRODUCTION

The presence of nanoparticles in a liquid points to two important aspects of fluid mechanics, namely pressure drops and heat transfer enhancement. A large part of this study focuses on these two features, which are compared with measured values in experiments. Most of the experimental studies in literature are concerned with forced convection, both laminar and turbulence, only a few works deal with mixed and natural convection. The common geometry for nanofluid tests is a circular tube for forced and a cavity for natural convection. A few reports for both of these are explained and compared with the simulation results of the present study for validation purposes. Due to the different nature of the flow in forced and natural convection, the interaction between flow and particles can vary depending on the geometry and intensity of the flow field. In other words, the important interactions in natural convective flow might not be the same as for the forced one. The other significant aspect of nanofluid simulations is to understand and explain the particle distribution inside the domain. All the above-mentioned are presented in this chapter. Firstly, simulations are conducted for forced tube convective flow via both conventional DPM and mixture models. Secondly, natural convective cavity flow is modelled via the developed mixture model proposed in this study. Finally, laminar nanofluid flow is simulated in a circular microchannel using DPM regarding some considerations in the present work.

SIMULATIONS OF NANOFLUID USING MIXTURE AND DPM APPROACHES IN FORCED CONVECTION

To understand some drawbacks of both approaches, a few early simulations are conducted and compared with the experimental results in literature. As explained in Chapter 3, the default version of the mixture model only assumes gravitational and centrifugal forces as the dominant slip mechanisms between particles and fluid. The default forces for the DPM model are drag, Saffman's lift, gravity, virtual mass, pressure

gradient, thermophoretic and Brownian motion. Because the comparison between experiments and simulations are made for a few geometries, the grid study and settings for each case are separately explained. The first case is a vertical pipe with laminar nanofluid conducted by Zhang [11] and Rea et al. [7]. Based on experimental works, two different diameter sizes of vertical tubes are simulated in this study, with the same length of 1 m. Rea et al. [7] used a stainless steel tube with ID 4.5 mm, and Zhang [11] with 5.537 mm. Both the tubes encountered constant heat flux on the outside of the tubes. Three types of nanoparticles as nanofluids were injected into the tubes consisting of Al2O3 and ZrO2 by Rea et al. [7] and SiO2 by Zhang [11]. In all the tests, the Reynolds number was below 2 000 and therefore the flow was laminar. They are described in Table 4-1 with the thermophysical properties of nanoparticles.

Table 4-1 Thermophysical properties of water and nanoparticles [96]

	$\rho(kg/m^3)$	$C_p(J/kg.K)$	$k(W/m.K)$	$\mu(kg/m.s)$	$d_p(nm)$
water	$765.33 + 1.8142 \times T$ $- 0.0035 \times T^2$	$(28.07 - 0.2817 \times T$ $+ 0.00125 \times T^2$ $- 2.48e - 6 \times T^3$ $+ 1.857e - 9 \times T^4) \times 1000$	$- 0.5752 + 0.006397 \times T$ $- 8.151e - 6 \times T^2$	$0.0967 - 8.207e - 4 \times T$ $+ 2.344e - 6 \times T^2$ $- 2.244e - 9 \times T^3$	-
Al2O3	3920	880	36	-	50
ZrO2	5600	418	2	-	50
SiO2	2200	745	1.38	-	20

Temperature is in terms of Kelvin.

Both 2D axisymmetric and 3D models were examined at the beginning of this study and the results showed that it was crucial to use a 3D model in laminar nanofluid flow, especially with the presence of gravity in the Lagrangian approach. It can be argued that 2D axisymmetric can only capture the radial migration of nanoparticles inside the fluid, while the difference between a 3D model and 2D axisymmetric simulation results proves that nanoparticles migrate from the wall both radially and tangentially.

53

The grid dependence study proves that a structured mesh with higher uniformity can provide more precise results by DPM than other meshes. However, a higher number of cells is needed in modelling nanofluid by DPM compared with other laminar single-phase flow in the same geometry. The final number of grids for this geometry is chosen to be 16 radially, 58 tangentially and 600 longitudinally ($16\times58\times600$), which are shown in Figure 4.1. The closest node to the wall is almost 1×10^{-4}m, which is less than 5% of tube radius. It is noted that the simulation results achieved by this mesh and even many times more than this without node-based averaging method are not in agreement with experimentations. Boundary conditions for DPM consist of the following: similar uniform velocity and temperature at the inlet for both particles and base flow, particle mass flow rate at the inlet based on particle volume fraction (it is important to make sure particles are uniformly distributed at the inlet), constant heat flux over the external surface of the tube, fully developed condition at the outlet and no-slip condition at the wall of the tube. The inlet conditions for particles are equivalent boundary and initial conditions for particles in the Lagrangian frame. Also, wall boundary conditions differ for the particles from base flow. Two main possibilities are that they can either rebound off the wall or stick to the wall. The simulation results showed that none of the mentioned conditions happened for particles. It means that particles never reached the wall or met the wall conditions. Mixture model B.C. is similar to base flow conditions in DPM.
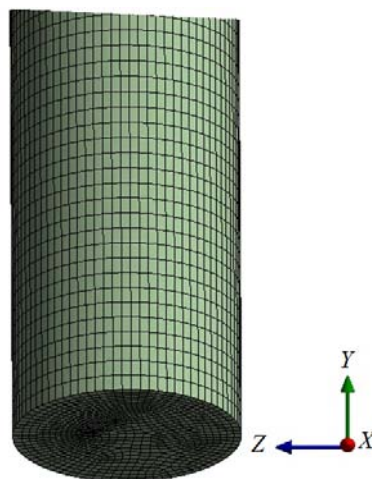

Figure 4.1: Generated mesh for CFD study with *Y* as vertical direction

As a first step, the extent of parameter *a* in the Gaussian distribution function in equation (3.109) needs to be chosen. Kaufmann et al. [97] successfully used *a*=6 in their study. Simulation results proved that any changes in *a* influenced mostly the particle concentration field and it had small impacts on pressure drops and heat transfer coefficient. The effects of *a* on alumina nanofluid with volume fraction 2.76% at the outlet of the tube can be seen in Figure 4.2. It can be seen that the larger amount of *a*=6 provides higher uniformity than the smaller one, but still the presence of the concentration gradient is obvious in all of them. Also, the same pattern of distribution can be observed for different ranges of *a*. However, *a*=6 was chosen for all the simulations here similar to Kaufmann et al. [97].

a)   *a* = 0.5   b)   *a* = 3.0   c)   *a* = 6.0
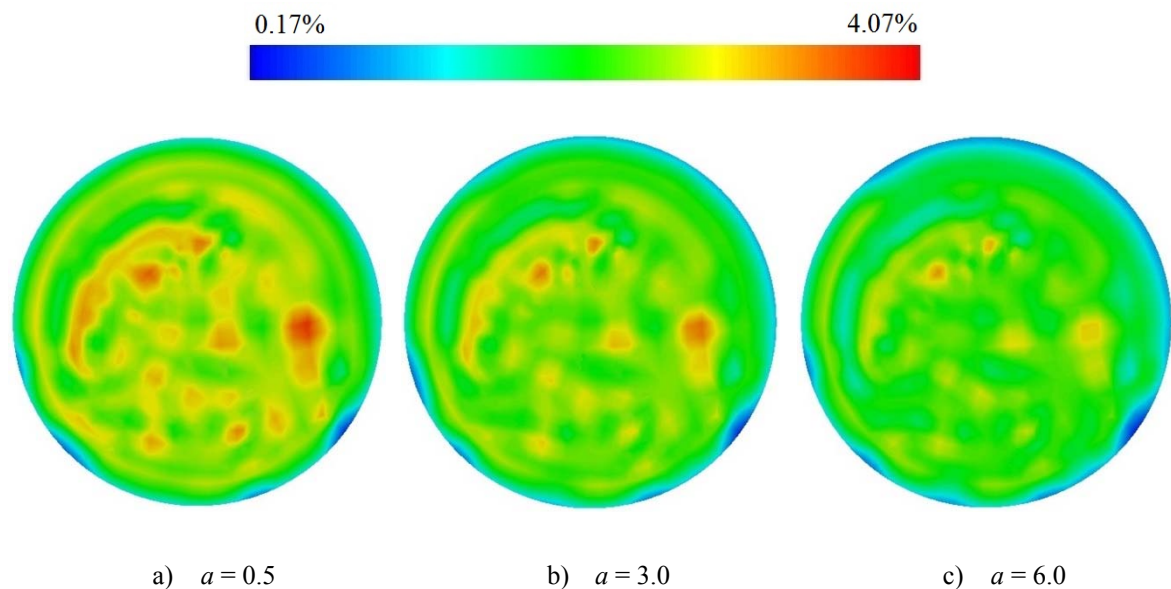
Figure 4.2: Effect of parameter *a* in Gaussian function on concentration distribution of alumina nanofluid with *α = 2.76%* at the outlet of the tube at *Re = 1 131, q″ = 18.7 kW/m²*.
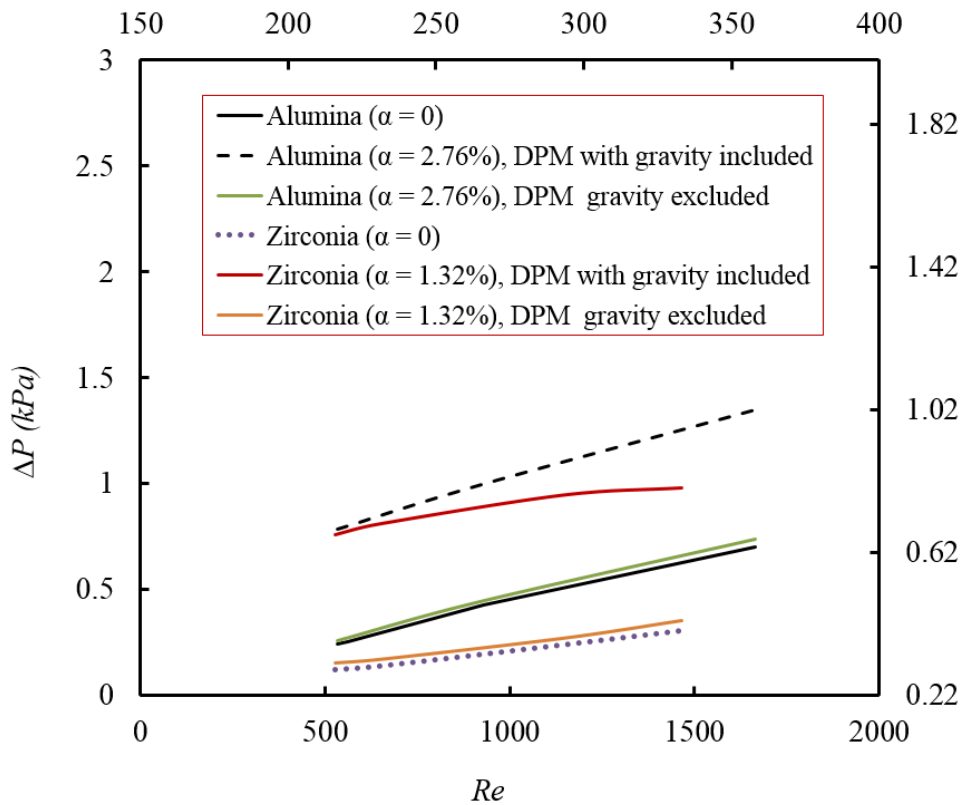
Figure 4.3: Effect of presence of gravity in DPM simulations for alumina and zirconia nanofluids, Left and bottom axis for alumina and right and top axis for zirconia.

The importance of gravity can be seen in Figure 4.3. When gravity is excluded from DPM, the pressure drops predicted by simulations are close to pressure drops with pure water, while DPM predicts more than twice the pressure loss with pure water. Hence considering no gravity in DPM may produce errors up to 200% in vertical laminar flow.

The dispersion of alumina and zirconia nanoparticles at the outlet section of the tube is illustrated in Figure 4.4, which shows the similar pattern of distribution for both alumina and zirconia nanofluids in different volume fractions. The percentage range of volume fraction in both nanoparticles with various particle loadings demonstrates that nanoparticles follow almost uniformly the base flow in lower volume fractions rather than in higher concentrations, notwithstanding the types of nanoparticles.
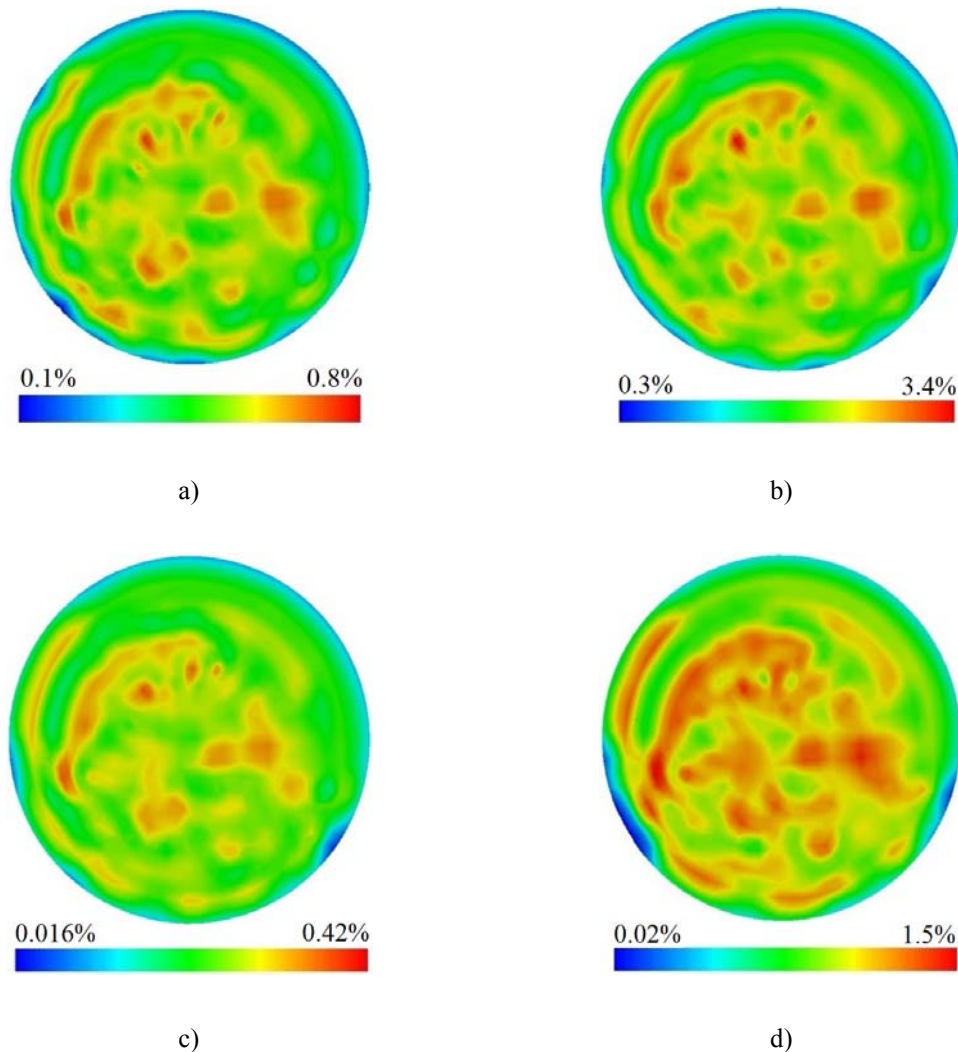
a)

b)

c)

d)

Figure 4.4: Distribution of nanoparticle volume fraction at the outlet for alumina and zirconia nanofluids. a) *0.65% alumina nanofluid, Re = 1 797, q″ = 18.6 kW/m² b) 2.76% alumina nanofluid, Re = 1 666, q″ = 25.3 kW/m² c) 0.32% zirconia nanofluid, Re = 356, q″ = 19.4 kW/m² d) 1.32% zirconia nanofluid, Re = 293, q″ = 16.4 kW/m²*

The concentration of nanoparticles rises in cells with an increase in particle loading, especially in an area slightly far from the wall and centroid region of tube, which can be clearly seen in Figure 4.4d. Again, the types of nanoparticles showed no impact on the dispersion of particles on the tube. Figure 4.4d also proves that the possibility of clustering may accelerate with growth in nanoparticle volume fraction. One of the reasons for no symmetry in particle distribution can be the Brownian motion and thermophoresis which occur at the same time. Brownian is random motion and happens everywhere in

57

cross-section and thermophoresis is strong close to the wall. The combination of both may disturb the cross-sectional concentration distribution. On the other hand, the mixture model results provided more uniform distribution of concentration than those of DPM for any types of nanoparticles and particle loadings. It means that the slip velocity assumed by the mixture model in the simulations is almost negligible. The nanofluid is treated as a homogeneous mixture with no relative velocity between solid and liquid parts.

4.1.1 Case study of heat transfer features

Heat transfer and hydrodynamic characteristics of laminar nanofluid in two vertical tubes are presented in this section. Figure 4.5 shows the good agreement between experiments and numerical solutions for heat transfer coefficient in base flow without nanoparticles for different Reynolds numbers. The heat transfer coefficient is simply calculated from $q'' / (T_w - T_b)$. The important parameter is the bulk temperature T_b, which can be defined as:

$$T_b = \frac{\int \rho c_p V T dA}{\int \rho c_p V dA} \tag{4.1}$$

The heat transfer coefficient and Nu number estimated by the mixture model and DPM compared with experimental results for three types of nanofluids are illustrated in Figure 4.6 and Figure 4.7. A wide range of Reynolds numbers from 290 to 1 800 and particle volume fraction from 0.2% to 2.76% was simulated for three common nanofluids, i.e. alumina, zirconia and silica nanofluid, with different diameters of nanoparticles.
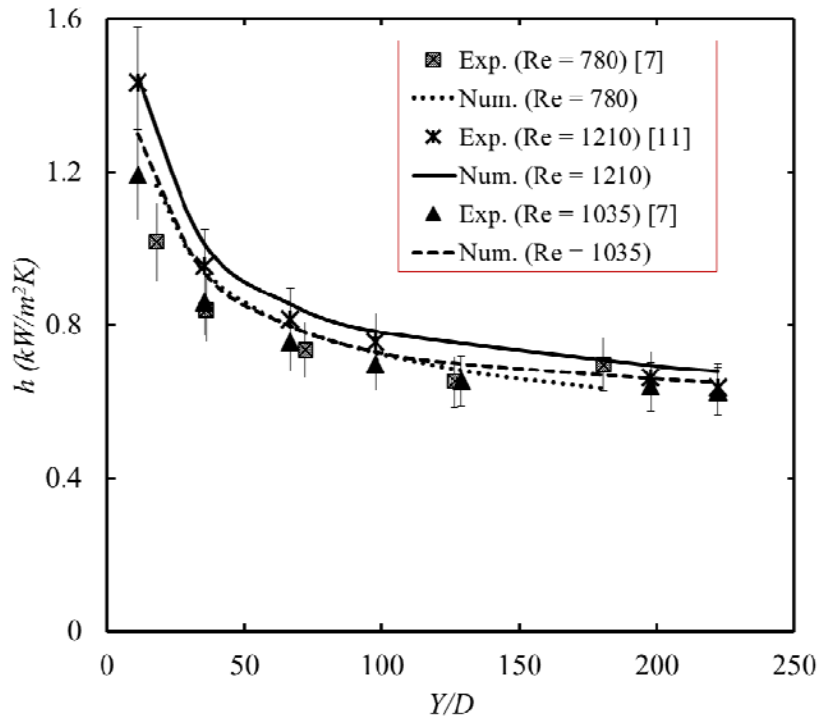
58

Figure 4.5: Heat transfer coefficient predicted by numerical solution and experimentally measured for laminar flow in vertical tubes

It is clear that both models provided findings in good agreement with experimental measurements. This conclusion is important, because empirical or theoretical correlations for thermophysical properties of nanofluid are needed to simulate this sort of fluid in tubes. DPM treats each component in nanofluid as it is and only some general correlations such as interaction or diffusion forces are required. As a result, DPM can be highly recommended for laminar nanofluid flow in vertical tubes to characterise the thermal features of nanofluids.

4.1.2 Study of hydrodynamic features

Pressure drops estimated by the mixture model and DPM are compared with the Darcy-Weisbach correlation in the error range of 20% in Figures 4.8, 4.9 and 4.10. The Darcy-Weisbach correlation is presented as:

$$\Delta P = \frac{64}{\text{Re}} \frac{L \rho V^2}{2 D_{tube} g} \tag{4.2}$$

59

All the properties for the Darcy-Weisbach correlation were borrowed from mixture properties presented in literature. The simulations were carried out for volume fraction below 3% and a good agreement was observed between modelling and the correlation. DPM showed a better trend for pressure loss prediction compared with the mixture model. The simulations were also conducted for higher 3% volume fractions. The DPM results were sometimes 100% different from the correlation, especially in the case of the higher velocity shown notwithstanding the type of nanofluid. The main differences between lower and higher volume fraction can be introduced as: firstly, rising the number of nanoparticles in each computational cell. One of the problems can come from inaccurate weight or Gaussian function to distribute the effects of particle variables to neighbouring cells. Secondly, the possibility of clustering and collision among nanoparticles will expand with an increase in volume fraction.

Due to a higher number of silica nanoparticles in each parcel compared with the other two nanoparticles with the same conditions, as shown in Figure 4.11, the percentage of difference for pressure drops in higher volume fraction was found much appreciable. It is noted that the number of particles is conserved in the entire domain when the particles are solved in Lagrangian frame. It means that it is important to assign the proper number of time steps for nanoparticles to make sure all the injected particles will leave the geometry domain. Moreover, the average difference between simulations and Darcy equation for pressure drops was found to be near 12% by the mixture model and 10% by DPM.

Non-dimensional temperature distribution of fluid and nanoparticles at the outlet is illustrated in Figures 4.12 and 4.13 for three nanofluids. With heat transfer parameters in this study consisting of heat flux, temperature, thermal conductivity and characteristic length, non-dimensional temperature can easily be defined as:

$$T^* = \frac{2\,(T - T_{in})\,k_c}{q''D_{tube}} \tag{4.3}$$
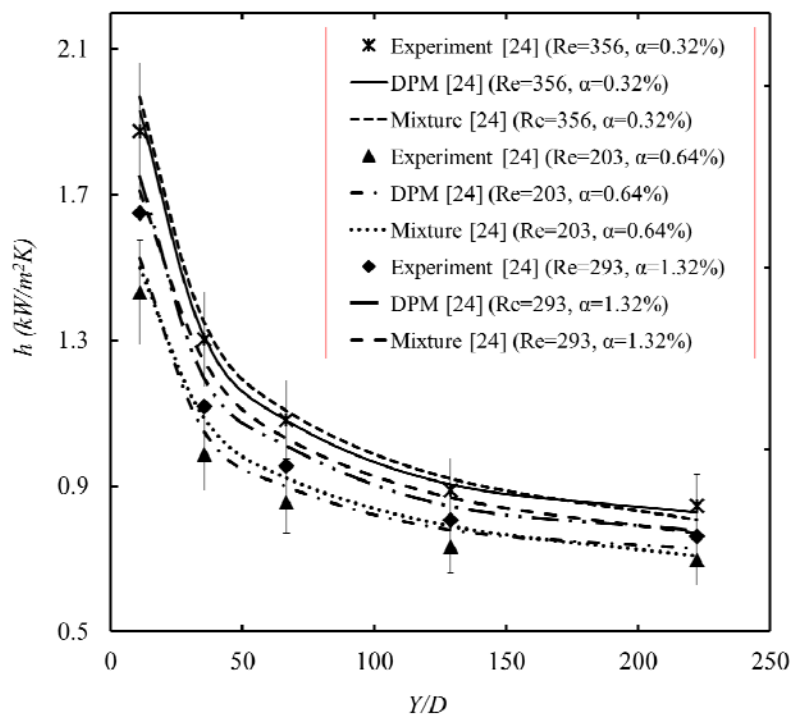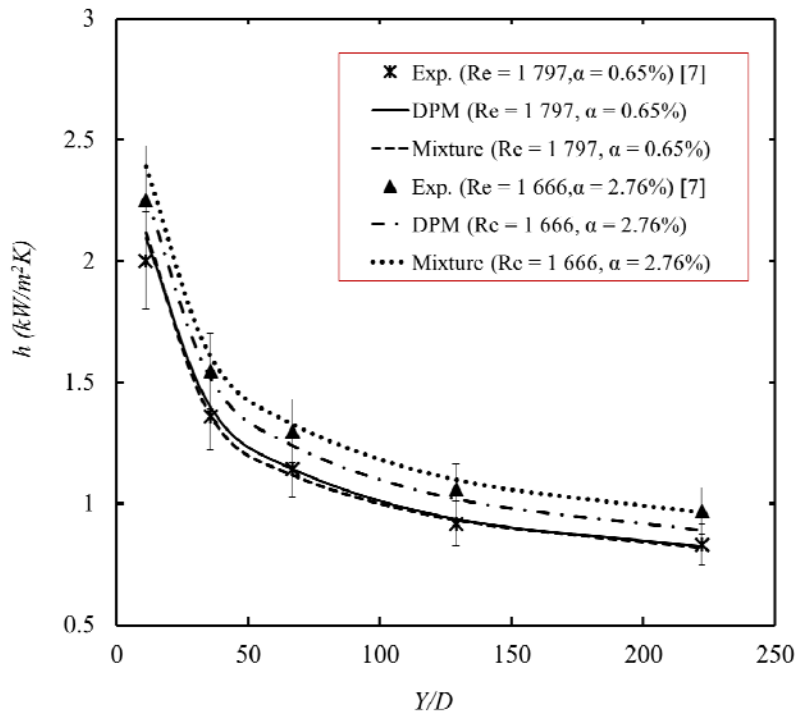
a)

b)

61

Figure 4.6: Comparison of experimental data and numerical predictions for heat transfer coefficient by the mixture model and DPM for a) alumina b) zirconia nanofluid.

Smooth parabolic profile of temperature for base fluid can be observed in all the simulations. It can be explained that nanoparticles cannot distort the parabolic shape of the temperature profile, and energy is mostly transported via nanoparticle migration. This makes more sense when fluid temperature is compared with the distribution of nanoparticle temperature in Figure 4.12 and Figure 4.13. The nanoparticle temperature profiles are distorted at the vicinity of the wall because of the higher temperature gradient. The trend is almost similar for lower and higher concentrations, although the distribution of temperature seems more uniform in the case of silica nanofluid with 0.2%.
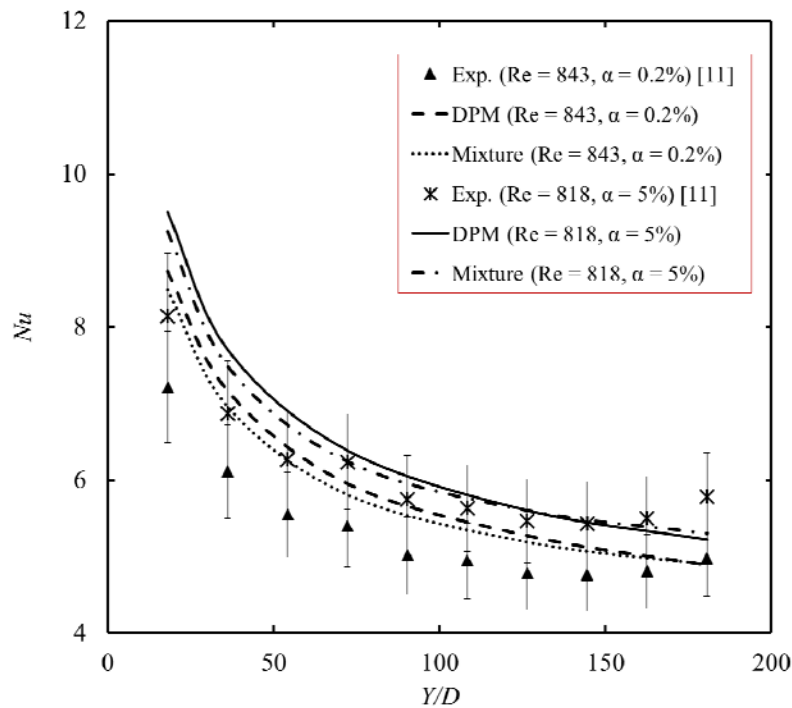

Figure 4.7: Nu number estimated by the mixture model and DPM in comparison with measured values for silica nanofluid
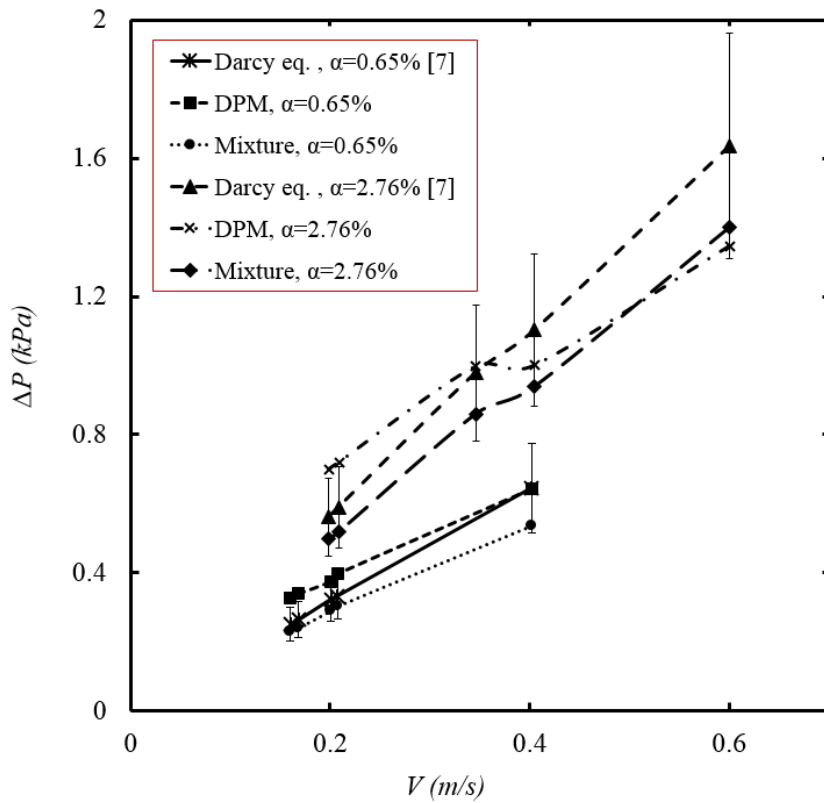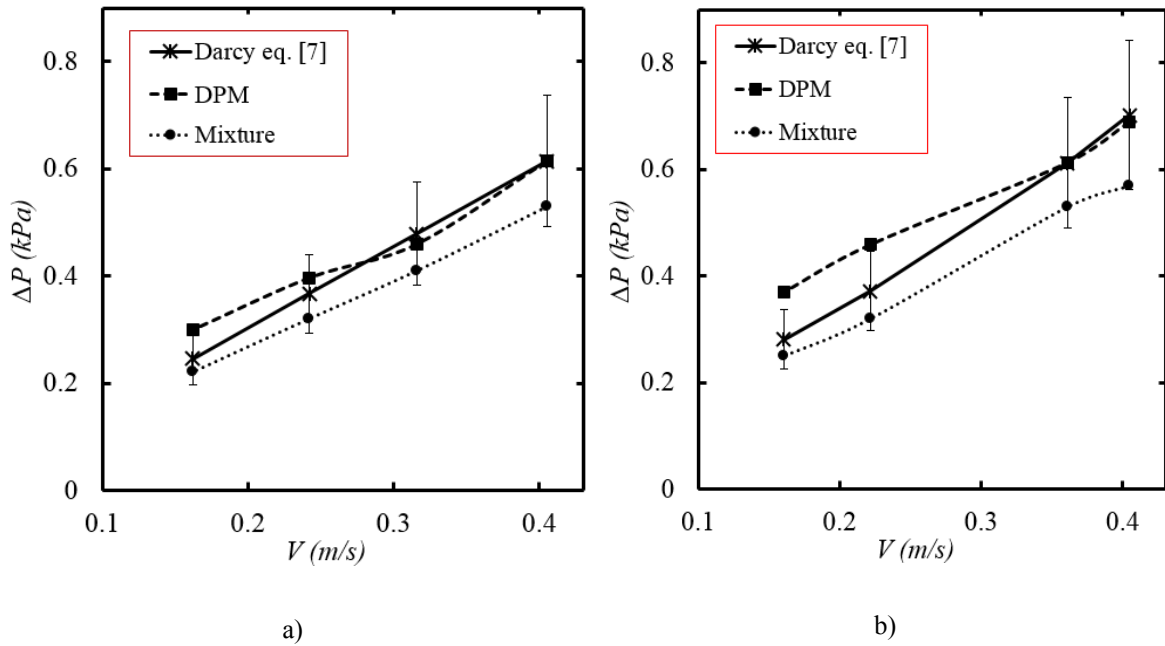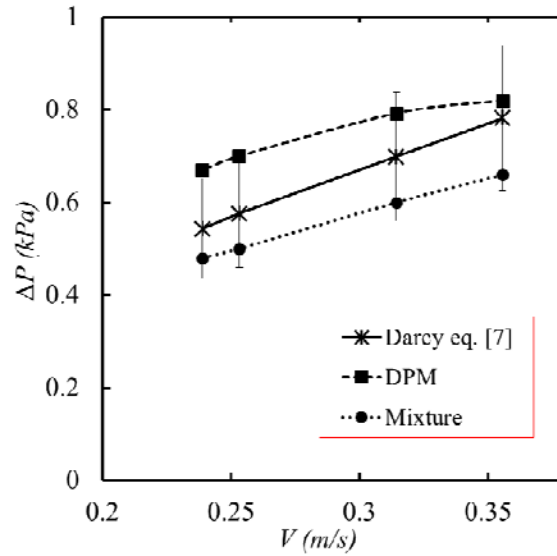
Figure 4.8: Prediction of pressure drops for alumina nanofluid by the mixture model and DPM in comparison with the correlation

a)   b)

(c)

Figure 4.9: Prediction of pressure drops for zirconia nanofluid by the mixture model and DPM in comparison with the correlation, zirconia nanofluid a) 0.32% vol. b) 0.64% vol. c) 1.32% vol.

Figure 4.14 presents the velocity profile at the outlet of tubes on the symmetry line predicted by two multiphase models. The model findings are compared with the fluid velocity affected by the nanoparticles. The gap between particles and model velocity can largely be seen close to the wall. The flow velocity profiles predicted by the mixture model and DPM are similar, while the nanoparticle velocity profile shows small slip velocity with base flow. It is noted that due to a high number of particles in the flow domain, this small amount of slip velocity can somehow produce noticeable pressure drops. From the figures, it seems that there is velocity for particles on the wall. The condition for particles is associated with collision between nanoparticles and wall (continuum is not held for dispersed particles). It means that if the nanoparticles do not reach the wall, the wall boundary conditions for particles are meaningless. On the other hand, because the nanoparticles are carried properly with the fluid, the simulations reveal that the nanoparticles never hit the wall in this study. Hence, the unreal velocity is chosen for nanoparticles at the wall, which is equal to the cell velocity at the vicinity of the wall. However, this unreal velocity has no effect on the modelling.
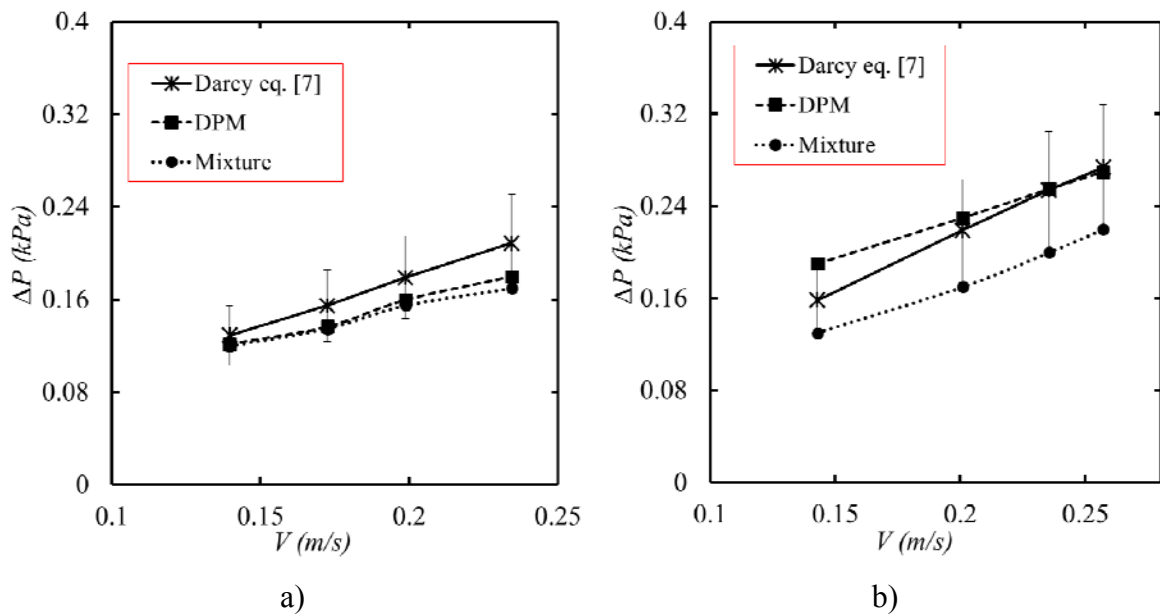
Figure 4.10: Prediction of pressure drops for silica nanofluid by the mixture model and DPM in comparison with the correlation for silica nanofluid a) 0.2% vol. b) 1% vol.

In summary, the two approaches can be compared as follows: the mixture model results highly depend on transport properties coming from experimentation. There is no need for the mixture properties for DPM, which only needs appropriate interaction or diffusion forces, empirical or analytical. The mixture model considers nanofluid as two phases. DPM treats the nanofluid as base fluid and solid separately, as it is in reality.
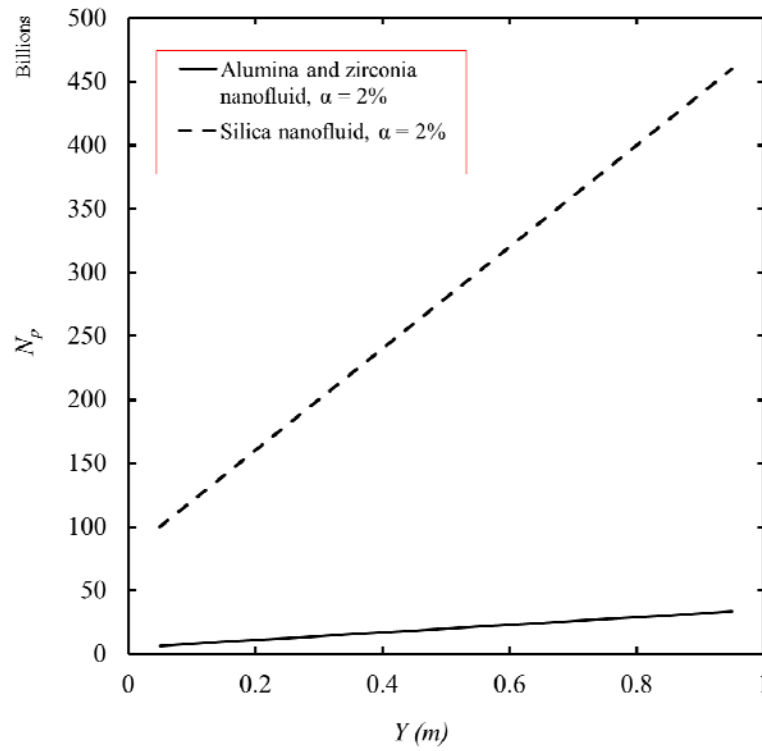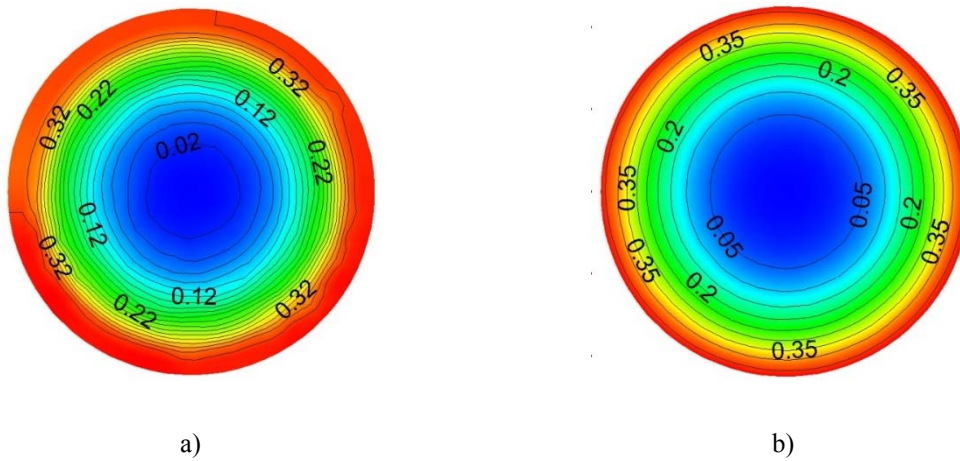
Figure 4.11: Changes in the number of nanoparticles in each parcel from inlet to outlet at the centre of the tube

a)

b)

66

c)   d)

Figure 4.12: Non-dimensional temperature distribution of base fluid and alumina nanofluid predicted by DPM, a) alumina nanoparticle, $\alpha = 0.65\%$, $Re = 1\ 797$ $q'' = 18.6$ kW/m^2. b) base flow, $Re = 1\ 797$, $q'' = 18.6\ kW/m^2$. c) alumina nanoparticle, $\alpha = 2.76\%$, $Re = 1\ 666$, $q'' = 25.3\ kW/m^2$. d) base flow $Re = 1\ 666$, $q'' = 25.3\ kW/m^2$.

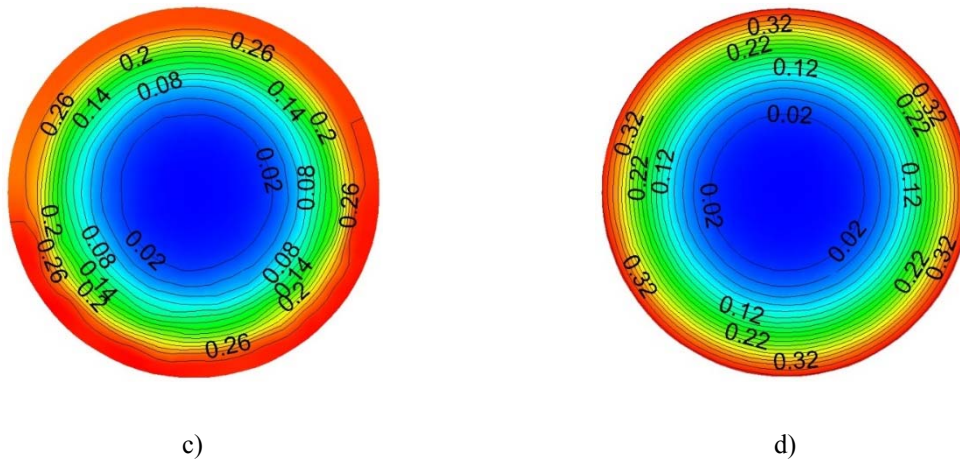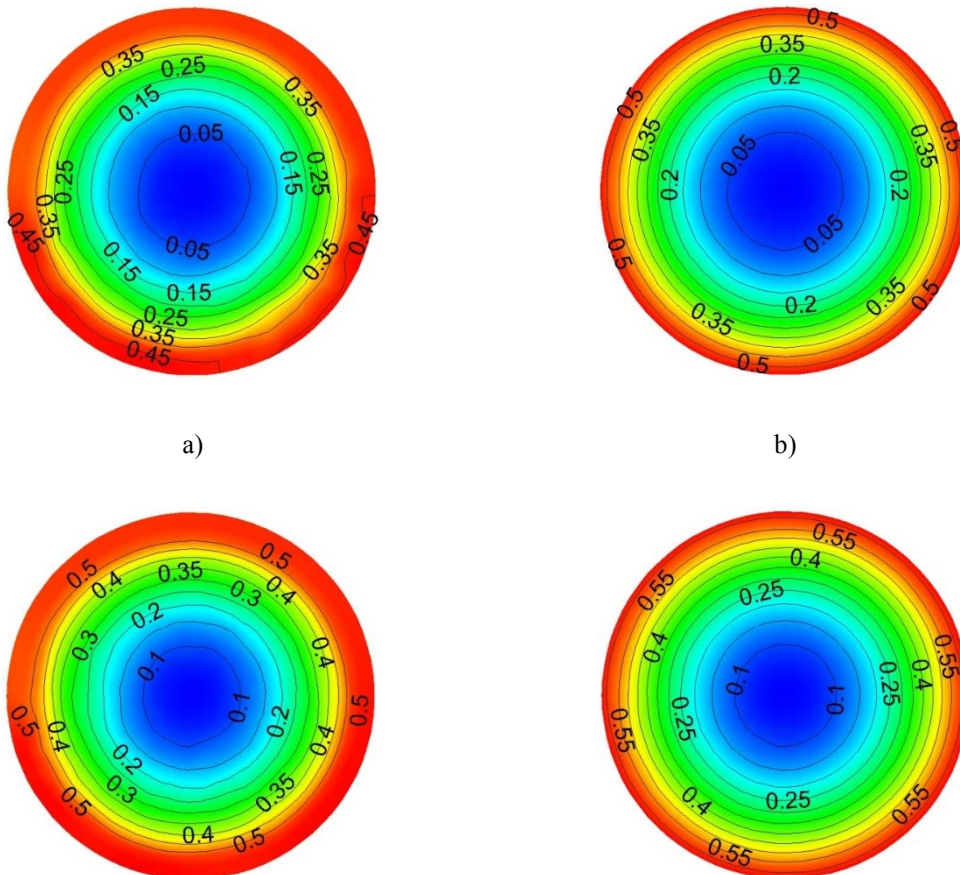

a)   b)

67

Figure 4.13: Non-dimensional temperature distribution of base fluid and nanofluid predicted by DPM. a) zirconia nanoparticle, $\alpha = 1.32\%$, $Re = 293$, $q'' = 16.3\ kW/m^2$, b) base flow, $Re = 293$, $q'' = 16.3\ kW/m^2$, c) silica nanoparticle, $\alpha = 0.2\%$, $Re = 843$, $q'' = 15.7\ kW/m^2$, d) base flow, $Re = 843$, $q'' = 15.7\ kW/m^2$

The thermophysical property correlations for nanofluid are not universal and change by fluid and nanoparticles. The empirical correlations for DPM interaction forces are not extensive and can be employed in most of the cases. The effects of slip mechanisms such as thermophoresis and Brownian can be seen as diffusion terms in mixture equations and need to be implemented in the program. In DPM, velocity is calculated for fluid and solid separately and finally, the relative velocity between them is the most important. DPM is weak to simulate higher nanoparticle loading due to the inclusion of other phenomena such as clustering and aggregating.
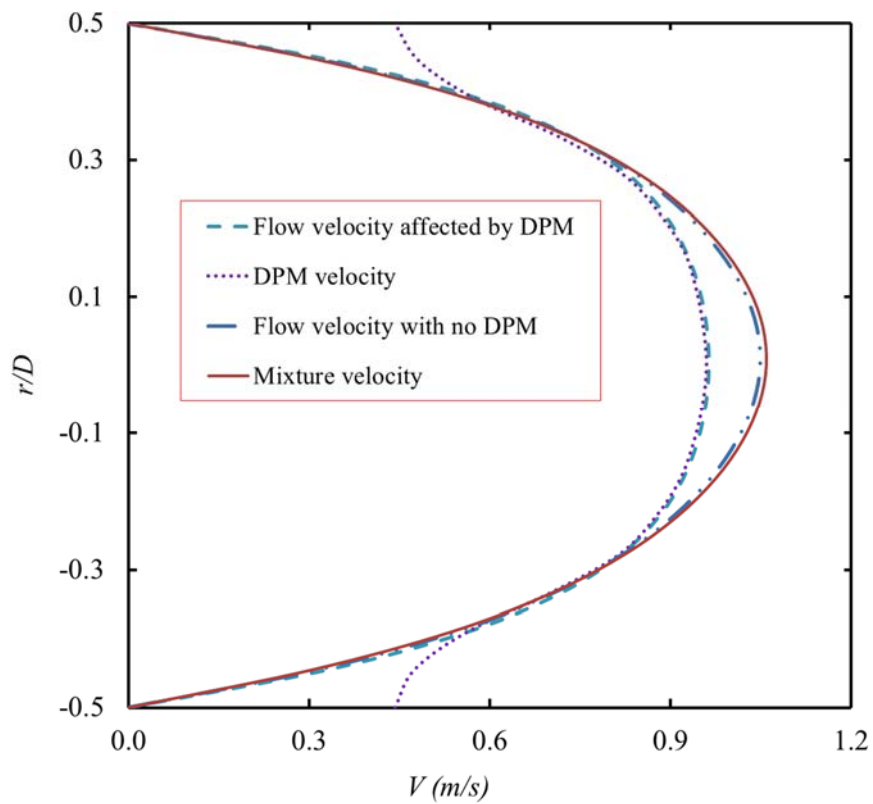
(a)
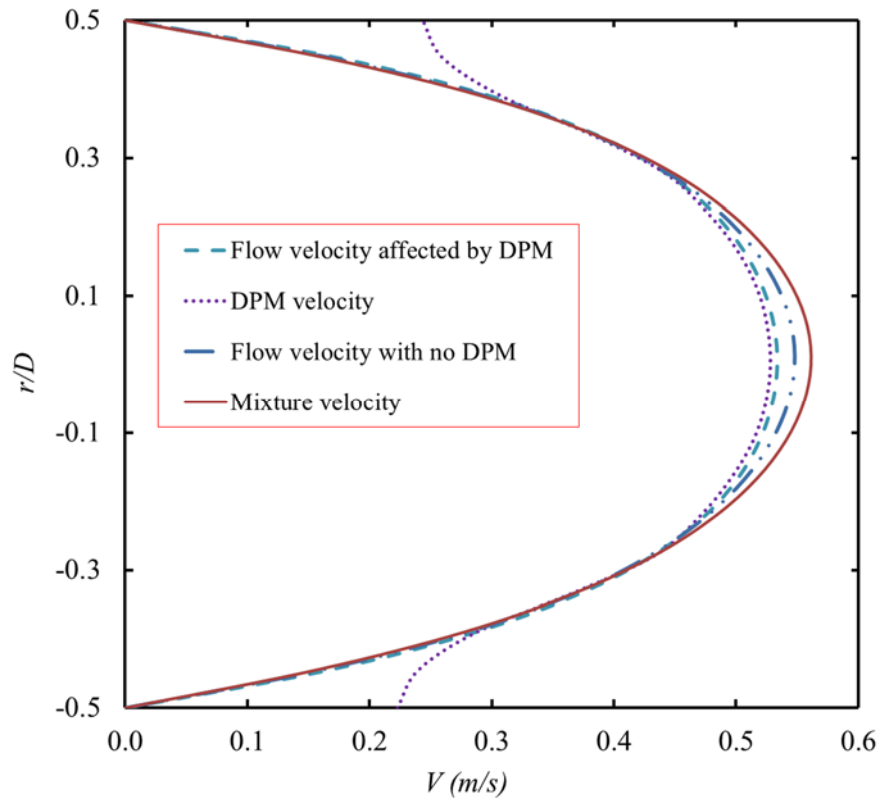
(b)

Figure 4.14: Velocity profile on the symmetry line at the outlet of tubes for alumina and zirconia nanofluids. a) alumina nanofluid, *Re = 1 680, α = 2.76%*, b) zirconia nanofluid, *Re = 1 060, α = 1.32%.*

SIMULATION OF NATURAL CONVECTION USING THE MODIFIED MIXTURE MODEL IN THE STUDY

The results of heat transfer and pressure drops in the previous section showed that both approaches can provide good prediction for laminar tube flow. But, the results of concentration distribution and particle migration can still be in doubt due to lack of all other phenomena involved in interactions. Therefore, the validity of the modified mixture model with diffusion approach presented in Chapter 3 is investigated for natural convection. In spite of the conventional mixture model, the modified one considers a range of slip mechanisms involved between nanoparticles and base flow. The experimental study of nanofluid natural convective flow in a rectangular cavity is

69

borrowed from the recently published paper by Ghodsinezhad et al. [98], conducted at the University of Pretoria.

The size of the cavity used was 96mm×120mm for cold and hot walls and the space between the walls was 102mm, therefore, the aspect ratio about unity. The entire schematic of the test section is shown in Figure 4.15. The hot and cold wall sides of the cavity are heated and cooled by two shell-and-tube heat exchangers with counterflow inside. All the materials of the heat exchangers were made from copper, including 4mm copper plates in each side of the cavity. The dimensions of the shell part of the heat exchanger were 96mm×120mm×18mm. To improve the heat transfer and uniformity of temperature inside the heat exchanger, the mass flow from and to the heat exchanger was split between shell and tube parts equally. The diameter of the tube was chosen to be 10.7mm ID and 1mm wall thickness. The hydraulic diameter of the shell part was calculated almost similar to the tube diameter to achieve the best distribution of mass and heat transfer inside heat exchangers. Also, three plates made of copper were installed inside heat exchangers as buffers to make the channel for the shell side.

With the calculation of Reynolds number in heat exchangers and Rayleigh number defined as $Ra = \dfrac{g\beta L^3 (T_{h-ave} - T_{c-ave})}{\alpha v}$, three separate types of flow regimes are recognised in the experiment: turbulent flow in hot heat exchanger, laminar flow in the cold heat exchanger and laminar natural convection flow in the cavity.

All the thermophysical and transport properties of the fluid were expressed in terms of temperature. Density in momentum equation was the non-Boussinesq term used in the cavity. Instead of the linear function of temperature for density by Boussinesq approximation as β∆T, a third-order polynomial function of temperature in Chapter 3 was employed. Also, the turbulence terms were ignored for laminar flow inside the cold heat exchanger and cavity. The realisable *k-ε* model was employed to simulate the fluctuating velocity and turbulent viscosity, which was successfully used by Bacharoudis et al. [99] and Teodosiu et al. [100].
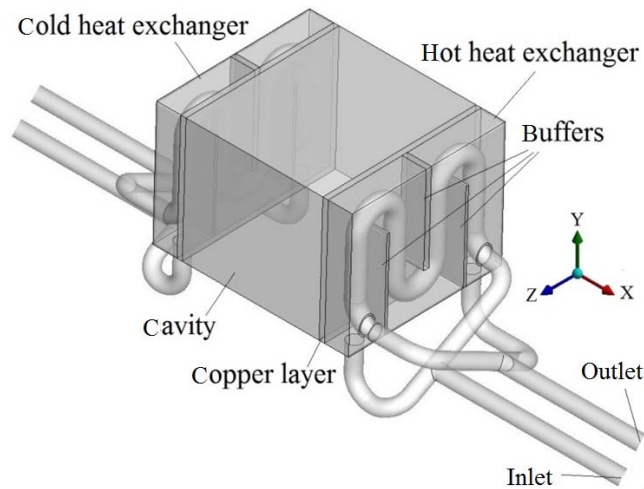
70

Figure 4.15: Schematic of the cavity with heat exchangers

Both structured and unstructured meshes were required for this kind of geometry, unstructured mesh for heat exchangers and the structured one for cavity and copper layers. Also, boundary layer meshes were added in heat exchangers due to the small size of the tube and existence of turbulent flow inside the hot section. Some interfaces were needed for the sections between heat exchangers and copper layers due to different types of meshes. The realisable *k-ε* model was operated with enhanced wall function as wall treatment in shell and tubes. The initial results exhibited the amount of y^+ at the vicinity of all walls less than 5, which was an acceptable amount for this method. On the other hand, the natural convection simulations inside the cavity proved that the mesh had to be fine enough in the vicinity of the walls to capture the entire influences of the small boundary layer due to natural convection. As a result, the closest node to the shell-and-tube walls was chosen as 0.3mm for the cavity. Three kinds of flow regimes existed in the model, namely turbulent forced convection, laminar forced convection and laminar natural convective flow. Therefore, it could be expected that a large number of iterations would be required to reach heat transfer balance in the cavity, which was the most important criteria for convergence. Various meshes were tried to find the optimum and best grid for each section in the model concerning the grid study (up to 2 million nodes in total). The criteria for comparison among different grids were chosen as heat flux in walls, temperature and velocity profile at the centre line of the cavity. Finally, the proper mesh was chosen as 912 081 unstructured cells for each heat exchanger, 226 981

71

structured cells for cavity and 2 078 644 cells for the entire model. The process of grid study compared with the chosen mesh is presented in Table 4-2.

Table 4-2 Grid study of the numerical simulation

Test case	Cells of a heat exchanger	Cavity cells	Total	Heat flux error compared with the chosen grid
1	413 578	91 125	931 431	9%
2	912 081	226 981	2 078 644	0%
3	1 325 421	421 875	3 111 168	-0.9%
4	1 968 780	912 673	4 937 765	-1.1%

a)

b)
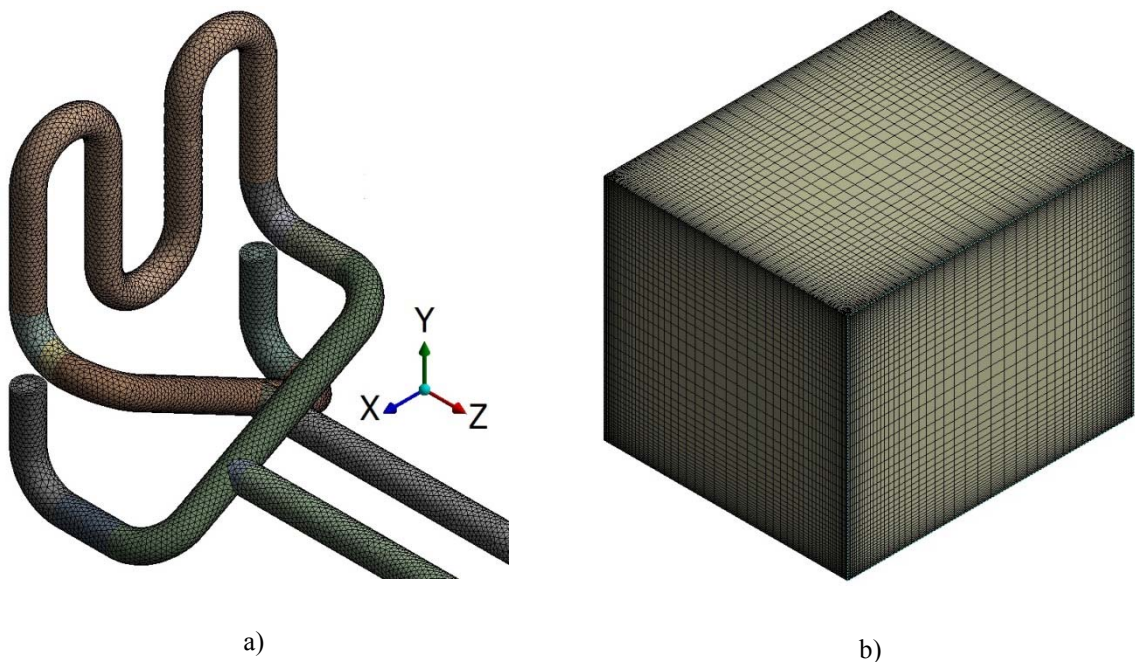
Figure 4.16: The generated mesh for a) tube of heat exchanger (unstructured) b) cavity (structured)

The simulations revealed that heat transfer balance in a range of 1% error happened after 15 000 iterations and it took three days for each case with eight processors 3.5GHz CPU. The generated mesh for the tube part of heat exchanger and cavity is shown in Figure 4.16. In addition, all the external walls of the tubes, heat exchangers and cavity were exposed to zero heat flux condition.

72

The nanoparticles used in this study were Al_2O_3 and ZnO; Al_2O_3 nanoparticles with manufactured claimed diameter of 30 nm and 99.9% purity and ZnO with claimed diameter of 20 nm. The other properties were as follows: Al_2O_3 density, heat capacity and thermal conductivity of 3950 kg/m^3, 765 J/kg.K and 36 w/m.K respectively, and ZnO density, heat capacity and thermal conductivity of 5606 kg/m^3, 523 J/kg.K and 25 w/m.K. Hadi et al. [98] report that the mean diameter of Al_2O_3 is 250nm and 127nm for ZnO using transmission electron microscopy (TEM). In this study, the reported particle diameter by manufacturers was not used in calculations and the measured one applied.

The robustness of the model proposed in the study was verified by the Nusselt number from measurements in Figure 4.17. A good agreement between experiment and modelling was observed. As can be seen, the Nusselt number dropped with an increase in concentration, but was still higher than distilled water in the case of alumina nanofluid. The drop and rise were also reported by Moradi et al. [45], Li and Peterson [37] and Rao and Srivastava [42] in these ranges of volume fraction. Moreover, alumina nanofluid provided a higher heat rate and in lower volume fractions. The measured temperature on the mid-vertical line of the cavity from bottom to top of the insulated walls was compared with the numerical results in Figure 4.18. This full agreement between simulation and experiment can be the main criterion for further predictions, especially for concentration distribution.

The conventional method in CFD software only includes the effect of gravitational force as the slip velocity and there are no terms for other slip mechanisms and diffusion of nanoparticles. This provides the wrong concentration distribution at the vicinity of the walls in Figure 4.19. The impacts of other mechanisms are noticeable from 0.5% vol. alumina to 1% vol. zinc oxide nanofluid. The higher amount of absolute value and gradient of volume fraction was clearly predicted close to the walls by the proposed method. It was caused by the presence of concentration and thermophoretic diffusion terms in mass equation, in particular next to the hot wall.
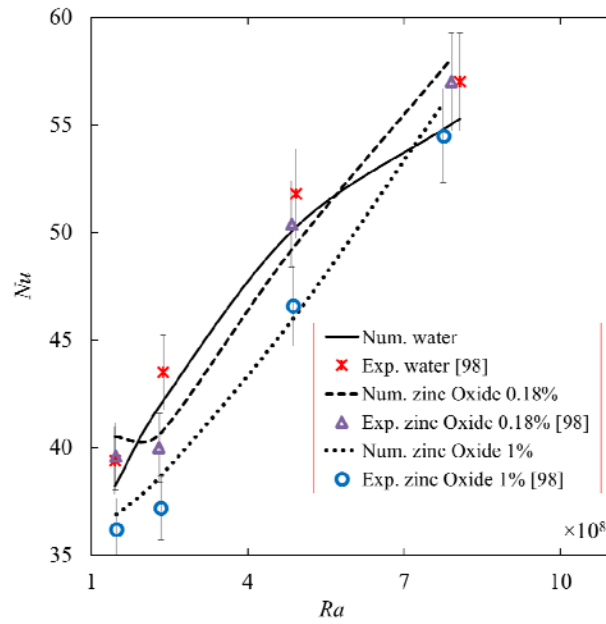
(a)
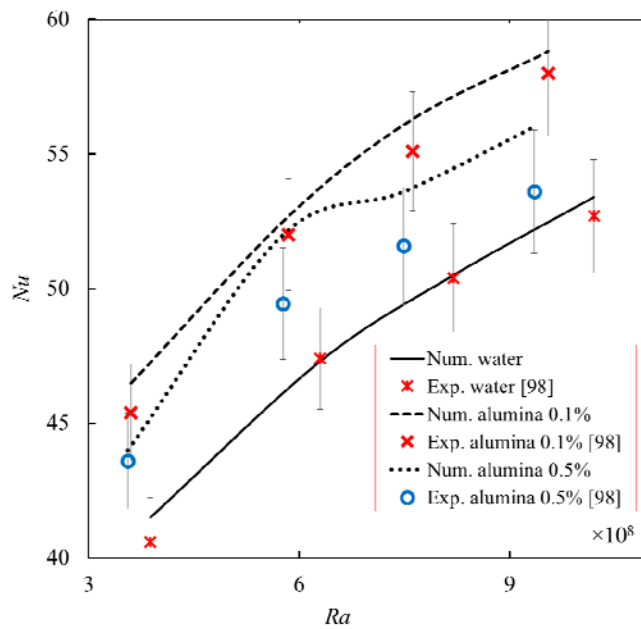
(b)

Figure 4.17: Comparison of Nusselt number measured during the experiments and calculated by the numerical model for alumina and zinc oxide nanofluids

One of the essential parts of prediction in this study is the concentration distribution of nanoparticles inside the cavity. It helps to have a deep understanding of particle migration along with the causes of changes in flow and thermal features, shown in Figure 4.20. The proposed method clearly presented a different distribution from the conventional method. The proposed method could predict the concentrated area at the bottom corners of the cavity and well dispersion in other regions.
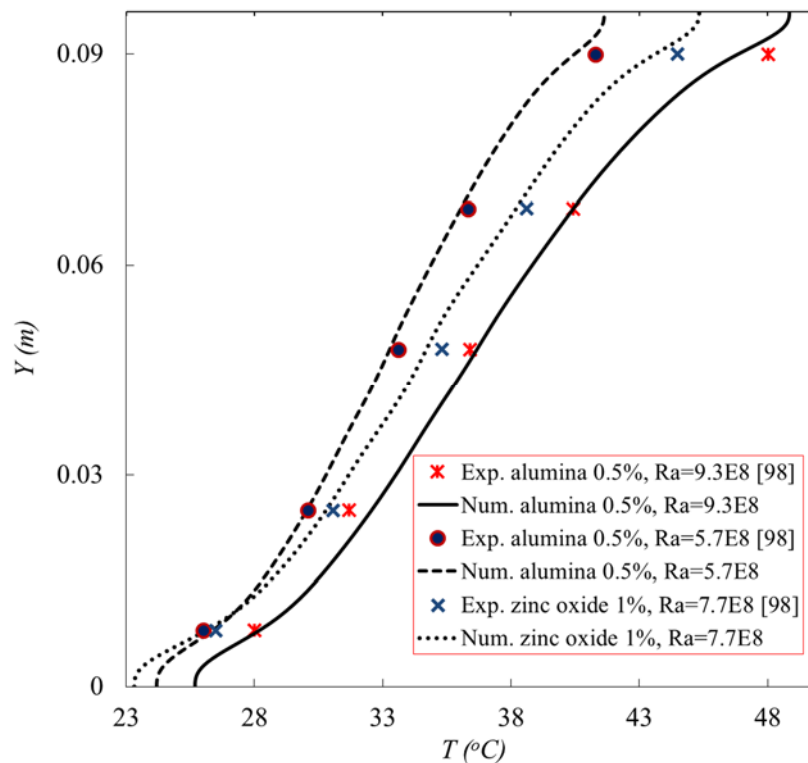
Figure 4.18: The profile of temperature in the Y-direction at the mid-vertical line of the cavity

The profiles of the non-dimensional Y velocity $V/\sqrt{g\beta\Delta TL}$ for alumina and zinc oxide nanofluid are compared with distilled water in Figure 4.21. The thickness of the hydrodynamic boundary layer is almost the same for all the cases. Because the concentration boundary layer of zinc oxide nanoparticles is thin close to the wall, no effects of particles on velocity profile are observed in the case of the zinc oxide nanofluid. It is mainly caused by buoyancy force on the zinc oxide nanoparticles with higher density than the alumina particles, producing a thicker concentration boundary layer at the bottom

of the cavity. In the case of alumina nanofluid, the competition among all the phenomena considered in this study will characterise the damping effects of particles on velocity. Therefore, the damping impacts on velocity in 0.5% vol. can be less than in the case of 0.1% vol.

The growth of hydrodynamic, concentration and thermal boundary layers could reveal many aspects of nanofluid flows, shown in Figure 4.22. The thermal boundary layer was the same for both nanofluids, and also the thickest among others. The increase of nanoparticle density and volume fraction from alumina to zinc oxide clearly affected the hydrodynamic boundary layer, particularly at the beginning of the growth. It was mainly caused by the presence of other slip mechanisms in momentum equation.

(a)

(b)

Figure 4.19: Concentration profile of alumina and zinc oxide nanoparticles at the vicinity of the hot wall (horizontal) and from the bottom of the cavity (vertical), a) alumina nanofluid *0.5%, Ra = 9.3E8*, b) zinc oxide *1%, Ra = 7.7E8*.

a)   b)
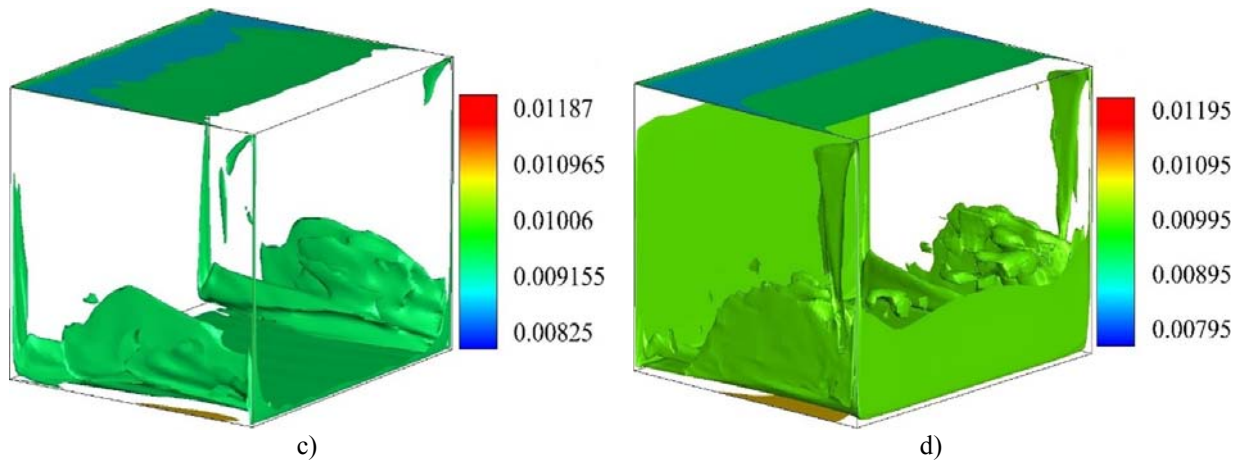
77
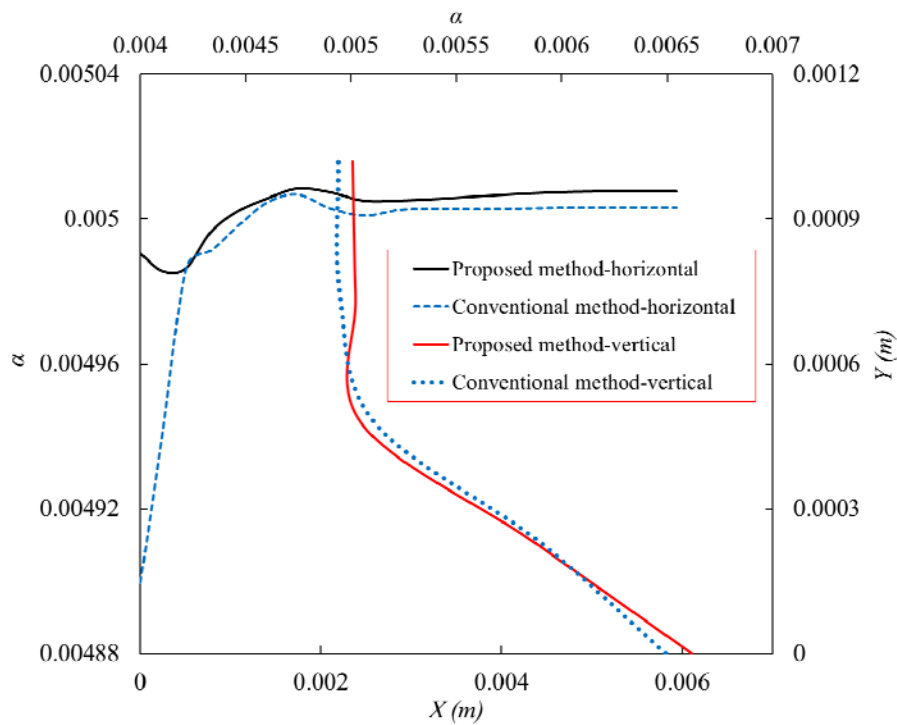
Figure 4.20: Three-dimensional distribution of nanoparticle concentration in a cavity, a) alumina *0.5%, Ra = 9.3E8*, conventional method, b) alumina *0.5%, Ra = 9.3E8*, proposed method, c) zinc oxide *1%, Ra = 7.7E8*, conventional method, d) zinc oxide *1%, Ra = 7.7E8*, proposed method

SIMULATION STUDY OF LAMINAR NANOFLUID FLOW IN A HORIZONTAL CIRCULAR MICROCHANNEL USING DISCRETE PHASE MODELLING

Laminar convective flow in a horizontal circular microchannel was simulated using DPM presented in Chapter 3. The experimental study done by Zhang et al. [101] was borrowed to validate the heat transfer results. Alumina nanofluid with particle average diameter 20 nm was used in a microchannel with the outside diameter of 1.5 mm and the inner diameter of 0.5 mm. The constant heat flux was applied to the outer section of the microchannel for the length of 100 mm. Because the amount of heat loss during the experiment was mentioned as less than 5%, it was included in the numerical considerations. In addition, the amount of 5% uncertainty in the calculation of Nusselt number was considered in illustrating the final results.

78

a) b)
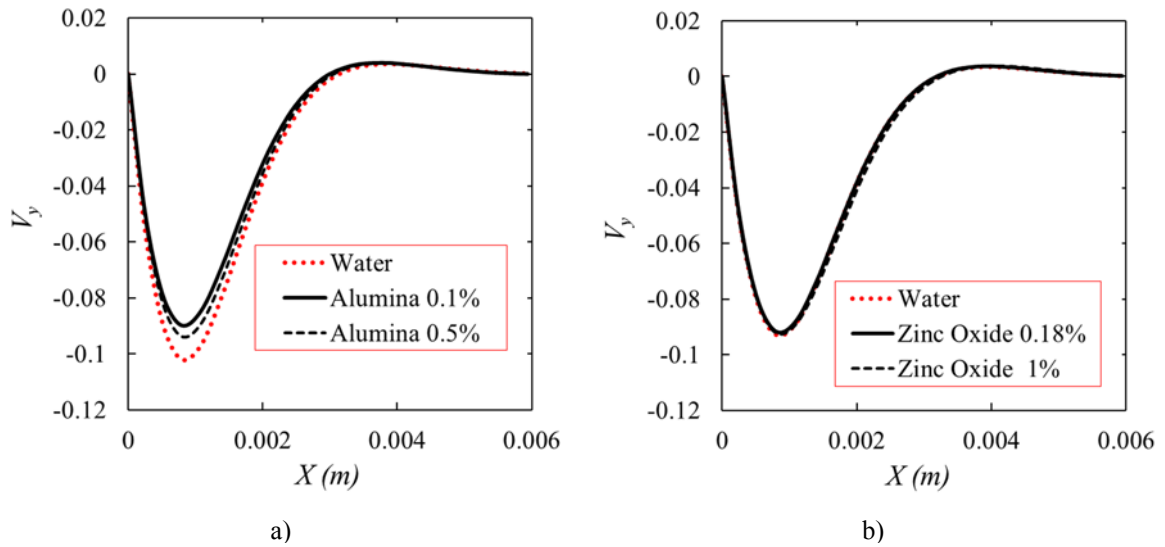
Figure 4.21: Non-dimensional Y velocity (V_y) at the vicinity of the cold wall

a) b)
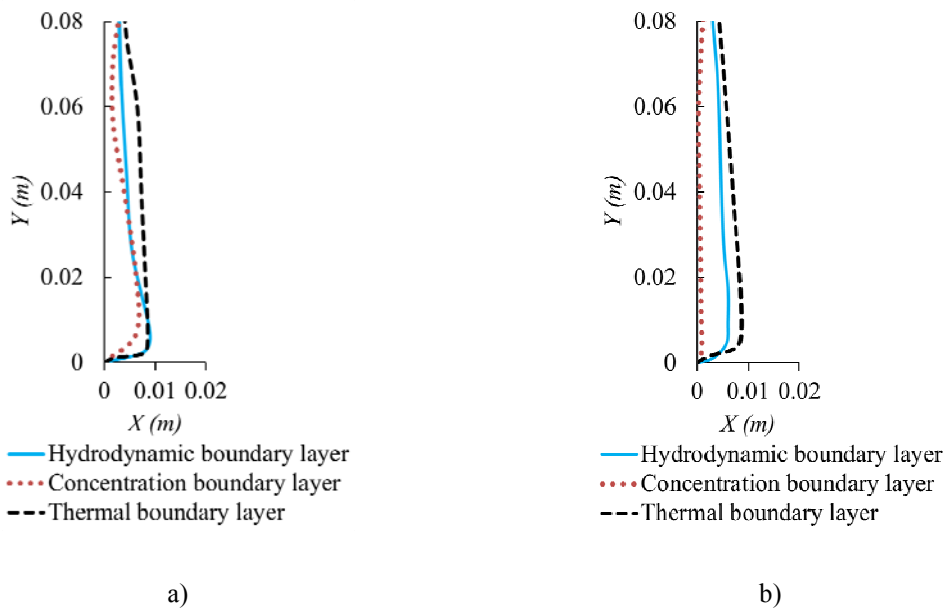
Figure 4.22: Flow, heat and mass boundary layers of nanofluids in natural convection near to the cold wall, a) alumina *0.5%, Ra = 9.3E8*, b) zinc oxide *1%, Ra = 7.7E8*.

The results of Nusselt number estimated by DPM are compared with measurements in Figure 4.23 considering the 5% error bar. Even though the values for various ranges of particle loading are close to each other, the impacts of nanoparticles in heat transfer enhancement are visible at Reynolds number higher than 1 500. This validation can be useful for further prediction of nanoparticle migration in the flow.

79
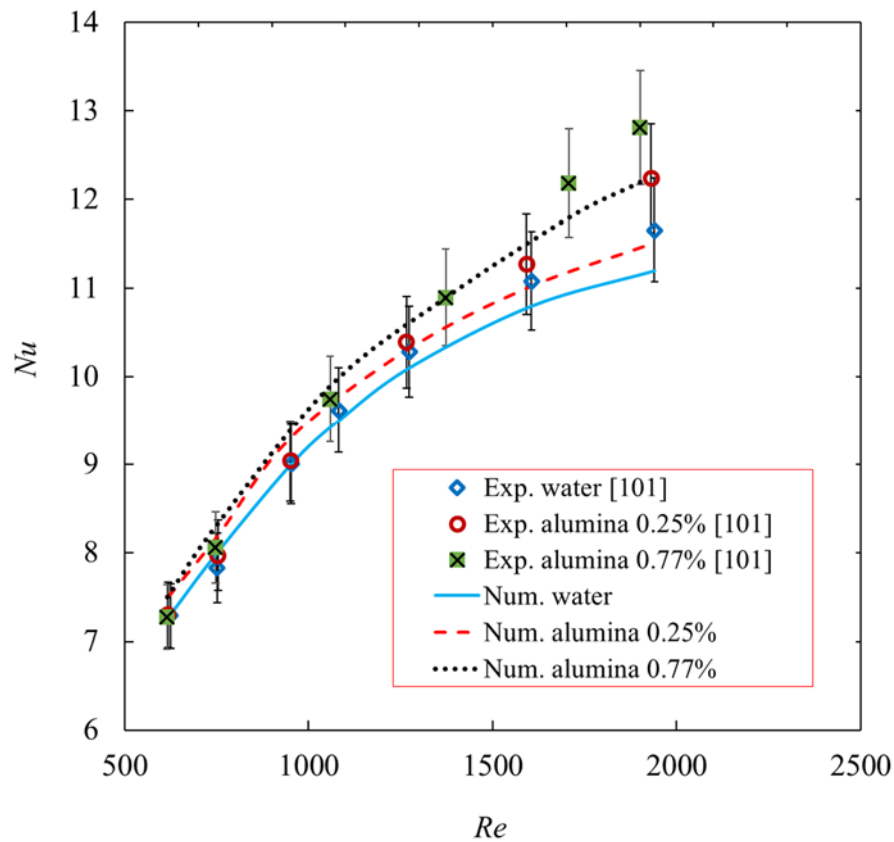
Figure 4.23: Nusselt number vs Reynolds number predicted by DPM compared with experimental measurements with 5% error bar

One of the most important issues in interactions between fluid and solid is to understand the significance of forces involved. The drag force can be considered the final result of all other forces. The importance of each force acting on the nanoparticles compared with the drag force is shown in Figure 4.24. Because some forces only interact in some specific directions, for example, gravity only in the Y-direction, the comparison is therefore presented in X-, Y- and Z-directions separately. The following conclusion can be made: The gravitational force can be safely neglected in laminar force flow for nanoparticles. The pressure gradient and virtual mass forces due to acceleration of the particle almost contain the minimum impacts on the particle in all directions. Due to lower ranges of particle concentration (<1% vol.), the long range attraction force of Van der Waals has a small effect on particle migration. It is noted that this force highly depends on particle-to-particle distance. The electric double-layer force can play a key role in particle-to-particle

80

interactions, but it depends on the final nanofluid solution and pH value. The pH is assumed 3 in this simulation.
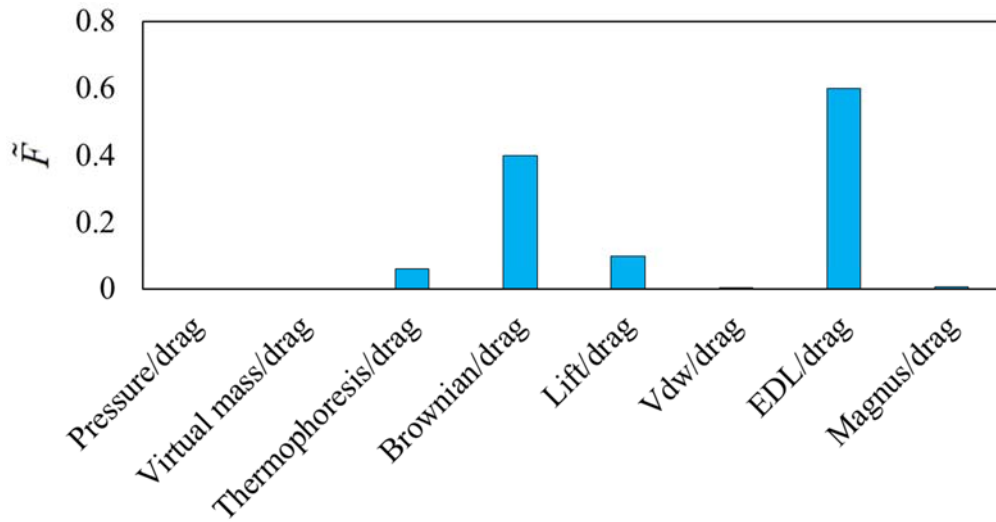
(a)
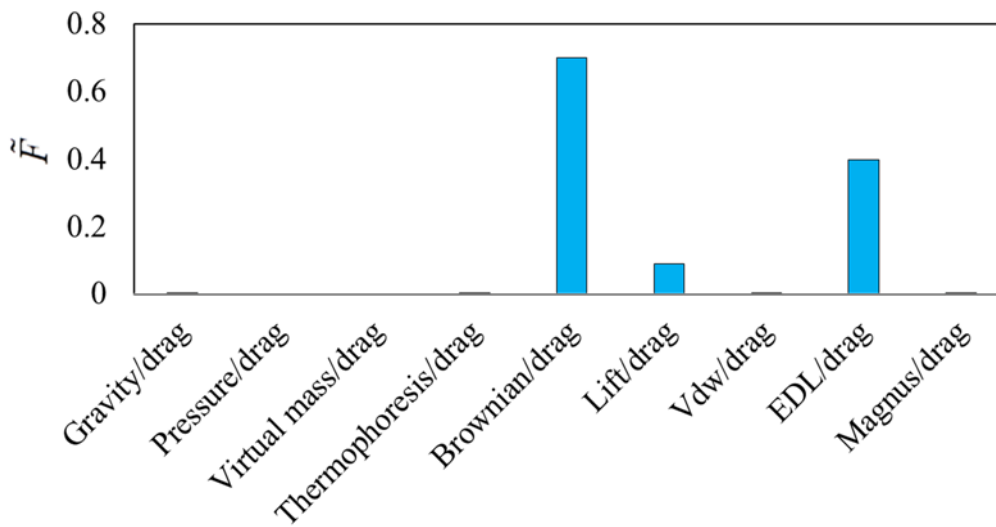
(b)
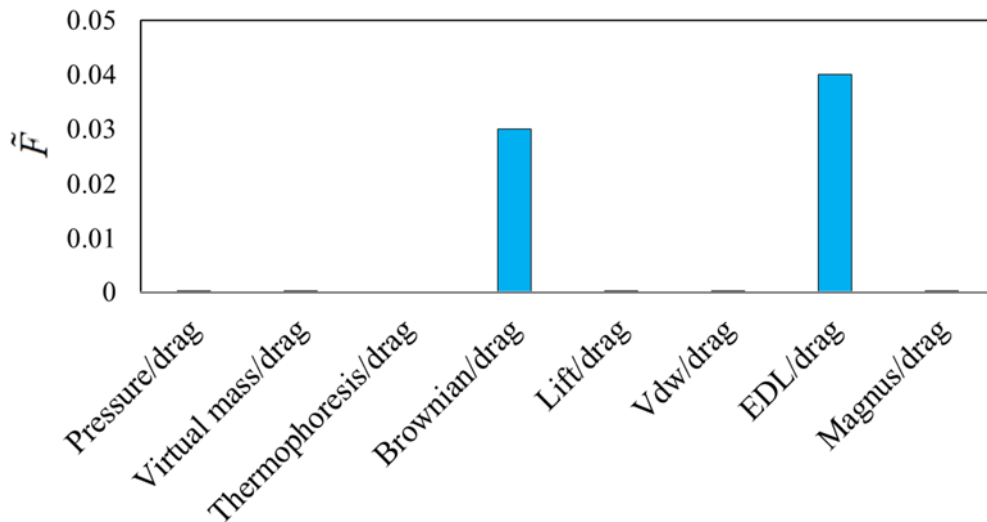
(c)

Figure 4.24: Comparative study of interaction forces between fluid and nanoparticles in a) X- b) Y- and c) Z-direction for alumina nanofluid 0.77% vol. Z-axis is flow direction

Because the main flow occurs in the Z-direction, the magnitude of the repulsive electric double-layer force decreases compared with drag force in this direction. The other important force is lift force due to shear stresses near to the wall towards the centre of the tube. This force can be strong in laminar nanofluid flow and mainly in the radial direction. Thermophoretic force only acts in radial direction due to temperature gradient. Thus, it can influence the particle migration near to the wall and it decreases towards the centre of the tube. Because the straight flow inside a circular tube can somehow be a rotational flow, the lift force due to rotation of the particle in the flow is taken into account, called Magnus force. The magnitude analysis indicates that this force can influence the particle migration in the radial direction, but not as much as Saffman's lift force. Brownian random force is the only effective force in all three directions and cannot be neglected, although the strong flow field and drag force in the Z-direction can even suppress those effects.

The distribution of nanoparticle concentration at different cross-sections of the microchannel is illustrated in Figure 4.25. The concentration boundary layer immediately

82

started growing after injection at the inlet and the early development was captured at Z=0.5 mm. Then, the particles gradually pushed away from the wall towards the centre of the microchannel due to thermophoresis, Saffman's lift and Magnus lift forces, seen at Z=1 mm. No bulk nanoparticles were concentrated near to the wall and the concentration area would be the middle way of the wall and microchannel centre in the developed flow region. This could also be explained by the fact that the tracking of the particles showed no hitting on the wall. Thus, none of the wall boundary conditions were met by the nanoparticles. In addition, the distribution was almost symmetric, meaning that the radial migration of the particles was the more dominant phenomenon than angular movement.

The angular movement of nanoparticles at different radial positions is presented in Figure 4.26. r=0.028 mm is the closest particle to the centre of the microchannel at the inlet and r=0.24mm means the particle near to the wall (the radius of the microchannel is 0.5 mm). The oscillations in angular position of the nanoparticles were clearly caused by the random Brownian motion in three directions. For the particle near to the wall, these random movements turned to less amplitude due to the effects of strong shear stress.

a)   b)

c)   d)
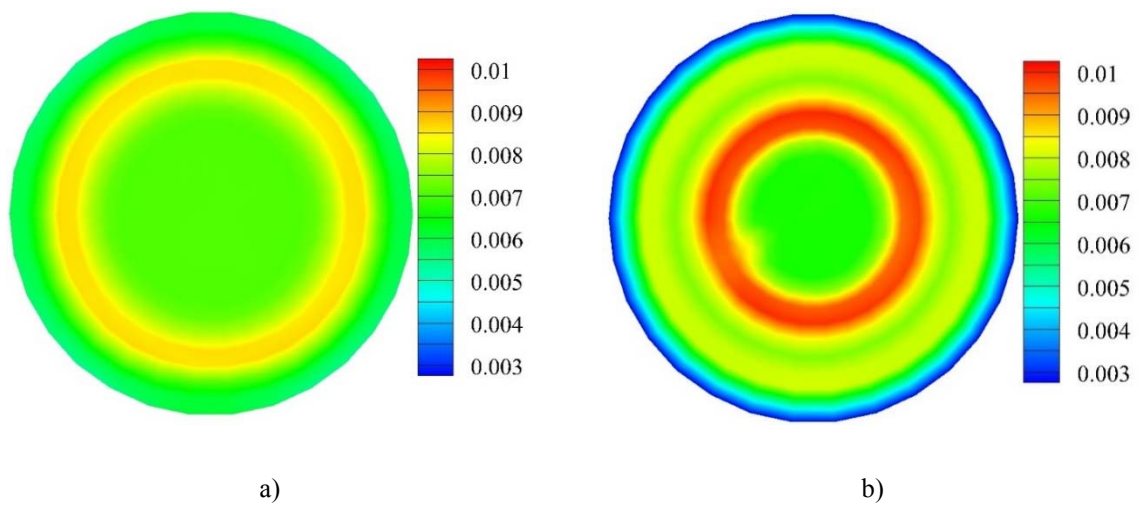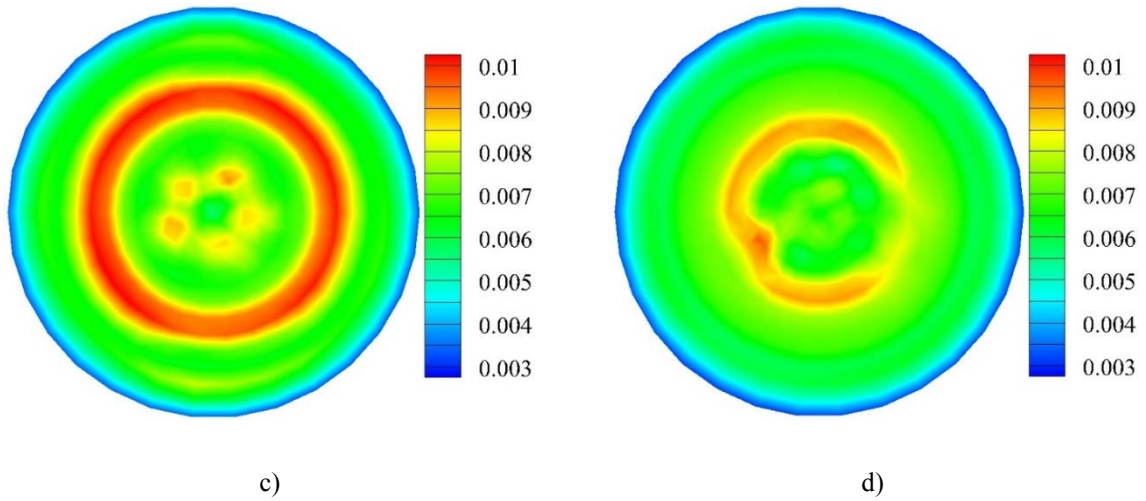
Figure 4.25: Concentration distribution of alumina nanoparticles 0.77% vol. at different cross-sections in flow direction in a horizontal microchannel at a) $Z = 0.5$ mm b) $Z = 1$ mm c) $Z = 10$ mm d) $Z = 100$ mm.

On the other hand, the maximum amplitude of the angular displacement occurred for the particles near to the centre of the microchannel. It meant that the Brownian motion was the dominant phenomenon near to the centre with minimum shear stresses and lift forces. Moreover, because the velocity magnitude got higher as the nanoparticles approached the centre line of the microchannel, it took longer to pass the entire domain reaching the outlet, shown in Figure 4.26a.

a)

84

b)

c)

d)

85

e)
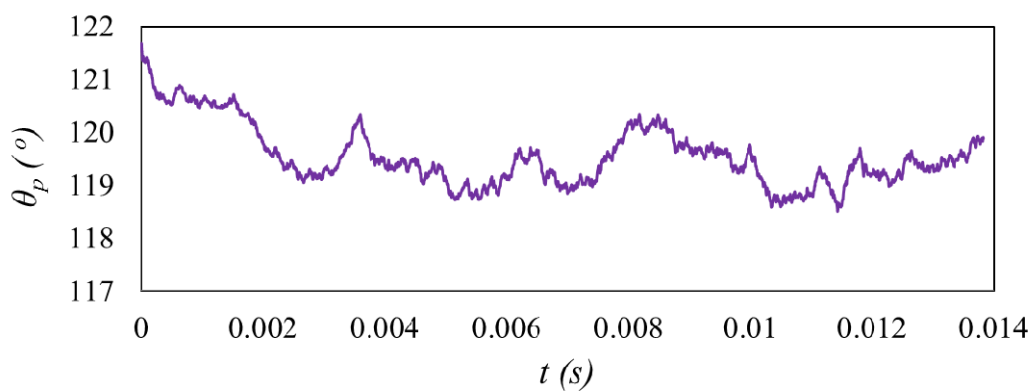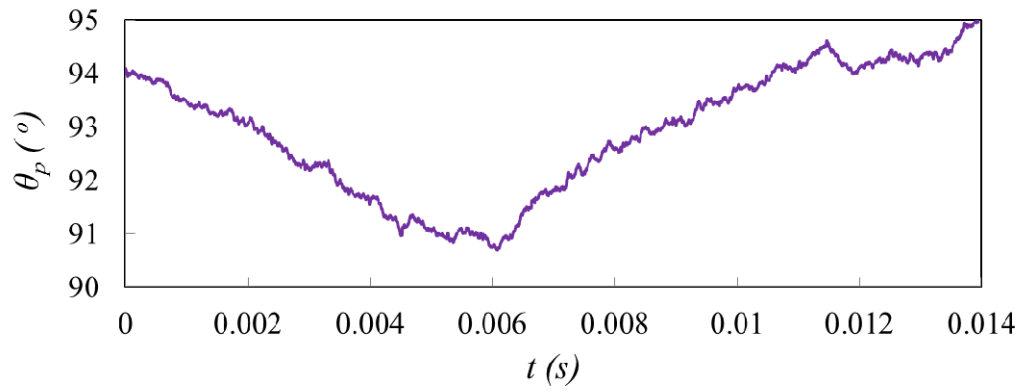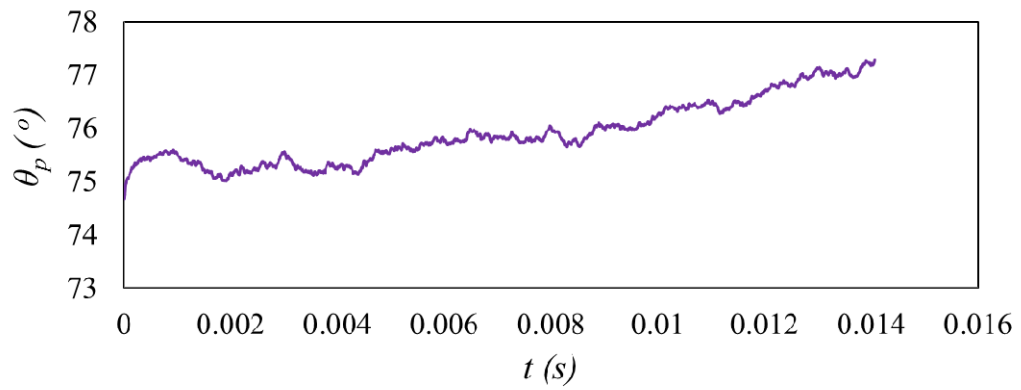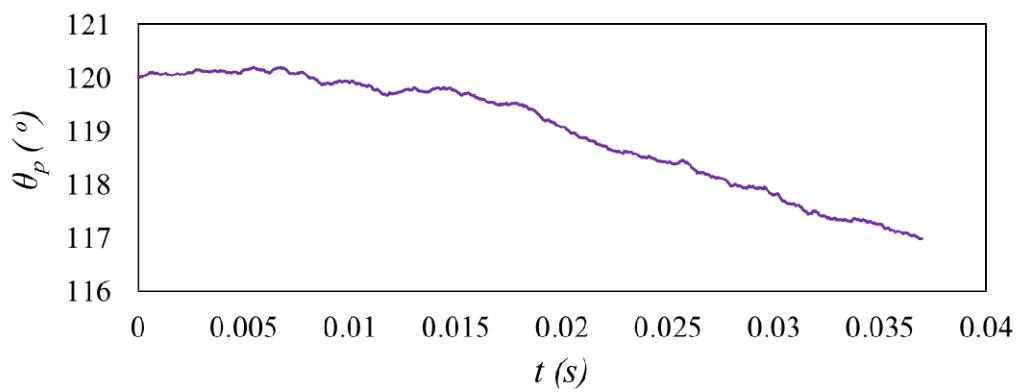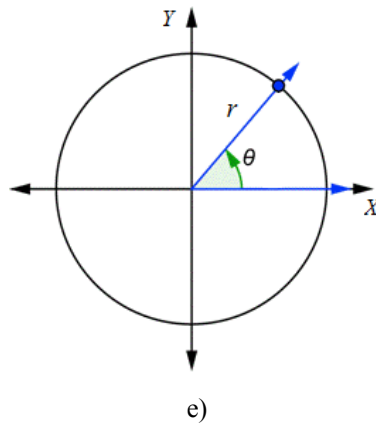
Figure 4.26: Angular movement of the nanoparticles from inlet to outlet at different radial positions. *r* is the initial radial position of the nanoparticle at the inlet or injection position. a) *r* = 0.028 mm b) *r* = 0.045 mm c) *r* = 0.061 mm d) *r* = 0.24 mm e) Polar coordinate system at a cross-section of the microchannel.

The radial migration of nanoparticles from the injection plane to the outlet is shown in Figure 4.26. The particles near to the wall took the highest displacement in radial direction due to all the forces caused by the temperature gradient and lift forces. Because most of the important interaction forces acted in the radial direction, such as thermophoresis, Saffman's and Magnus forces, the oscillations in displacement from one frame to another would be small due to fewer impacts of random Brownian motion. The trend of radial migration was more or less similar in all the nanoparticles. They took the path towards the centre of the microchannel while the concentration boundary layer grew. Then, the displacement grew up to reach the asymptotic value in the developed flow region.
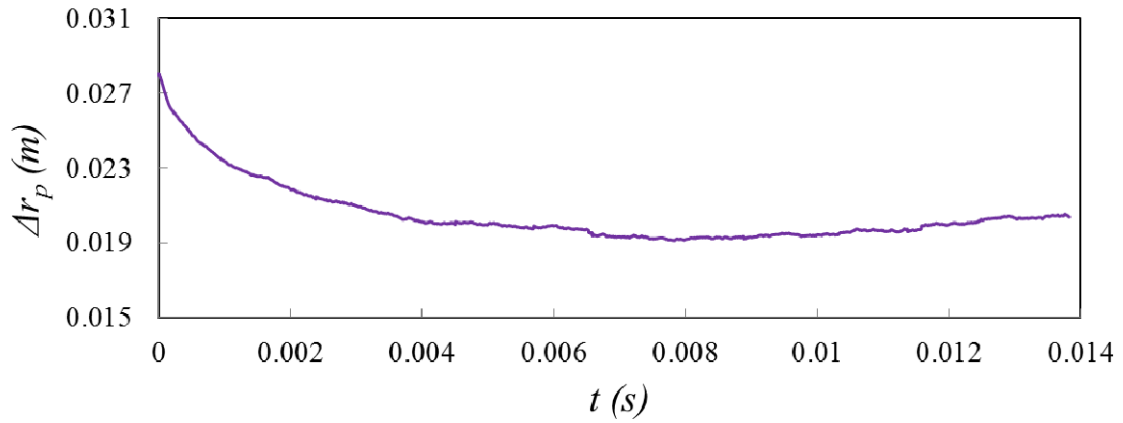
a)
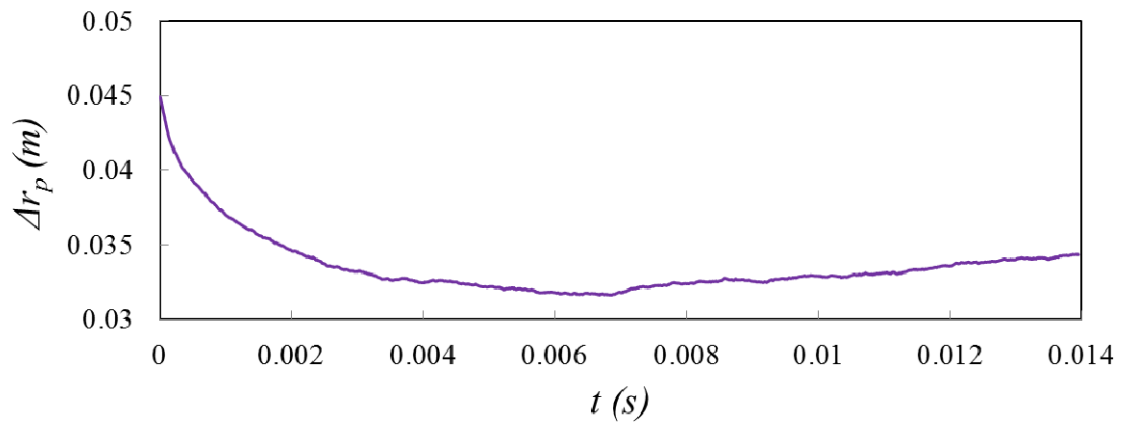
b)
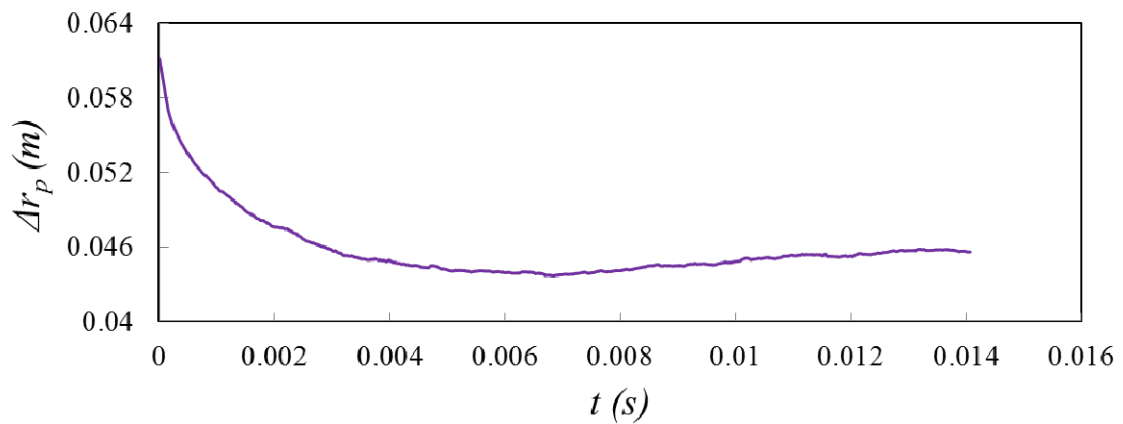
c)

(To be continued on the next page)

87
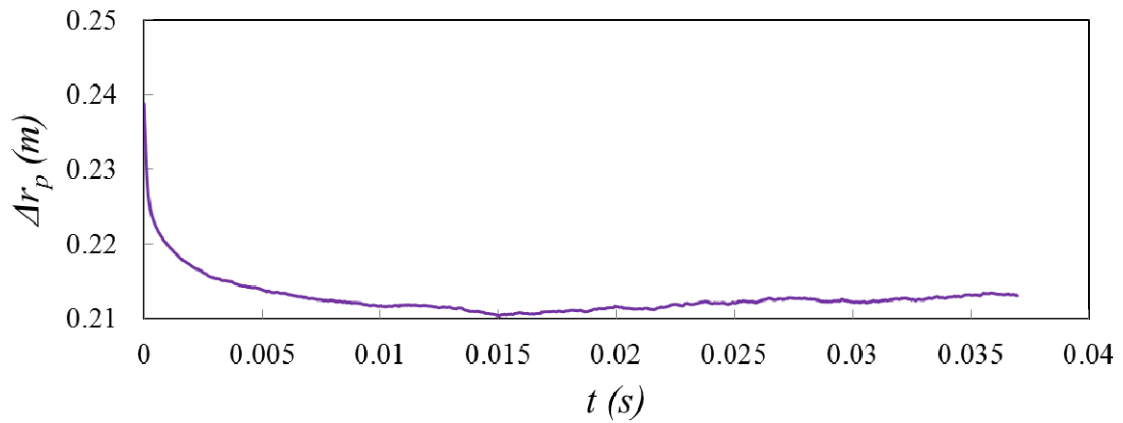
d)

Figure 4.27: Radial displacement of nanoparticles from inlet to outlet
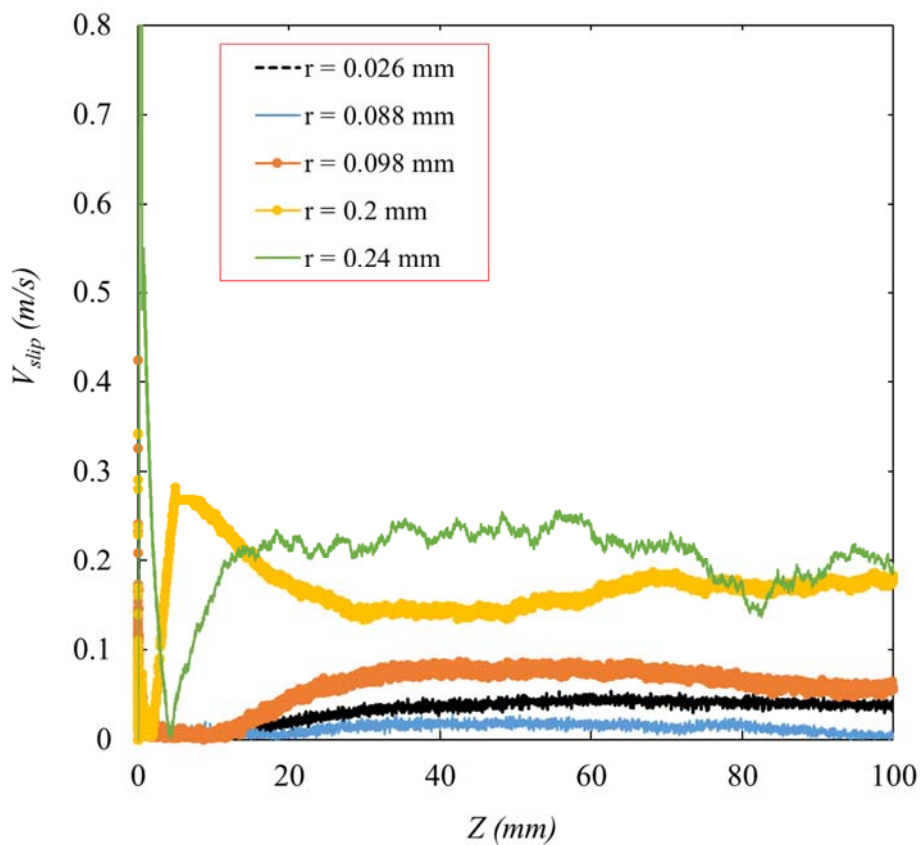
Figure 4.28: Evolution of relative velocity between nanoparticles and fluid in the microchannel at different injected radial positions

One of the most important parameters in solid-liquid flows is the slip velocity between particles and base fluid, shown in Figure 4.28. Due to migration of the nanoparticles in

88

the radial direction, the magnitude of the slip velocity may considerably vary in the computational domain. The radial positions of r = 0.2 mm and r = 0.24 mm were near to the wall and inside the hydrodynamic boundary layer of the flow. Hence early expanded slip velocity at the entrance region was expected for these nanoparticles.

a)

b)

89
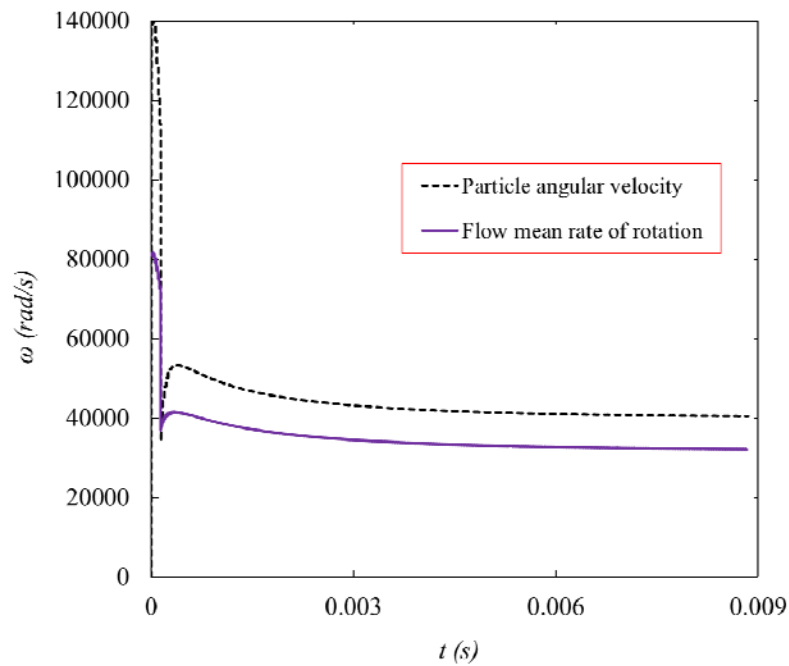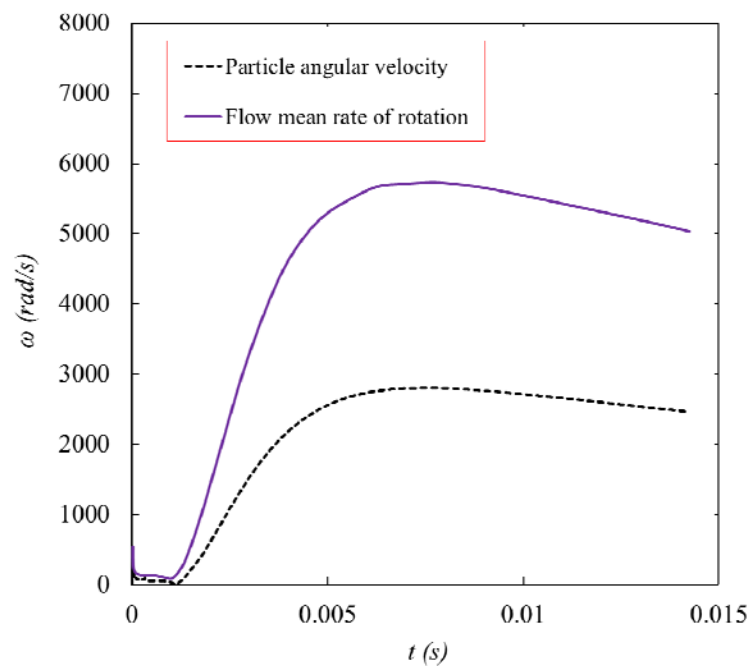
Figure 4.29: Nanoparticles and flow angular velocity a) near to the wall and b) centre of the microchannel.

But for other particles, for instance, near to centroid regions at r=0.026 mm, the particles were involved in hydrodynamic boundary layer further, after Z=20 mm in this case. It meant that the slip velocity only started growing after Z=20 mm in the flow direction for those nanoparticles.

The effective parameter for determining the Magnus force is the angular velocity of the nanoparticles and vorticity of the fluid flow. The parallel flow in a microchannel is a rotational flow with the condition $\nabla \times \mathbf{v}_c \neq 0$. The nanoparticles gained their rotation mainly from the flow and it finally led to Magnus lift force, especially near to the wall. The nanoparticle angular velocity is compared with flow mean rotation $\frac{1}{2}\nabla \times \mathbf{v}_c$ in Figure 4.29. The values of angular velocity near to the wall were enormous compared with the centroid region and could not be neglected in Magnus force. The particles could increase the rotation also due to their inertia and Brownian motion. The noticeable amount of shear stress at the entrance region produced the highest values of angular rotation, shown in Figure 4.29a.

CONCLUSION

In this chapter, the models developed in Chapter 3 were employed in simulations and the results were explained. Published experimental measurements were used to validate the results of heat transfer and hydrodynamic features. It was found that the mixture model might be the most straightforward model to characterise the heat transfer features of nanofluid due to high dependency of the model on the thermophysical properties. But, it could not provide a proper understanding of nanoparticle distribution and migration in the flow. To improve the shortcoming of the mixture model, the important slip mechanisms were implemented in the simulations. The results showed that the diffusion caused by temperature and concentration gradient, electrostatic forces and gravity played key roles in nanofluid distribution in natural convection.

Discrete phase modelling was used to simulate nanoparticle flow in a microchannel. The advantage of this model has concerned the real physical model of the simulations where there was no need for extra thermophysical properties. The results for DPM were found in good agreement for laminar flow in a horizontal microchannel. Most of the possible phenomena involved in nanoparticle interactions were included. Brownian random motion and electrostatic forces were found to be present in all the domains, but others were effective only near to the wall.

The other forces including Saffman's lift, Magnus lift and thermophoresis were scalable only in the radial direction. Virtual mass, pressure gradient and gravity can be safely neglected in nanofluid laminar flow. The impacts of the lift due to rotation of nanoparticles in rotational flow or Magnus force could be observed on particle radial distribution. Brownian motion was found the essential reason of particle migration, especially angular displacement, but the impacts deteriorated when the nanoparticles approached the wall. Higher amplitude of the angular displacement occurred near to the centre of the microchannel. Van der Waals attraction force highly depended on particle-to-particle distance and could be weak for volume fractions of less than 1%. On the other hand, the electric double-layer force could play an important role in particle distribution.

The abilities and weaknesses of the mixture model for nanofluid are summarised as follows:

The mixture model results highly depend on transport properties coming from experimentation. It considers nanofluid as two phases. The thermophysical property correlations for nanofluid are not universal and change by base fluid and nanoparticles. The effects of slip mechanisms such as thermophoresis and Brownian can be presented as diffusion terms in mixture equations and need to be implemented in the program.

The abilities and weaknesses of DPM for nanofluid are summarised as follows:

For the DPM model, there is no need for the nanofluids' properties, but appropriate interaction or diffusion forces, empirically or analytically. It treats the nanofluid as base fluid and solid separately, as it is in reality. The empirical correlations for DPM

91

interaction forces are not extensive and can be employed in most of the cases. The velocity is calculated for fluid and solid separately and eventually, the relative velocity between them is the most important parameter.

There are some aspects of nanofluid simulations which are recommended here: possibility of clustering and agglomeration inside the flow, and somehow sedimentation, size distribution of the nanoparticles in the computational domain for the mixture model, finding a way to combine both the mixture model and DPM, further development of modelling the electric double layer around the particle.

.

CHAPTER 5:   CONCLUSIONS AND RECOMMENDATIONS

SUMMARY

The effect of the heat transfer enhancement of nanofluid has been the focus of many researchers in recent years. A large number of experimental studies proved the effectiveness of the presence of nanoparticles in a base fluid. Because of the complexity of the interactions between solid and liquid, only a few methods have been developed in recent years regarding the simulations. Most of the studies in this field of science were briefly presented in Chapter 2 of this thesis.

The aim of this investigation is to develop new ideas in nanofluid flow regarding the solid-liquid interaction phenomena. The mixture model as a common model in simulations of nanofluid flow was presented and developed in Chapter 3. New slip velocity was developed and implemented through some UDFs in ANSYS-Fluent. Only thermophoresis and concentration diffusions were implemented in mass and energy equations separately. The other interactions such as pressure gradient, virtual mass, lift, gravity and electrostatic slip mechanisms were implemented in momentum equation as a separate UDF.

Due to many restrictions in DPM, only a few studies were found in literature. In this study, an attempt was made to consider most of the phenomena involved in nanofluid mixtures in DPM. The validity of the final results was compared with other experimental measurements. The findings covered the heat transfer and hydrodynamic features of the flow, nanoparticle migration and concentration distribution. Electrostatic forces were implemented in ANSYS-Fluent through some UDFs. Also, the new heat transfer equation of particles was implemented as a new heat law with small predefined time steps in a separate UDF.

CONCLUSIONS

Two different flow regimes were investigated in this study consisting of forced and natural convective flows. Natural convection was studied in a rectangular cavity with

93

nanofluid suspended and simulated with the developed mixture model. The results of heat transfer were found in good agreement with experimental data. The conventional mixture model in CFD software only considered the effect of the gravitational force as the slip velocity. This provided the wrong concentration distribution at the vicinity of the walls. Higher absolute value and gradient of volume fraction was predicted close to the walls by the proposed method. The results showed that the diffusion caused by temperature and concentration gradient, electrostatic forces and gravity played key roles in nanofluid distribution in natural convection. The hydrodynamic boundary layer was the same for most of the cases. The concentration boundary layer of zinc oxide nanoparticles was found thin close to the wall and it had no effect on the velocity profile. It was mainly caused by buoyancy force on zinc oxide nanoparticles with higher density than alumina particles. The thermal boundary layer was the same for both alumina and zinc oxide nanofluids. The increase of nanoparticle density and volume fraction from alumina to zinc oxide clearly influenced the hydrodynamic boundary layer, particularly at the beginning of the growth.

The discrete phase modelling was used to simulate nanoparticle flow in a horizontal microchannel with laminar flow. This model was developed for particles in sizes larger than nanoscale. Hence many of the interactions involved in micro-sizes might be negligible in nano-sizes and other phenomena should be implemented. The heat transfer results of DPM were found in good agreement with experimental data. Most of the possible phenomena involved in nanoparticle interactions were included. Brownian random motion and electrostatic forces were found to be present in all the domains, but other parameters were effective only near to the wall. The other forces including Saffman's lift, Magnus lift and thermophoresis were scalable only in the radial direction and mainly near to the wall. Virtual mass, pressure gradient and gravity could be safely neglected in nanofluid laminar flow. The lift due to rotation of nanoparticles in rotational flow or Magnus force could have an impact on particle radial distribution. Brownian motion was found to be the most significant cause of particle migration, especially angular displacement. However, the effect deteriorated when the particle approached the wall because of the presence of other forces. Higher amplitude of the angular

displacement occurred for the particles near to the centre of the microchannel. It meant that Brownian motion was the phenomenon near to the centre with minimum shear stresses and lift forces. Van der Waals attraction force highly depended on the particle-to-particle distance and could be weak for volume fraction less than 1%. On the other hand, the electric double-layer force could play a key role in particle distribution, depending on the pH of the solution and zeta potential on the particles. The analysis of slip velocity between nanoparticles and base fluid showed that, firstly, a stronger shear flow region produced higher values of slip velocity. Secondly, the magnitude of the slip velocity was found one order less than the fluid velocity, or even less.

In summary, the abilities of both the developed mixture model and DPM were studied in this research. The following differences between these models were indicated:

1. The mixture model considered nanofluid as two phases. DPM treated the nanofluid as base fluid and solid separately, as in reality.

2. The effect of slip mechanisms such as thermophoresis and Brownian could be presented as diffusion terms in mixture equations and needed to be implemented in the program. In DPM, velocity was calculated for fluid and solid separately and eventually, the relative velocity between them was the most important parameter.

RECOMMENDATIONS

There are many untouched aspects of nanofluid in terms of both experimentations and simulations. The following recommendations are provided for further investigation:

1. Only a few experimental measurements are available in literature for nanofluids to show the precise amount of heat transfer and hydrodynamic feature enhancement. Therefore, further experimental studies are recommended to provide the concentration distribution during convective heat transfer

2. One of the important aspects of nanofluid is the possibility of clustering and agglomeration inside the flow, and somehow sedimentation. This phenomenon are too complicated and should be considered in future simulation

95

3. The mixture model cannot consider the size distribution of the nanoparticles in the computational domain, as DPM does. Further development for this case is needed.

4. Finding a way to combine both the mixture model and DPM can be one of the new approaches in this field of study.

5. Because the liquid electrons are rearranged around a particle, called double layer, it can be assumed that a new type of phase is added to the system. The surface tension between this new phase and base fluid can be one of the phenomena involved. Further investigation is needed.

REFERENCES

[1]   K.S. Hwang, S.P. Jang, S.U.S. Choi, Flow and convective heat transfer characteristics of water-based Al2O3 nanofluids in fully developed laminar flow regime, Int. J. Heat Mass Transf. 52 (2009) 193–199. doi:10.1016/j.ijheatmasstransfer.2008.06.032.

[2]   Y. Ding, H. Alias, D. Wen, R.A. Williams, Heat transfer of aqueous suspensions of carbon nanotubes (CNT nanofluids), Int. J. Heat Mass Transf. 49 (2006) 240–250. doi:10.1016/j.ijheatmasstransfer.2005.07.009.

[3]   D. Wen, Y. Ding, Experimental investigation into convective heat transfer of nanofluids at the entrance region under laminar flow conditions, Int. J. Heat Mass Transf. 47 (2004) 5181–5188. doi:10.1016/j.ijheatmasstransfer.2004.07.012.

[4]   Y. Yang, Z.G. Zhang, E.A. Grulke, W.B. Anderson, G. Wu, Heat transfer properties of nanoparticle-in-fluid dispersions (nanofluids) in laminar flow, Int. J. Heat Mass Transf. 48 (2005) 1107–1116. doi:10.1016/j.ijheatmasstransfer.2004.09.038.

[5]   Y. He, Y. Jin, H. Chen, Y. Ding, D. Cang, H. Lu, Heat transfer and flow behaviour of aqueous suspensions of TiO 2 nanoparticles (nanofluids) flowing upward through a vertical pipe, Int. J. Heat Mass Transf. 50 (2007) 2272–2281.

[6]   D. Kim, Y. Kwon, Y. Cho, C. Li, S. Cheong, Y. Hwang, J. Lee, D. Hong, S. Moon, Convective heat transfer characteristics of nanofluids under laminar and turbulent flow conditions, Curr. Appl. Phys. 9 (2009) 119–123. doi:10.1016/j.cap.2008.12.047.

[7]   U. Rea, T. McKrell, L. wen Hu, J. Buongiorno, Laminar convective heat transfer and viscous pressure loss of alumina-water and zirconia-water nanofluids, Int. J. Heat Mass Transf. 52 (2009) 2042–2048. doi:10.1016/j.ijheatmasstransfer.2008.10.025.

[8]   K.B. Anoop, T. Sundararajan, S.K. Das, Effect of particle size on the convective heat transfer in nanofluid in the developing region, Int. J. Heat Mass Transf. 52

97

(2009) 2189–2195. doi:10.1016/j.ijheatmasstransfer.2007.11.063.

[9] B. Kolade, K.E. Goodson, J.K. Eaton, Convective Performance of Nanofluids in a Laminar Thermally Developing Tube Flow, J. Heat Transfer. 131 (2009) 52402. doi:10.1115/1.3013831.

[10] W.-Y. Lai, Experiments on Laminar Convective Heat Transfer with gamma-Al 2O3 Nanofluids, Arizona State University, 2010.

[11] Z. Zhang, Experimental evaluation of heat transfer characteristics of silica nanofluid, Massachusetts Institute of Technology, 2010.

[12] M.M. Derakhshan, M.A. Akhavan-Behabadi, S.G. Mohseni, Experiments on mixed convection heat transfer and performance evaluation of MWCNT-Oil nanofluid flow in horizontal and vertical microfin tubes, Exp. Therm. Fluid Sci. 61 (2015) 241–248. doi:10.1016/j.expthermflusci.2014.11.005.

[13] Y.L. Zhai, G.D. Xia, X.F. Liu, Y.F. Li, Heat transfer enhancement of Al2O3-H2O nanofluids flowing through a micro heat sink with complex structure, Int. Commun. Heat Mass Transf. 66 (2015) 158–166. doi:10.1016/j.icheatmasstransfer.2015.05.025.

[14] C.. Tang, S. Tiwari, M.W. Cox, Viscosity and friction factor of aluminum oxide--water nanofluid flow in circular tubes, J. Nanotechnol. Eng. Med. 4 (2013) 21004.

[15] A.T. Utomo, E.B. Haghighi, A.I.T. Zavareh, M. Ghanbarpourgeravi, H. Poth, R. Khodabandeh, B. Palm, A.W. Pacek, The effect of nanoparticles on laminar heat transfer in a horizontal tube, Int. J. Heat Mass Transf. 69 (2014) 77–91. doi:10.1016/j.ijheatmasstransfer.2013.10.003.

[16] D. Liu, L. Yu, Single-phase thermal transport of nanofluids in a minichannel, J. Heat Transfer. 133 (2011) 31009. doi:10.1115/1.4002462.

[17] B.C. Pak, Y.I. Cho, Hydrodynamic and heat transfer study of dispersed fluids with submicron metallic oxide particles, Exp. Heat Transf. 11 (1998) 151–170.

doi:10.1080/08916159808946559.

[18]   Y. Xuan, Q. Li, Investigation on convective heat transfer and flow features of nanofluids, J. Heat Transfer. 125 (2003) 151. doi:10.1115/1.1532008.

[19]   W. Williams, J. Buongiorno, L.-W. Hu, Experimental investigation of turbulent convective heat transfer and pressure loss of alumina/water and zirconia/water nanoparticle colloids (nanofluids) in horizontal tubes, J. Heat Transfer. 130 (2008) 42412. doi:10.1115/1.2818775.

[20]   W. Yu, D.M. France, D.S. Smith, D. Singh, E. V. Timofeeva, J.L. Routbort, Heat transfer to a silicon carbide/water nanofluid, Int. J. Heat Mass Transf. 52 (2009) 3606–3612. doi:10.1016/j.ijheatmasstransfer.2009.02.036.

[21]   W. Duangthongsuk, S. Wongwises, An experimental study on the heat transfer performance and pressure drop of TiO2-water nanofluids flowing under a turbulent flow regime, Int. J. Heat Mass Transf. 53 (2010) 334–344. doi:10.1016/j.ijheatmasstransfer.2009.09.024.

[22]   L.S. Sundar, K. V. Sharma, Turbulent heat transfer and friction factor of Al2O3 Nanofluid in circular tube with twisted tape inserts, Int. J. Heat Mass Transf. 53 (2010) 1409–1416. doi:10.1016/j.ijheatmasstransfer.2009.12.016.

[23]   S. Torii, Y. Satou, Y. Koito, Experimental study on convective thermal-fluid flow transport phenomena in circular tube using nanofluids, Int. J. Green Energy. 7 (2010) 289–299. doi:10.1080/15435071003796061.

[24]   S.S. Ferrouillat, A.A. Bontemps, J.-P.J.P. Ribeiro, J.-A.A. Gruss, O. Soriano, Hydraulic and heat transfer study of SiO 2/water nanofluids in horizontal tubes with imposed wall temperature boundary conditions, Int. J. Heat Fluid Flow. 32 (2011) 424–439. doi:10.1016/j.ijheatfluidflow.2011.01.003.

[25]   A.R. Sajadi, M.H. Kazemi, Investigation of turbulent convective heat transfer and pressure drop of TiO2/water nanofluid in circular tube, Int. Commun. Heat Mass

99

Transf. 38 (2011) 1474–1478. doi:10.1016/j.icheatmasstransfer.2011.07.007.

[26] L.G. Asirvatham, B. Raja, D. Mohan Lal, S. Wongwises, Convective heat transfer of nanofluids with correlations, Particuology. 9 (2011) 626–631. doi:10.1016/j.partic.2011.03.014.

[27] S. Suresh, M. Chandrasekar, P. Selvakumar, Experimental studies on heat transfer and friction factor characteristics of CuO/water nanofluid under laminar flow in a helically dimpled tube, Heat Mass Transf. Und Stoffuebertragung. 48 (2012) 683–694. doi:10.1007/s00231-011-0917-2.

[28] L.S. Sundar, M.T. Naik, K.V. Sharma, M.K. Singh, T.C. Siva Reddy, Experimental investigation of forced convection heat transfer and friction factor in a tube with Fe3O4 magnetic nanofluid, Exp. Therm. Fluid Sci. 37 (2012) 65–71. doi:10.1016/j.expthermflusci.2011.10.004.

[29] W.H. Azmi, K. V. Sharma, P.K. Sarma, R. Mamat, S. Anuar, V. Dharma Rao, Experimental determination of turbulent forced convection heat transfer and friction factor with SiO2 nanofluid, Exp. Therm. Fluid Sci. 51 (2013) 103–111. doi:10.1016/j.expthermflusci.2013.07.006.

[30] B. Sahin, G.G. Gültekin, E. Manay, S. Karagoz, Experimental investigation of heat transfer and pressure drop characteristics of Al2O3-water nanofluid, Exp. Therm. Fluid Sci. 50 (2013) 21–28. doi:10.1016/j.expthermflusci.2013.04.020.

[31] K. Wusiman, H. Chung, J.N. Md, A. Handry, Y. Eom, J. Kim, H. Jeong, Heat transfer characteristics of nanofluid through circular tube, J. Cent. South Univ. 20 (2013) 142–148. doi:10.1007/s11771-013-1469-z.

[32] L.S. Sundar, M.K. Singh, I. Bidkin, A.C.M. Sousa, Experimental investigations in heat transfer and friction factor of magnetic Ni nanofluid flowing in a tube, Int. J. Heat Mass Transf. 70 (2014) 224–234. doi:10.1016/j.ijheatmasstransfer.2013.11.004.

[33]   N. Putra, W. Roetzel, S.K. Das, Natural convection of nano-fluids, Heat Mass Transf. Und Stoffuebertragung. 39 (2003) 775–784. doi:10.1007/s00231-002-0382-z.

[34]   D. Wen, Y. Ding, Formulation of nanofluids for natural convective heat transfer applications, Int. J. Heat Fluid Flow. 26 (2005) 855–864. doi:10.1016/j.ijheatfluidflow.2005.10.005.

[35]   A.G.A. Nnanna, Experimental Model of Temperature-Driven Nanofluid, J. Heat Transfer. 129 (2007) 697. doi:10.1115/1.2717239.

[36]   B.H. Chang, A.F. Mills, E. Hernandez, Natural convection of microparticle suspensions in thin enclosures, Int. J. Heat Mass Transf. 51 (2008) 1332–1341. doi:10.1016/j.ijheatmasstransfer.2007.11.030.

[37]   C.H. Li, G.P. Peterson, Experimental studies of natural convection heat transfer of Al2O3/DI water nanoparticle suspensions (Nanofluids), Adv. Mech. Eng. 2010 (2009). doi:10.1155/2010/742739.

[38]   C.J. Ho, W.K. Liu, Y.S. Chang, C.C. Lin, Natural convection heat transfer of alumina-water nanofluid in vertical square enclosures: An experimental study, Int. J. Therm. Sci. 49 (2010) 1345–1353. doi:10.1016/j.ijthermalsci.2010.02.013.

[39]   R. Ni, S.Q. Zhou, K.Q. Xia, An experimental investigation of turbulent thermal convection in water-based alumina nanofluid, Phys. Fluids. 23 (2011). doi:10.1063/1.3553281.

[40]   M.R. Khadangi Mahrood, S.G. Etemad, R. Bagheri, Free convection heat transfer of non Newtonian nanofluids under constant heat flux condition, Int. Commun. Heat Mass Transf. 38 (2011) 1449–1454. doi:10.1016/j.icheatmasstransfer.2011.08.012.

[41]   Y. Hu, Y. He, S. Wang, Q. Wang, H. Inaki Schlaberg, Experimental and Numerical Investigation on Natural Convection Heat Transfer of TiO2–Water

101

Nanofluids in a Square Enclosure, J. Heat Transfer. 136 (2013) 22502. doi:10.1115/1.4025499.

[42] S.S. Rao, A. Srivastava, Interferometry-based whole field investigation of heat transfer characteristics of dilute nanofluids, Int. J. Heat Mass Transf. 79 (2014) 166–175. doi:10.1016/j.ijheatmasstransfer.2014.07.097.

[43] C.J. Ho, D. Chen, W. Yan, O. Mahian, Buoyancy-driven flow of nanofluids in a cavity considering the Ludwig – Soret effect and sedimentation : Numerical study and experimental validation, 77 (2014) 684–694. doi:10.1016/j.ijheatmasstransfer.2014.05.059.

[44] H. Li, Y. He, Y. Hu, B. Jiang, Y. Huang, Thermophysical and natural convection characteristics of ethylene glycol and water mixture based ZnO nanofluids, Int. J. Heat Mass Transf. 91 (2015) 385–389. doi:10.1016/j.ijheatmasstransfer.2015.07.126.

[45] H. Moradi, B. Bazooyar, A. Moheb, S.G. Etemad, Optimization of natural convection heat transfer of Newtonian nanofluids in a cylindrical enclosure, Chinese J. Chem. Eng. 23 (2015) 1266–1274. doi:10.1016/j.cjche.2015.04.002.

[46] S.S. Rao, A. Srivastava, Interferometric study of natural convection in a differentially-heated cavity with Al2O3-water based dilute nanofluids, Int. J. Heat Mass Transf. 92 (2016) 1128–1142. doi:10.1016/j.ijheatmasstransfer.2015.09.074.

[47] Y. Xuan, W. Roetzel, Conceptions for heat transfer correlation of nanofuids, Int. J. Heat Mass Transf. 43 (2000) 3701–3707.

[48] S. Sidi El Becaye Maiga, S.J. Palm, C.T. Nguyen, G. Roy, N. Galanis, Heat transfer enhancement by using nanofluids in forced convection flows, Int. J. Heat Fluid Flow. 26 (2005) 530–546. doi:10.1016/j.ijheatfluidflow.2005.02.004.

[49] J. Buongiorno, Convective Transport in Nanofluids, J. Heat Transfer. 128 (2006) 240. doi:10.1115/1.2150834.

102

[50]   A. Akbarinia, R. Laur, Investigating the diameter of solid particles effects on a laminar nanofluid flow in a curved tube using a two phase approach, Int. J. Heat Fluid Flow. 30 (2009) 706–714. doi:10.1016/j.ijheatfluidflow.2009.03.002.

[51]   V. Bianco, O. Manca, S. Nardini, Numerical investigation on nanofluids turbulent convection heat transfer inside a circular tube, Int. J. Therm. Sci. 50 (2011) 341–349. doi:10.1016/j.ijthermalsci.2010.03.008.

[52]   R. Mokhtari Moghari, A. Akbarinia, M. Shariat, F. Talebi, R. Laur, Two phase mixed convection Al2O3-water nanofluid flow in an annulus, Int. J. Multiph. Flow. 37 (2011) 585–595. doi:10.1016/j.ijmultiphaseflow.2011.03.008.

[53]   Z. Haddad, E. Abu-Nada, H.F. Oztop, A. Mataoui, Natural convection in nanofluids: Are the thermophoresis and Brownian motion effects significant in nanofluid heat transfer enhancement?, Int. J. Therm. Sci. 57 (2012) 152–162. doi:10.1016/j.ijthermalsci.2012.01.016.

[54]   H.A. Pakravan, M. Yaghoubi, Analysis of nanoparticles migration on natural convective heat transfer of nanofluids, Int. J. Therm. Sci. 68 (2013) 79–93. doi:10.1016/j.ijthermalsci.2013.04.007.

[55]   E. Rossi di Schio, M. Celli, A. Barletta, Effects of Brownian Diffusion and Thermophoresis on the Laminar Forced Convection of a Nanofluid in a Channel, J. Heat Transfer. 136 (2013) 22401. doi:10.1115/1.4025376.

[56]   M. Shariat, R.M. Moghari, A. Akbarinia, R. Rafee, S.M. Sajjadi, Impact of nanoparticle mean diameter and the buoyancy force on laminar mixed convection nanofluid flow in an elliptic duct employing two phase mixture model, Int. Commun. Heat Mass Transf. 50 (2014) 15–24. doi:10.1016/j.icheatmasstransfer.2013.11.003.

[57]   M. Goodarzi, M.R. Safaei, K. Vafai, G. Ahmadi, M. Dahari, S.N. Kazi, N. Jomhari, Investigation of nanofluid mixed convection in a shallow cavity using a two-phase mixture model, Int. J. Therm. Sci. 75 (2014) 204–220.

doi:10.1016/j.ijthermalsci.2013.08.003.

[58] M. Hejazian, M.K. Moraveji, A. Beheshti, Comparative study of Euler and mixture models for turbulent flow of Al2O3 nanofluid inside a horizontal tube, Int. Commun. Heat Mass Transf. 52 (2014) 152–158. doi:10.1016/j.icheatmasstransfer.2014.01.022.

[59] Y. Abbassi, A.S. Shirani, S. Asgarian, Two-phase mixture simulation of Al2O3/water nanofluid heat transfer in a non-uniform heat addition test section, Prog. Nucl. Energy. 83 (2015) 356–364. doi:10.1016/j.pnucene.2015.04.009.

[60] F. Garoosi, B. Rohani, M.M. Rashidi, Two-phase mixture modeling of mixed convection of nanofluids in a square cavity with internal and external heating, Powder Technol. 275 (2015) 304–321. doi:10.1016/j.powtec.2015.02.015.

[61] S. Kakac, A. Pramuanjaroenkij, Single-phase and two-phase treatments of convective heat transfer enhancement with nanofluids - A state-of-the-art review, Int. J. Therm. Sci. 100 (2016) 75–97. doi:10.1016/j.ijthermalsci.2015.09.021.

[62] Y. He, Y. Men, Y. Zhao, H. Lu, Y. Ding, Numerical investigation into the convective heat transfer of TiO2 nanofluids flowing through a straight tube under the laminar flow conditions, Appl. Therm. Eng. 29 (2009) 1965–1972. doi:10.1016/j.applthermaleng.2008.09.020.

[63] V. Bianco, F. Chiacchio, O. Manca, S. Nardini, Numerical investigation of nanofluids forced convection in circular tubes, Appl. Therm. Eng. 29 (2009) 3632–3642. doi:10.1016/j.applthermaleng.2009.06.019.

[64] K. Jin, Modeling Nano-Particle Migration in Pipe Flow through Eulerian-Lagrangian Approach, Lehigh University, 2011. http://preserve.lehigh.edu/cgi/viewcontent.cgi?article=2253&context=etd.

[65] S. Laín, M. Sommerfeld, Numerical calculation of pneumatic conveying in horizontal channels and pipes: Detailed analysis of conveying behaviour, Int. J.

Multiph. Flow. 39 (2012) 105–120. doi:10.1016/j.ijmultiphaseflow.2011.09.006.

[66] S. Tahir, M. Mital, Numerical investigation of laminar nanofluid developing flow and heat transfer in a circular channel, Appl. Therm. Eng. 39 (2012) 8–14. doi:10.1016/j.applthermaleng.2012.01.035.

[67] H. Bahremand, A. Abbassi, M. Saffar-Avval, Experimental and numerical investigation of turbulent nanofluid flow in helically coiled tubes under constant wall heat flux using Eulerian-Lagrangian approach, Powder Technol. 269 (2014) 93–100. doi:10.1016/j.powtec.2014.08.066.

[68] M. Ishii, T. Hibiki, Thermo-fluid dynamics of two-phase flow, Springer Science & Business Media, 2010.

[69] M. Manninen, V. Taivassalo, S. Kallio, On the mixture model for multiphase flow, Technical Research Centre of Finland Finland, VTT publications 288, 1996.

[70] P.G.T. Saffman, The lift on a small sphere in a slow shear flow, J. Fluid Mech. 22 (1965) 385–400.

[71] J.S. Marshall, S. Li, Adhesive particle flow, Cambridge University Press, 2014.

[72] A.R. Petosa, Transport , deposition and aggregation of metal oxide nanoparticles in saturated granular porous media : role of water chemistry , collector surface and particle coating, McGill University, Canada, 2013.

[73] D.G. Kröger, Air-cooled heat exchangers and cooling towers. Appendix A: Properties of Biological Fluids, PennWell Books, 2004. doi:10.1016/B978-0-08-087780-8.00143-1.

[74] E.E.S. Michaelides, Heat and mass transfer in particulate suspensions, Springer Science & Business Media, 2013.

[75] M. Corcione, Empirical correlating equations for predicting the effective thermal conductivity and dynamic viscosity of nanofluids, Energy Convers. Manag. 52

(2011) 789–793. doi:10.1016/j.enconman.2010.06.072.

[76]   F. Podczeck, Particle-particle adhesion in pharmaceutical powder handling, World Scientific, 1998.

[77]   R.J. Hunter, Foundations of colloid science, Oxford University Press, 2001.

[78]   Sa. Morsi, A.J. Alexander, An investigation of particle trajectories in two-phase flow systems, J. Fluid Mech. 55 (1972) 193–208.

[79]   A. Haider, O. Levenspiel, Drag coefficient and terminal velocity of spherical and nonspherical particles, Powder Technol. 58 (1989) 63–70.

[80]   B. Oesterle, T.B. Dinh, Experiments on the lift of a spinning sphere in a range of intermediate Reynolds numbers, Exp. Fluids. 25 (1998) 16–22. doi:10.1007/s003480050203.

[81]   S.C.R. Dennis, S.N. Singh, S.B. Ingham, The steady flow due to a rotating sphere at low and moderate Reynolds numbers, J. Fluid Mech. 101 (1980) 257–279. doi:10.1017/S0022112080001656.

[82]   A.Y. Varaksin, J. Melorose, R. Perroy, S. Careas, Turbulent particle-laden gas flows, Springer, 2007. doi:10.1017/CBO9781107415324.004.

[83]   X. Zheng, Z. Silber-Li, The influence of Saffman lift force on nanoparticle concentration distribution near a wall, Appl. Phys. Lett. 95 (2009) 24–27. doi:10.1063/1.3237159.

[84]   W. Kraipech, A. Nowakowski, T. Dyakowski, A. Suksangpanomrung, An investigation of the effect of the particle-fluid and particle-particle interactions on the flow within a hydrocyclone, Chem. Eng. J. 111 (2005) 189–197. doi:10.1016/j.cej.2005.02.022.

[85]   G.S. McNab, A. Meisen, Thermophoresis in liquids, J. Colloid Interface Sci. 44 (1973) 339–346. doi:10.1016/0021-9797(73)90225-7.

[86] M. Ahmed, M. Eslamian, Numerical Simulation of Natural Convection of a Nanofluid in an Inclined Heated Enclosure Using Two-Phase Lattice Boltzmann Method: Accurate Effects of Thermophoresis and Brownian Forces, Nanoscale Res. Lett. 10 (2015) 296. doi:10.1186/s11671-015-1006-0.

[87] E.E. Michaelides, Brownian movement and thermophoresis of nanoparticles in liquids, Int. J. Heat Mass Transf. 81 (2015) 179–187. doi:10.1016/j.ijheatmasstransfer.2014.10.019.

[88] A. Li, G. Ahmadi, Dispersion and Deposition of Spherical Particles from Point Sources in a Turbulent Channel Flow, Aerosol Sci. Technol. 16 (1992) 209–226. doi:10.1080/02786829208959550.

[89] J. Koo, C. Kleinstreuer, A new thermal conductivity model for nanofluids, J. Nanoparticle Res. 6 (2004) 577–588. doi:10.1007/s11051-004-3170-5.

[90] H.E. Patel, T. Sundararajan, T. Pradeep, A. Dasgupta, N. Dasgupta, S.K. Das, A micro-convection model for thermal conductivity of nanofluids, Pramana - J. Phys. 65 (2005) 863–869. doi:10.1007/BF02704086.

[91] W.E. Ranz, Evaporation from drops: Part II, Chem. Engng. Prog. 48 (1952) 173–180.

[92] E.E. Michaelides, Z. Feng, Heat transfer from a rigid sphere in a nonuniform flow and temperature field, Int. J. Heat Mass Transf. 37 (1994) 2069–2076. doi:10.1016/0017-9310(94)90308-5.

[93] J.H. Ferziger, M. Peric, Computational methods for fluid dynamics, Springer Science & Business Media, 2012.

[94] S. V Apte, K. Mahesh, T. Lundgren, Accounting for finite-size effects in simulations of disperse particle-laden flows, Int. J. Multiph. Flow. 34 (2008) 260–271.

[95] D.M. Snider, An incompressible three-dimensional multiphase particle-in-cell

107

model for dense particle flows, J. Comput. Phys. 170 (2001) 523–549.

[96] ASHRAE, American society of heating, refrigerating and air-conditioning engineers, Fundamentals. Appendix A, 2009.

[97] A. Kaufmann, M. Moreau, O. Simonin, J. Helie, Comparison between Lagrangian and mesoscopic Eulerian modelling approaches for inertial particles suspended in decaying isotropic turbulence, J. Comput. Phys. 227 (2008) 6448–6472. doi:10.1016/j.jcp.2008.03.004.

[98] H. Ghodsinezhad, M. Sharifpur, J.P. Meyer, Experimental investigation on cavity flow natural convection of Al2O3–water nanofluids, Int. Commun. Heat Mass Transf. 76 (2016) 316–324. doi:10.1016/j.icheatmasstransfer.2016.06.005.

[99] E. Bacharoudis, M.G. Vrachopoulos, M.K. Koukou, D. Margaris, A.E. Filios, S.A. Mavrommatis, Study of the natural convection phenomena inside a wall solar chimney with one wall adiabatic and one wall under a heat flux, Appl. Therm. Eng. 27 (2007) 2266–2275. doi:10.1016/j.applthermaleng.2007.01.021.

[100] C. Teodosiu, F. Kuznik, R. Teodosiu, CFD modeling of buoyancy driven cavities with internal heat source - Application to heated rooms, Energy Build. 68 (2014) 403–411. doi:10.1016/j.enbuild.2013.09.041.

[101] H. Zhang, S. Shao, H. Xu, C. Tian, Heat transfer and flow features of Al2O3-water nanofluids flowing through a circular microchannel - Experimental results and correlations, Appl. Therm. Eng. 61 (2013) 86–92. doi:10.1016/j.applthermaleng.2013.07.026.

A

APPENDIX A: User-Defined Functions

APPENDIX A.1: UDFs for the developed mixture model, slip velocity approach

```
/*************************************************************************
This UDF is to define a new slip velocity due to diffusion in mixture model equation
This code needs to be either interpreted or compiled and all DEFINE_ADJUST functions
are needed to be hooked up.
*************************************************************************/
/*Hint for temp gradianet from Help: Note that gradient variables are available only when
the equation for that variable is being solved.
*/

#define diam 137.e-9                    //particle diameter
# define kB 1.3806e-23                  //Boltzmann constant
# define pi 3.1415
# define PH 3                    //PH of the nanofluid
# define e0 8.854e-12             //vaccum permitivity
# define er 80                //relative permitivity (in this case for water
# define Fa 96485             //Faraday constant
# define Rg 8.31
# define zetap 30e-3
# define Ham 4e-20              //Hamaker constant(in this case for alumina nanofluid
# define kp 36           //particle thermal conductivity
DEFINE_ADJUST(adjust_T, domain)    //new scalar for Temp
{
    int n = 0;
    Thread *t;
    cell_t c;
    face_t f;
    domain = Get_Domain(1);
    thread_loop_c(t, domain)
    {
        begin_c_loop(c, t)
        {
            C_UDSI(c, t, 0) = C_T(c, t);
        }
        end_c_loop(c, t)
    }
    thread_loop_f(t, domain)
    {
        if (NULL != THREAD_STORAGE(t, SV_UDS_I(0)))
        {
```

```
        begin_f_loop(f, t)
        {
            real T1 = 0.;
            if (NULL != THREAD_STORAGE(t, SV_T))
                T1 = F_T(f, t);
            else if (NULL != THREAD_STORAGE(t->t0, SV_T))
                T1 = C_T(F_C0(f, t), t->t0);
            F_UDSI(f, t, 0) = T1;
        }
        end_f_loop(f, t)
    }
}
}

DEFINE_ADJUST(adjust_vof, domain)
{
    Thread *t;
    cell_t c;
    face_t f;
    domain = Get_Domain(2);
    // Fill UDS with the vof.
    thread_loop_c(t, domain)
    {
        begin_c_loop(c, t)
        {
            C_UDSI(c, t, 1) = 1 - C_VOF(c, t);
        }
        end_c_loop(c, t)
    }

    thread_loop_f(t, domain)
    {
        if (THREAD_STORAGE(t, SV_UDS_I(1)) != NULL)
            begin_f_loop(f, t)
            {
                F_UDSI(f, t, 1) = 1 - F_VOF(f, t);
            }
        end_f_loop(f, t)
    }
}

//slip velocity will be added
DEFINE_VECTOR_EXCHANGE_PROPERTY(custom_slip, c, mixture_thread,
primary_phase, secondary_phase, vector_result)
{
```

```
real gravity[2] = { 0., -9.81 };
real phi, T, rho_c, rho_m, mu_c, rhop;
        real taup;
        real C_Brownian, kf, ST;
        real C_thermophes;
        real D_B;
        real Vp_x, Vp_y, Vp;
        real CB;
real Umgrad_x, Umgrad_y;
        real Vmgrad_x, Vmgrad_y;
        real Vm, Um;
        real a_x, a_y;
real Vs_x_BTGC, Vs_y_BTGC;
        real fvm_x, fvm_y;
        real fp_x, fp_y;
        real Vs_x_vm, Vs_y_vm;
        real xx;
        real Vs_x_p, Vs_y_p;
real Io, kk;
        real Fvdw, Fedl;
        real Fdlvo_x, Fdlvo_y;
real Vs_x_dlvo=0;
real Vs_y_dlvo=0;
real curlu;
        real Rew;
        real CL;
        real fL_x, fL_y;
        real Vs_x_L, Vs_y_L;
Thread *pt;        // thread pointers for primary phases
Thread *st;        // thread pointers for secondary phases
pt = THREAD_SUB_THREAD(mixture_thread, primary_phase);
st = THREAD_SUB_THREAD(mixture_thread, secondary_phase);
phi = C_VOF(c, st); //vof second phase (or particle)
// at this point the phase threads are known for primary (0) and secondary(1) phases
T = C_T(c, pt);
rho_c = 765.33 + 1.8142*T - 0.0035*pow(T, 2);      //fluid density
rho_m = C_R(c, mixture_thread);          //mixture density
kf = -0.00000718*pow(T, 2) + 0.00575419*T - 0.46662403;    //water thermal
conductivity
        mu_c = 0.000000000029885*pow(T, 4) - 0.00000040781184*pow(T, 3)
        + 0.000020927097596*pow(T, 2) - 0.004792184560427*T +
        0.414092804247831;       //laminar fluid (water) viscosity
rhop = C_R(c, st);              //secondary (particle) density
taup = rhop*diam*diam / 18. / mu_c;       //particle relaxation time

D_B = kB*T / 3.0 / pi / mu_c / diam;
```

```
C_Brownian = rho_m *D_B / (phi*(1 - phi)*rho_c);
ST = 0.26*kf / (2.0 * kf + kp);
C_thermophes = rho_m*ST*mu_c / ((1 - phi)*rho_c*rho_c);

Um = C_U(c, mixture_thread);
Vm = C_V(c, mixture_thread);
Umgrad_x = C_U_G(c, mixture_thread)[0];      //U mixture velocity gradianet in x-
direction
Umgrad_y = C_U_G(c, mixture_thread)[1];      //U mixture velocity gradianet in y-
direction
Vmgrad_x = C_V_G(c, mixture_thread)[0];      //V mixture velocity gradianet in x-
direction
Vmgrad_y = C_V_G(c, mixture_thread)[1];      //V mixture velocity gradianet in y-
direction

a_x = gravity[0] - Um*Umgrad_x - Vm*Umgrad_y;   //acceleration in x-direction
a_y = gravity[1] - Um*Vmgrad_x - Vm*Vmgrad_y;   //acceleration in y-direction
          Vs_x_BTGC = taup*(rhop - rho_m)*a_x / rhop -
          C_thermophes*C_UDSI_G(c, pt, 0)[0] / T - C_Brownian*C_UDSI_G(c,
          st, 1)[0];
          Vs_y_BTGC = taup*(rhop - rho_m)*a_y / rhop -
          C_thermophes*C_UDSI_G(c, pt, 0)[1] / T - C_Brownian*C_UDSI_G(c,
          st, 1)[1];

          fvm_x = rho_c*0.5*(C_U(c, pt)*C_U_G(c, pt)[0] + C_V(c, pt)*C_U_G(c,
          pt)[1]);
fvm_y = rho_c*0.5*(C_U(c, pt)*C_V_G(c, pt)[0] + C_V(c, pt)*C_V_G(c, pt)[1]);
Vs_x_vm = taup*fvm_x / rhop;//slip velocity due to virtual mass force in x-axis
Vs_y_vm = taup*fvm_y / rhop;
/////////////////////////pressure gradient  slip velocity
fp_x = rho_c*(C_U(c, pt)*C_U_G(c, pt)[0] + C_V(c, pt)*C_U_G(c, pt)[1]);
fp_y = rho_c*(C_U(c, pt)*C_V_G(c, pt)[0] + C_V(c, pt)*C_V_G(c, pt)[1]);
Vs_x_p = taup*fp_x / rhop;
Vs_y_p = taup*fp_y / rhop;
/////////////////////////// Saffman lift force
curlu = C_V_G(c, pt)[0] - C_U_G(c, pt)[1];
Rew = rho_c*fabs(curlu)*diam*diam / mu_c;
if (Rew == 0)
    CL = 0.076;
else
    CL = 3.*6.46 / (2. * pi*sqrt(Rew));

fL_x = CL*rho_c*phi*curlu*vector_result[1];
fL_y = CL*rho_c*phi*curlu*vector_result[0];
Vs_x_L = taup*fL_x / rhop;
Vs_y_L = taup*fL_y / rhop;
```

```c
//////////////////////////// van der waals attraction and repulsion (electrical double layer)
forces
    xx =pow((pi / 6 / phi), 0.333333333333333)-1;     //xx is h/d, surface distance to
diameter of particle
    if (PH > 7)
        Io = 0.5*pow(10, (PH - 14));            //ionic strength
    else
        Io = 0.5*pow(10, -PH);

    kk = sqrt(2000 * pow(Fa, 2)*Io / e0 / er / Rg / T);          //Debye parameter, 1/kk is
Debye lenght
    if (xx > 1 / kk / diam)
    {
        Fvdw = Ham / 6.0 / diam / (pow(xx, 2.0)*pow((xx + 1), 3)*pow((xx + 2), 2.0));
        Fedl = pi*diam*kk*e0*er*zetap*zetap*exp(-kk*xx*diam);
        if (C_U(c, pt) > 0)
            Fdlvo_x = Fvdw - Fedl;
        else
            Fdlvo_x = Fedl - Fvdw;

        if (C_V(c, pt) > 0)
            Fdlvo_y = Fvdw - Fedl;
        else
            Fdlvo_y = Fedl - Fvdw;

        Vs_x_dlvo = Fdlvo_x / (3 * pi*mu_c*diam);
        Vs_y_dlvo = Fdlvo_y / (3 * pi*mu_c*diam);
    }
    vector_result[0] = Vs_x_BTGC + Vs_x_vm + Vs_x_p - Vs_x_dlvo + Vs_x_L;
    vector_result[1] = Vs_y_BTGC + Vs_y_vm + Vs_y_p - Vs_y_dlvo + Vs_y_L;
    C_UDMI(c, pt, 0) = Fvdw / Fedl;
    C_UDMI(c, pt, 1) = Vs_x_dlvo / Vs_x_BTGC;
    C_UDMI(c, pt, 2) = Vs_x_L / Vs_x_BTGC;
    C_UDMI(c, pt, 3) = Vs_y_dlvo / Vs_y_BTGC;
    C_UDMI(c, pt, 4) = Vs_y_L / Vs_y_BTGC;
}
////////////////////////////////////////////////////////////////////////////////////////////////////////////////////////////////
////////
DEFINE_PROPERTY(airviscosity, c, t)
{
    real T = C_T(c, t);
    real alfa = C_VOF(c, t);
    real muair, muwater;
            real mumixture;
```

```
            muwater = 0.000000000029885*pow(T, 4) - 0.000000040781184*pow(T,
            3) + 0.000020927097596*pow(T, 2) - 0.004792184560427*T +
            0.414092804247831;
    mumixture = muwater / (1-34.87*pow(diam/3e-10,-0.3)*pow(alfa,1.03));
    if (alfa == 0)
        muair = .0008;
    else
        muair = (mumixture - (1 - alfa)*muwater) / alfa;
    return muair;
}

DEFINE_PROPERTY(airconductivity, c, t)
{
    real T = C_T(c, t);
    real alfa = C_VOF(c, t);
    real kbf, kair;
            real knf;
            real mu_c = 0.000000000029885*pow(T, 4) -
            0.000000040781184*pow(T, 3) + 0.000020927097596*pow(T, 2) -
            0.004792184560427*T + 0.414092804247831;  //laminar fluid (water)
            viscosity
    real rho_c = 765.33 + 1.8142*T - 0.0035*pow(T, 2);  //fluid density
    real cp_c = -0.00014301*pow(T, 3) + 0.15359377*pow(T, 2) - 54.08920728*T +
10444.58656104;
    real ub, Re, Pr_f;
    ub = 2 * kB*T / (pi*mu_c*diam*diam);
    Re = rho_c*ub*diam / mu_c;
            kbf = -0.00000718*pow(T, 2) + 0.00575419*T - 0.46662403;
    Pr_f = cp_c*mu_c / kbf;
    knf = kbf*(1 + 4.4*pow(Re, 0.4)*pow(Pr_f, 0.66)*pow(T / 273.15, 10.)*pow(kp /
kbf,0.03)*pow(alfa, 0.66));
    if (alfa == 0)
        kair = .6;
    else
        kair = (knf - (1 - alfa)*kbf) / alfa;
    return kair;
}
```

APPENDIX A.2: UDFs for the developed mixture model, diffusion approach

114

```
/*************************************************************************
```
Only the following code is added to the above mentioned code and diffusion of thermophoresis and Brownian is removed in slip velocity section. it is avoided mentioning it here (with some modifications)
```
*************************************************************************/


//source term in mass equation of second phase

DEFINE_SOURCE(mass_source, c, t, dS, eqn)
{
    real source;
                real T, Cp_c, DB;
                real kf, mu_c, rho_c;
                real ST, DT;
                real Gphi_GT;
                real GT_GT;
                real G2phi;
                real G2T;
    T = C_T(c, t);
    Cp_c = -0.00014301*pow(T, 3) + 0.15359377*pow(T, 2) - 54.08920728*T +
10444.58656104;
    kf = -0.00000718*pow(T, 2) + 0.00575419*T - 0.46662403;
                mu_c = 0.000000000029885*pow(T, 4) - 0.000000040781184*pow(T, 3)
                + 0.000020927097596*pow(T, 2) - 0.004792184560427*T +
                0.414092804247831;   //laminar fluid (water) viscosity
    rho_c = 765.33 + 1.8142*T - 0.0035*pow(T, 2);
    DB = kB*T / 3.0 / pi / mu_c / diam;            //for laminar
    ST = 0.26*kf / (2.0 * kf + kp);

    DT = ST*mu_c*C_UDSI(c, t, 4) / rho_c;

    Gphi_GT = C_UDSI(c, t, 5) * C_UDSI(c, t, 1) + C_UDSI(c, t, 6) * C_UDSI(c, t, 2) +
C_UDSI(c, t, 7) * C_UDSI(c, t, 3);
    G2phi = C_UDSI_G(c, t, 5)[0] + C_UDSI_G(c, t, 6)[1] + C_UDSI_G(c, t, 7)[2];
    G2T = C_UDSI_G(c, t, 1)[0] + C_UDSI_G(c, t, 2)[1] + C_UDSI_G(c, t, 3)[2];
    source = rhop*((DB / T + ST*mu_c / rho_c / T)*Gphi_GT + DB*G2phi + DT*G2T /
T);
    dS[eqn] = rhop* ST*mu_c *G2T / rho_c / T;

    return source;
}
///////////////////////////////////////////////////////////////////////////////////////////////////////////////////////////
/////////////////////////////////////////////////
//source term in mixture enrgy equation
DEFINE_SOURCE(Heat_source, c, t, dS, eqn)
{
```

```
    real source;
                real T, Cp_c, DB;
                real kf, mu_c, rho_c;
                real ST, DT;
                real Gphi_GT;
                real GT_GT;
                real G2phi;
                real G2T;
    T = C_T(c, t);
    Cp_c = 28070 - 281.7*T + 1.25*pow(T, 2) - 0.00248*pow(T, 3) + 1.857e-06*pow(T, 4);
    kf = -.5752 + 6.397*.001*T - 8.151*.001*.001*pow(T, 2);   //water thermal
conductivity
    mu_c = .0967 - .0008207*T + 2.344*pow(10., -6)*pow(T, 2) - 2.244*pow(10., -9)*pow(T, 3);
    rho_c = 765.33 + 1.8142*T - 0.0035*pow(T, 2);

    DB = kB*T / 3.0 / pi / mu_c / diam;
    ST = 0.26*kf / (2.0 * kf + kp);
    DT = ST*mu_c*C_UDSI(c, t, 3) / rho_c;          //thermophesis coefficient

                Gphi_GT = C_UDSI_G(c, t, 3)[0] * C_UDSI_G(c, t, 0)[0] +
                C_UDSI_G(c, t, 3)[1] * C_UDSI_G(c, t, 0)[1] + C_UDSI_G(c, t, 3)[2] *
                C_UDSI_G(c, t, 0)[2];
    GT_GT = C_UDSI_G(c, t, 1)[0] + C_UDSI_G(c, t, 2)[1] + C_UDSI_G(c, t, 3)[2];
    source = rhop*Cp_p*(DB*Gphi_GT + DT*GT_GT/T);
    dS[eqn] = rhop*Cp_p *(kB*Gphi_GT / 3.0 / pi / mu_c / diam);
    return source;
}
//the following boundary conditions are applied in the case of cavity
DEFINE_PROFILE(temp_hot, t, i)
{
    real x[ND_ND];    /* this will hold the position vector */
    real y;
    face_t f;
    begin_f_loop(f, t)
    {
        F_CENTROID(x, f, t);
        y = x[1];
        F_PROFILE(f, t, i) = -363.56*pow(y, 2.) + 74.527*y + 313.39;
    }
    end_f_loop(f, t)
}

DEFINE_PROFILE(temp_cold, t, i)
{
```

116

```
    real x[ND_ND];    /* this will hold the position vector */
    real y;
    face_t f;
    begin_f_loop(f, t)
    {
        F_CENTROID(x, f, t);
        y = x[1];
        F_PROFILE(f, t, i) = 32.941*y + 294.17;
    }
    end_f_loop(f, t)
}
```